NTNU
Institutt for materialteknologi

HYDROGEN-BASED IRON RECOVERY FROM BAUXITE RESIDUE

BACHELOR'S THESIS

HYDROGENBASERT JERN-UTVINNING FRA RØDSLAM

BACHELOROPPGAVE

WRITTEN BY

Skibelid, Olivia Bogen

Velle, Sander Ose

Vollan, Frida

ACADEMIC SUPERVISORS

Jafar Safarian
Arman Hoseinpur-Kermani
Casper Van der Eijk (external)

INITIATOR

The HARARE project, funded by the European Union

IMA-B-12-2022
Security classification: open
19.05.2022, TRONDHEIM

Preface

Our thesis; "Hydrogen-based Iron Recovery from Bauxite Residue" is based on scientific research exploring the further utilization of bauxite residue. The thesis has been written as a part of the bachelor's degree in chemical engineering at the Department of Material Science and Engineering at the Norwegian University of Science and Technology, NTNU. It is written in cooperation with the European EU project HARARE, which is based on previous research carried out by SINTEF Industry and NTNU through the ENSUREAL EU project, commissioned 2017-2022. HARARE's overall objective is to eliminate waste from the metallurgical industry while recovering valuable materials and encouraging the use of hydrogen in the industry. The project has received funding from the European Union's Horizon 2020 Research and Innovation Program under grant agreement No. 958307.

We are incredible grateful for being able to contribute at an innovative project such as HARARE. The work has been very fulfilling, although it has been challenging. Since the thesis work mainly is within the material sciences, the work required some adaptation on our behalf. Many hours were spent acquiring the proper knowledge, including understanding the mechanisms behind our experimental work. In addition, the latter demanded an excessive amount of time. Fortunately, our supervisors always made time for our inquiries. We would like to express our immense gratitude to Assoc. Professor Jafar Safarian, NTNU, for all the guidance and feedback, during the entirety of the project. Dr. Arman Hoseinpur-Kermani, NTNU, for going above and beyond when helping in all the experimental aspects of this project. Dr. Casper van der Eijk, for introducing us to the project, and being our link to SINTEF. We would also like to direct a special thanks to Ina Merete Stuen, for guidance throughout the entire degree. In addition, NTNU and SINTEF is acknowledged for permitting the use of their equipment, instruments and laboratories.

We hope our thesis offers some valuable insight, and that it can contribute to a more sustainable industry in the long term.

Olivia Bogen Skibelid

Sander Ose Velle

Frida Vollan

Trondheim, 19.05.2022

Abstract

Valorization of bauxite residue is of great importance for sustainable production of aluminium, and the research in this field is continued in this bachelor thesis. Hydrogen reduction of iron in a mixture of bauxite residue and limestone was studied based on experimental work. In addition, the leaching of the reduced samples was done to research the extraction of aluminium trihydroxide and further acquisition of alumina. The research was done with the intention of further valorization of bauxite residue, eliminating the waste of the aluminium industry. Hydrogen was purposefully used as reductant to reduce the carbon emissions of the process.

To enable reduction of the mixture, it was pelletized and sintered. The sintered pellets were then reduced at three different temperatures (1000, 1100 and 1200°C) and four durations (0.5, 1.5, 2 and 2.5 h). The variation of temperature and time was done to investigate their influence on the production of metallic iron, both separately and cooperatively, to determine the optimal reduction conditions. Comparison of the reduction experiments indicate that temperature is the most important parameter considering the overall yield of metallic iron, even though time remains important, especially at higher temperatures.

Various analytical methods and instruments were used to characterise the samples. With use of XRF, each sample's contents were quantified prior to reduction. Consequently, the reduced samples were studied with SEM and XRD to inspect the morphology and composition. The leached samples were analysed with XRD for determining composition, in addition to qualitative analysis through ICP-MS.

The results from the reduction experiments revealed that reduction 4 (1000°C, 2.5 h) was the most beneficial for reducing iron, with a yield of 82.9%. When considering the extraction of aluminium after leaching, reduction 2 (1000°C, 1 h) yielded the most with 86.6%. When combining the results from the reduction and leaching experiments, it was concluded that reduction 4 was the most beneficial, giving the greatest combined yield of both iron (82.9%) and aluminium (82.0%), granting the best overall valorization of bauxite residue.

Sammendrag

Valorisering av bauksittavfall er essensielt for bærekraftig produksjon av aluminium, og undersøkes videre i denne bacheloroppgaven. Hydrogenreduksjon av jernoksider i en blanding av bauksitt-avfall og kalkstein ble studert basert på eksperimentelle forsøk. De reduserte prøvene ble i tillegg behandlet under basiske forhold for å undersøke ekstraksjonen av aluminiumtrihydroksid, som videre muliggjør uthenting av alumina. Forskningen ble gjort med den hensikt å skape verdi av bauxittrester, og begrense avfallet fra aluminiumindustrien. Hydrogen ble bevisst brukt som reduksjonsmiddel, for å redusere karbonutslippene fra prosessen.

For å muliggjøre reduksjon av blandingen ble det laget pellets av blandingen. Disse ble sintret, og deretter redusert ved tre forskjellige temperaturer (1000, 1100 og 1200°C) og tider (0.5, 1, 2, og 2.5 t). Variasjonen av temperatur og tid ble gjort for å undersøke deres innflytelse på produksjonen av metallisk jern, og dermed finne de optimale reduksjonsbetingelsene. Sammenligning av reduksjons-eksperimentene indikerer at temperatur er den viktigste parameteren med hensyn på det overordnede utbyttet av rent jern, selv om tid forblir en viktig parameter, spesielt ved høyere temperaturer.

Ulike analysemetoder og instrumenter ble brukt for å karakterisere prøvene. Ved hjelp av XRF ble prøvenes innhold kvantifisert før reduksjon. Følgelig ble de reduserte prøvene studert med SEM og XRD for å undersøke morfologien og den strukturelle sammensetningen. Etter utlutingen ble residuumet analysert med XRD, og filtratet ble analysert med ICP-MS for kvantifisering av løsningen.

Resultatene fra reduksjonseksperimentene viste at reduksjonen uført ved 1000°C i 2.5 timer var den mest gunstige reduksjonsparallellen med et utbytte av rent jern på 82.9%. Med hensyn på ekstraksjonen av aluminium etter utlutingen var reduksjonen utført ved 1000°C i 1 time den som gav det største utbyttet med 86.6%. Ved sammenfatning av eksperimentene fra reduksjonene og utlutningene ble det konkludert med at reduksjon 4 var den overordnet mest gunstige da den gav det samlet største utbyttet av både jern (82.9%) og aluminium (82.0%) og dermed den beste utnyttelsen av bauksittavfallet.

Table of contents

List of figures

List of tables

Abbreviations

RM – Red mud

BR – Bauxite residue

SEM – Scanning electron microscope

- SEI – Secondary electron imaging
- BEI – Backscattering electron imaging
- EDS – Dispersive x-ray spectroscopy

XRD – X-ray diffraction analysis

XRF – X-ray fluorescence analysis

ICP-MS – Inductive coupled plasma mass spectrometry

wt% – weight percentage

1 Introduction

1.1 Background and motivation

Global warming is a threat to humanity and every living being on the earth. In 2015, the Paris agreement was a turning point from which 196 parties united to act against climate change in a legally binding agreement. The long-term goal is to achieve a climate neutral world by mid-century[1, 2]. The sixth intergovernmental panel on climate change (IPCC) report from august 2021, reports that only with massive and immediate cuts in greenhouse emissions, will the 1.5°C or 2.0°C rise in average global temperature be avoided[3]. As a paradox, the energy demand in the world increases, and to ensure a sustainable future for the generations to come, a shift from fossil fuels to renewable energy sources is essential. One of the great contributors to CO_2-emissions is the metallurgical industry. This industry alone, accounts for 70 million tons direct CO_2-emissions annually per 2017[4]. Nonetheless, because of the high demand of metals such as aluminium and iron, connected to the shift to renewable energy, restraining metal production is not an option. The only option would be to make the metal industry more sustainable.

The present commercial process to extract and produce alumina is done by the Bayer Process. In addition to producing CO_2 and being generally energy consuming, it also produces 170 million tons red mud worldwide annually, per 2019[5]. Depending on the quality of the mined bauxite ore, up to two kg of red mud is produced for every kg aluminium produced[6]. Red mud is the main by-product of the Bayer Process and there are severe environmental issues concerning its disposal. The most practised way to dispose of this very alkaline and heavy metal containing waste, is to store it in ponds around the world. The ponds percolate into the local environments and can potentially flood large areas. Its alkalinity makes it damaging to agriculture and life depending on groundwater, which threatens the ecosystems surrounding the deposits. Despite being hazardous, the red mud contains considerable amounts of useful minerals and metals like iron, remnants of aluminium and rare earth elements. Red mud can contain up to 50 precent iron oxides and 10 percent aluminium oxides[7]. These perfectly good raw materials are simply dumped in large deposits - a glaring example of how the linear economy and short-term cycles of supply and demand disregard long-term planning for conservation of natural resources for future generations[7].

Because of the environmental challenges the Bayer process presents, other solutions have been sought out these past few years. Several of these projects are based on the Pedersen Process. The Pedersen Process differentiate from the Bayer Process in several ways. The most important differences are that the Pedersen process reduce CO_2 emissions and produces grey mud, a usable by-product as opposed to red mud, which needs further processing before it can be utilized. The main by-product in the process is pig iron which can further be turned into steel. It also produces CO_2 in the early stages of the process, although it is reused in later stages; which results in lower overall emissions[8]. Even though the Pederson process seems to be more eco-friendly than the Bayer Process, it is economically inferior and is not used commercially for this reason.

The ENSURAL Project is an example of previous research further exploring the use of the Pedersen Process. The project's main objective is ensuring zero waste production of alumina in Europe. This optimalization of the Pederson Process also include extracting rare earth elements[9]. To further ensure eco-friendly metal production, the HARARE Project was started in 2021 and is a consortium of universities, research institutes and industrial companies from Norway, Greece, Germany and Belgium[2, 4]. This project is based both on the Pedersen Process and the ENSUREAL project. The main modifications to the Pedersen Process, is firstly that the crude material is dried red mud (also called

bauxite residue) instead of bauxite ore. The second, very important change, is that the bauxite residue is reduced with hydrogen gas instead of coke. This ensures no direct CO_2-emisson from the process, as the only bi-product is H_2O and grey mud. This bachelor thesis is written in collaboration with, and as a part of, the HARARE project.

The main motivation to write this bachelor thesis is to be involved in creating a more sustainable future. As mentioned earlier, the IPCC states that it is crucial to act as soon as possible, and as members of the younger generation, this is of high importance. The HARARE project aims to be a pioneer in sustainable pathways to remove waste and valorize materials. In the process, it may inspire a more ethically conscious metallurgical industry. The subject is very interesting and the ability to provide information which will make changes for the better is very appealing.

1.2 Scope of research

This bachelor project aims to investigate an iron and aluminium extraction process which eliminates waste and carbon emissions compared to other processes in the same field. The project is included in HARARE's second work package (WP2). This package concerns the hydrogen reduction process and mainly focuses on the production of reduced pellets proper for further iron recovery by magnetic separation (WP4). In addition, the obtained lab scale results in WP2 will be used to upscale the process to pilot size in WP3 of the project. The approach to the experimental work is to carry out the reduction isothermally, adding H_2 at target temperature and vary the temperature and duration of the reduction to inspect how the parameters change the amount of metallic iron produced. The produced iron metal will also be attempted separated magnetically from the rest of the sample before the samples will be leached to obtain the aluminium from each sample.

The experimental procedure of this bachelor project is extensive. The main research activities and learnings, are:

- Pelletizing of bauxite residue
- Sintering at elevated temperature
- Hydrogen reduction at elevated temperature
- Characterization methods
- Alkaline leaching

Before being truly familiarized with the theory, it was decided to create a hypothesis based on optimizing the reduction conditions. Between the parameters of temperature and time, it was believed that temperature would prove to affect the reduction the most. This claim was based on knowledge from previous subjects regarding kinetics and thermodynamics. In relation to which time would be the most efficient for the reduction, and it was believed that the longest duration of reduction would result in the greatest yield of metallic iron.

The main objective of the project is to provide valuable insight in the process for further sustainable valorization of bauxite residue, using hydrogen metallurgy. If possible, the work will be able to contribute to a more sustainable metal industry in a long-term perspective.

2 Literature survey

2.1 Bayer process and bauxite residue

Bauxite is the primary material used for alumina production in the metallurgical industry and contain many different minerals such as hydrous aluminium and iron bearing minerals, silicates and titanium minerals[10]. The composition of the ore varies depending on if it is lateritic or karst ore deposits. Lateritic deposits are soils which are found in areas around the equator consisting of gibbsite (γ-$Al(OH)_3$) and boehmite (γ-AlO(OH)). Lateritic deposits are considered as high-grade bauxite which indicates a mass ratio of Al_2O_3 to SiO_2 greater than 6.25 and/or high Al_2O_3 to Fe_2O_3 ratio. Karst bauxite deposits consisting of boehmite and diaspore (α-AlO(OH)) can also be extracted from areas outside the equator. These ores are usually more rigid, are harder to leach (like diaspore) and contain more silica (SiO_2) and/or hematite (Fe_2O_3) and demand more processing to use[11-13].

The Bayer process is the main hydrometallurgical method to produce alumina from bauxite. It was invented by Carl Josef Bayer in 1888 and utilizes the amphoteric abilities of aluminium ions in solution. The process from bauxite ore to alumina can be simplified to five steps: milling, leaching, classification, precipitation and calcination. A simplified flowsheet of this process is shown in figure 1[14].

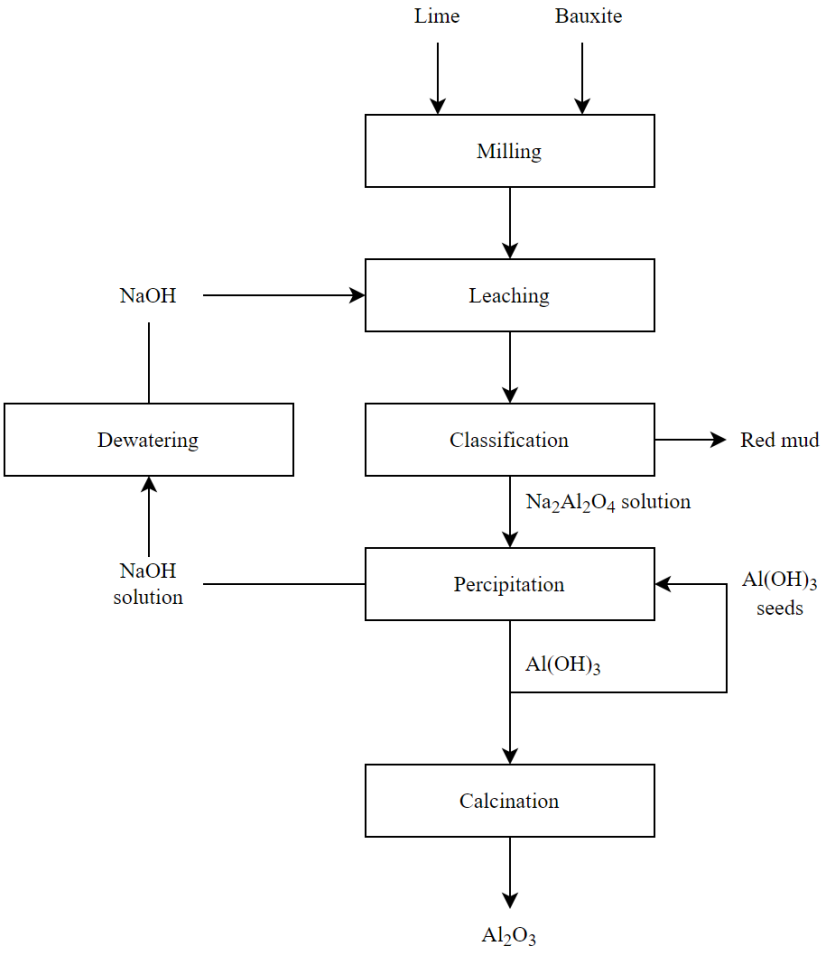

Figure 1. Simplified overview of the Bayer process[14]

Firstly, the bauxite ore is mixed with limestone and crushed in a mill to separate the different minerals in the ore and increase the surface area of the particles. Afterwards the finely crushed ore is transferred to leaching in order to extract the aluminium containing compounds. The mineral mixture is digested in a caustic solution at high pressures with temperatures between 150-250°C. In this step hydrous aluminium compounds like gibbsite, boehmite and diaspore react with the sodium hydroxide as shown in equations 1 and 2[13-15].

$$Al(OH)_{3(s)} + NaOH_{(aq)} \rightarrow Na^{+}_{(aq)} + Al(OH)^{-}_{4(aq)} \quad (1)$$

$$AlO(OH)_{(s)} + NaOH_{(aq)} + H_2O_{(l)} \rightarrow Na^{+}_{(aq)} + Al(OH)^{-}_{4(aq)} \quad (2)$$

The aluminium compounds dissolve in the solution while other insoluble minerals such as hematite remain. When the leaching is complete, the slurry is cooled down and continues to settle tanks for clarification. This is where the sodium aluminiumhydroxide solution gets separated from the suspended solid particles. With addition of flocculants, the bauxite residue is removed and washed to regenerate the caustic solution to the process. Depending on the requirements of the red mud (RM) storage facility, the residue may have to be further processed to be transferred to its disposal area. The sodium aluminiumhydoxide solution may also have to be cleansed of impurities[13-15].

When solution and the sediment is separated, the saturated sodium aluminiumhydroxide solution is cooled down to precipitate solid aluminium trihydroxide ($Al(OH)_3$). With addition of fine crystal $Al(OH)_3$ seeds, the solution starts to crystallize and aluminium trihydroxide and sodium hydroxide is recovered from the solution as shown in equation 3[13-15].

$$Na^{+}_{(aq)} + Al(OH)^{-}_{4(aq)} \rightarrow Al(OH)_{3(s)} + NaOH_{(aq)} \quad (3)$$

The recovered sodium hydroxide is recycled to the leaching step while some of the fine aluminium trihydroxide is reused as seeds for crystallization.

In the final step of the process the precipitated $Al(OH)_3$ is fed to a calcination furnace. At temperatures ranging from 960-1100°C the volatile components of the aluminium trihydroxide are driven off, producing alumina solids (Al_2O_3) as shown in equation 4[13-15].

$$Al(OH)_{3\,(s)} \rightarrow Al_2O_{3\,(s)} + 3H_2O_{(g)} \quad (4)$$

The Bayer process is the most commercially efficient method in alumina production, but it has its disadvantages. The amount of RM disposed worldwide is about 2.7 billion tonnes and is expected to increase by about 170 million tonnes per year[5, 16]. Depending on the composition of the bauxite which is used in the Bayer process, the amount of RM produced from one metric tonne of alumina is between 0,8-1,5 metric tonnes[10]. Low-grade bauxites demand tougher leaching conditions, produce large amounts of RM and are not ideal for the Bayer process. Composition analysis of RM internationally shows direct loss of valuable materials like iron and aluminium oxides among other minerals such as titanium oxide. The loss of iron oxides lies between 25-50 wt% while aluminium oxide is around 12-25 wt%. Considering the vast amount of RM disposed around the world, the total loss of minerals is significant[14, 16].

The environmental impact of RM production is of great significance. After leaching, the caustic soda is regenerated from the slurry. However, the RM still has alkalinity which makes the slurry hazardous.

How different facilities and companies dispose of the slurry varies. One of the most common and cheapest ways to treat the RM is to mix it with water to pump it out of the system more efficiently. The slurry is then transported to large holding ponds where it is disposed of. These holding ponds form a threat to its surroundings through the risk of flooding and accidents have already happened. In 2010 a holding pond collapsed releasing around 700,000 m^3 of RM sludge through the city of Ajka in Hungary, killing ten, injuring hundreds of people and destroying 40 km^2 of agricultural fields[14, 16]. The International Federation of Red Cross and Red Societies (IFRC) case study on the accident claims the flood was closer to 2 000 000 m^3 of red mud with about 120 people hospitalized and 300 injuries[17]. Pictures of the disaster are shown in figure 2.

Figure 2. Pictures of the flooding of Devescer (left) and the breach of the holding pond in Ajka (right)[17], ©MTI.

With holding ponds the groundwater can also get contaminated, which can be devastating for people and the environment. With further processing of the RM slurry accidents can be prevented. For instance, the slurry can be filtered and dewatered to remove the moisture content, resulting in bauxite residue (BR). It can also be treated with CO_2 to remove its alkalinity. These measures ensure a safer storage of the BR[14, 16].

2.2 Valorization of bauxite residue

Research and patents on how to utilize the BR is plentiful. With sufficient treatment of the RM to remove its hazardous properties, it can be used in mine backfilling and substituents in construction materials, such as cement. Other patents such as bricks, tiles and road construction are also considered. However, with considerable amounts of iron, aluminium and titanium oxides, the BR still has great value in terms of minerals. It is used for iron production and extraction of other oxide minerals remaining in the BR. Additionally, quantitative analysis of BR identifies traces of rare earth minerals within the material. Elements such as scandium (Sc), gallium (Ga), lithium (Li) and others are sought after, and extraction should be considered. Considering the vast amount of BR around the world and the materialistic value it holds, the processing of the material should be encouraged[14, 18].

As mentioned, aluminium is extracted through the Bayer process which yields a highly alkaline waste product. A more eco-friendly alternative to this process is the Pedersen process. It was introduced in 1920s by Norwegian Professor, Harald Pedersen and for almost 50 years the process made 17 000 ton per year in Høyanger, Norway. The Pedersen process prevents the hazardous red mud generation and instead forms consumable pig iron and grey mud (carbonate) products. In addition to being more eco-friendly, the Pedersen process functions better with low-grade bauxite, as opposed to the Bayer process.

The process is shown schematically in figure 3. Removing metallic iron from the bauxite through a smelting-reduction with coke, yields pig iron as well as a further processable calcium-aluminate slag. To extract the aluminium from this slag, it is milled and leached with a sodium carbonate solution. The residue from the leaching constitutes the grey mud. Further addition of carbon dioxide is done to precipitate the aluminium hydroxide. The waste of this step is a sodium carbonate solution, which is reused in the leaching. As seen in the figure, carbon dioxide produced in the first step is also reused in the precipitation of aluminium hydroxide[14, 16, 19].

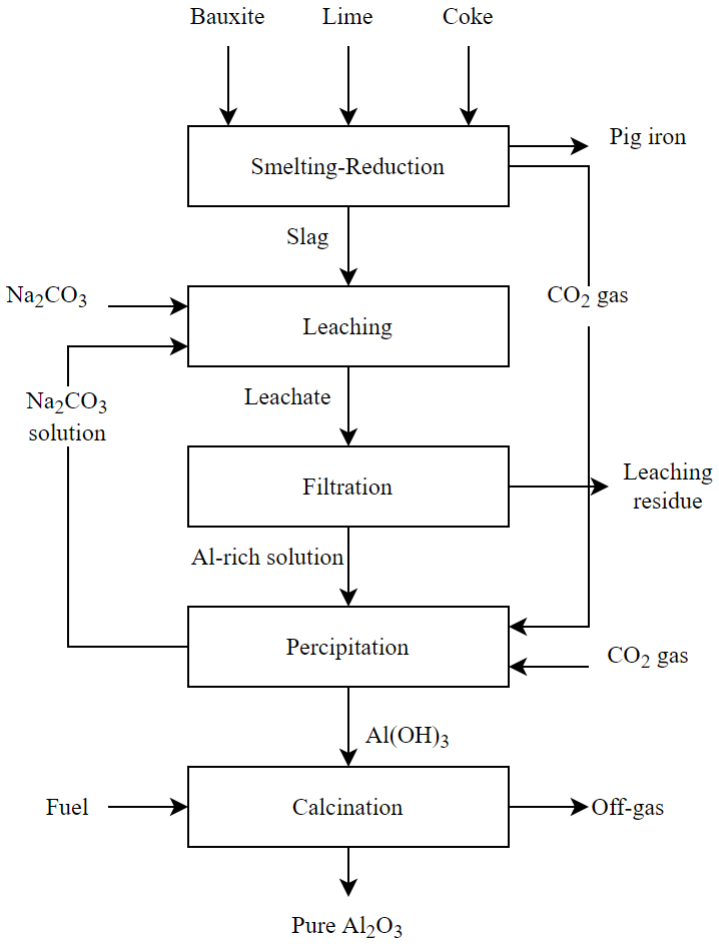

Figure 3. Flowsheet of the Pedersen process[20].

In addition to yielding more environment friendly products throughout the process, the Pedersen process has multiple advantages compared to the Bayer process. Besides being reused in the process, the sodium carbonate solution is much less alkaline than a pure sodium hydroxide solution. The leaching only requires about a third of the energy needed for heating, relative to the Bayer process, as well as avoiding the energy required to pressure the solution, as the process is performed at atmospheric pressure. The further precipitation demands a slightly higher temperature; however, the process only lasts for 6-10 hours, contrary to the Bayer process' 48-70 hours. The Pederson process requires approximately 10% higher energy consumption and about 40% higher raw materials costs than the Bayer process. On the contrary the Pederson process is more flexible and has 30-50% lower process costs per unit mass of alumina[14].

2.3 Hydrogen reduction of iron oxide

When dried BR is being used for iron extraction, the mixture of it with additives needs to be pelletized and sintered to handle and process it properly in practice. With addition of limestone, the mixture is pelletized and dried to remove excess moisture content. The dried pellets are then transferred to a muffle furnace for sintering. At 1200°C the iron particles start to agglomerate and volatile components such as hydroxides and carbonates evaporate, removing most of the remaining hydrogen and carbon content in the mixture. The evaporation of carbonates is shown in equation (5). The sintering process hardens the pellets, makes new mineral phases simultaneously as making the material porous. Minerals such as calcite ($CaCO_3$) with a melting point of 1339°C[21] release carbon dioxide and form new calcium phases such as calcium titanium oxide. Hematite also changes during sintering to brownmillerite ($Ca_2(Al,Fe^{3+})_2O_5$) . However, it is difficult to determine a specific melting point for many of these phases as they vary in composition and morphology. Porosity is important for minimizing the resistance to gas flow through the pellets, which is essential for the gaseous reduction[22].

$$CaCO_{3(s)} \rightarrow CaO_{(s)} + CO_{2(g)} \quad (5)$$

In bauxite, iron is mainly found in the oxide form called hematite. Throughout reduction of the iron oxide with hydrogen, it will form magnetite (Fe_3O_4) before further reduction to metallic iron[10]. Depending on the temperature at reduction, the process forms different intermediate oxides. When reduction is performed at temperatures above 570°C, it will form wüstite (FeO) before metallic iron (Fe) is formed[23]. This can be seen in figure 4, which shows the binary Fe-O system. The diagram displays the different iron and iron-oxides stability areas formed at various temperatures and oxygen concentrations.

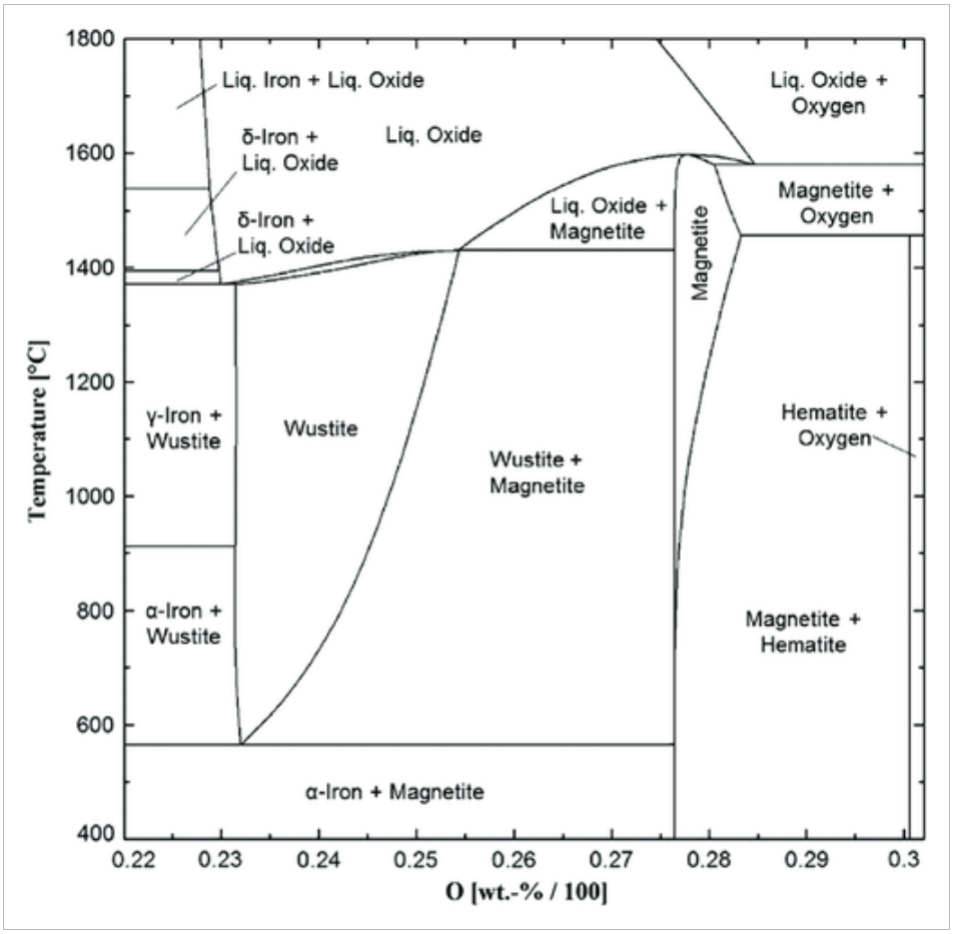

Figure 4. Binary Fe-O system in relation to temperature and oxygen share[23].

As seen, the formation of wüstite is limited to temperatures above 570°C and below 1400°C. For increasing the formation of metallic iron, the oxygen should be below 23.25% and above the initial wüstite formation temperature. The reactions at 700°C are shown in formula 6, 7, 8 and 9, with coherent change in enthalpy[24]. Total reduction with hydrogen is endothermic, which means that the process requires energy. This is supplied in practice via the introduction of reducing gas with higher temperature. The first reaction explains the formation of magnetite from hematite, while the two subsequent reactions explain the further reduction of magnetite. As seen, reduction of hematite can result in both metallic iron and wüstite. Furthermore, wüstite is reduced to metallic iron.

$$3Fe_2O_{3(s)} + H_{2(g)} \rightarrow 2Fe_3O_{4(s)} + H_2O_{(g)}, \qquad \Delta H_{700°C} = 5279\ kJ \tag{6}$$

$$Fe_3O_{4(s)} + 4H_{2(g)} \rightarrow 3Fe_{(s)} + 4H_2O_{(g)}\ , \qquad \Delta H_{700°C} = 95.551 kJ \tag{7}$$

$$Fe_3O_{4(s)} + H_{2(g)} \rightarrow 3FeO_{(s)} + H_2O_{(g)}, \qquad \Delta H_{700°C} = 52.086\ kJ \tag{8}$$

$$FeO_{(s)} + H_{2(g)} \rightarrow Fe_{(s)} + H_2O_{(g)}, \qquad \Delta H_{700°C} = 14.488\ kJ \tag{9}$$

Figure 5 shows a Baur-Glassner diagram, which describes the thermodynamics of iron oxide reduction when it is exposed to H_2-H_2O mixtures. The diagram displays the stability areas of different iron oxide phases. This is dependent on temperature and gas oxidation degree (GOD). Gas oxidation degree is defined as the ratio of oxidized gas components over the sum of oxidised and oxidizable gas components, $H_2O/(H_2+H_2O)$. The GOD value of a gas composition is a good indicator of its reduction force; a lower GOD represents a higher reduction force for the gas mixture. When reducing iron, it is preferable with a low GOD, as this increases the chances of forming metallic iron. As seen in the figure, the area in which metallic iron is stable, expands with increasing temperature. The same applies for wüstite. Accordingly, from a thermodynamic perspective, the temperature ought to be as high as possible[23].

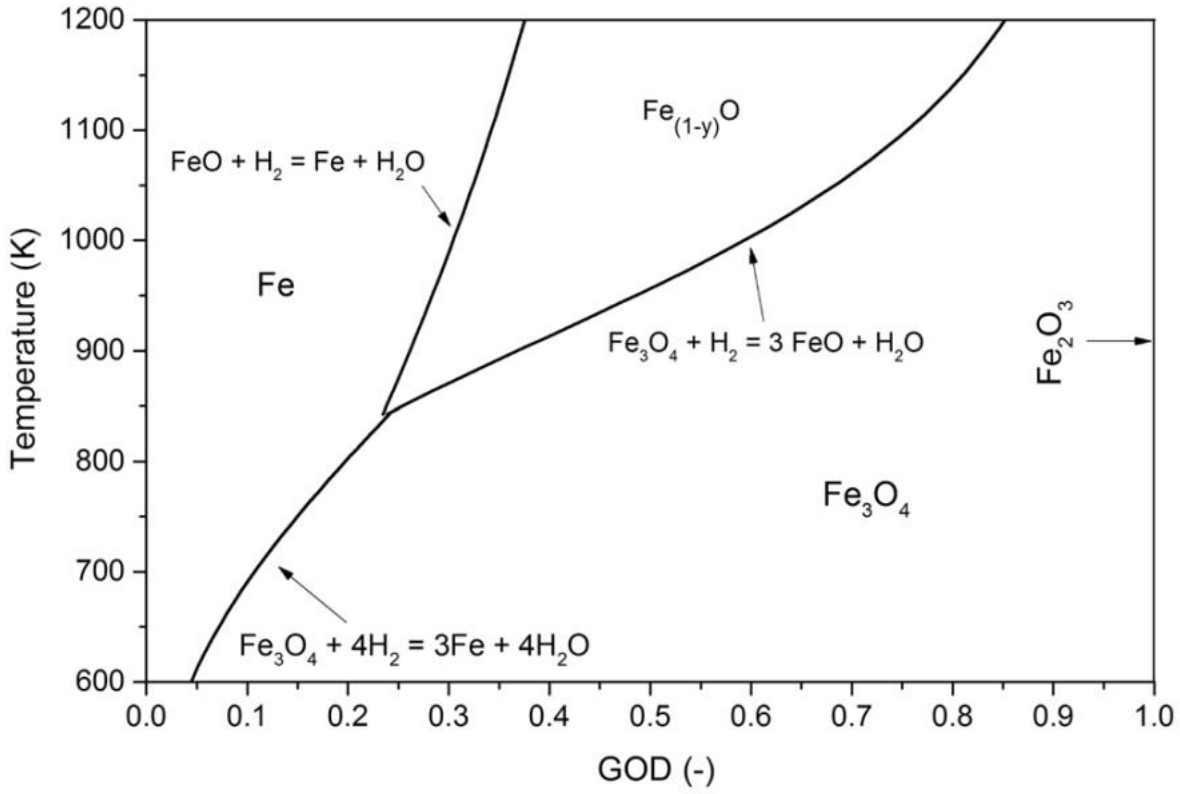

Figure 5. Baur-Glassner diagram for the Fe-O-H_2 system[23].

As mentioned, the figures indicates that a higher temperature results in increasing probability of forming metallic iron. From this statement it is possible to resonate that a hydrogen-reduction should be performed isothermal, to obtain a proper overview of how the target temperature affects the process rate, as well as the extent of reduction and the properties of the reduction product. On the other hand, starting reduction at lower temperature and possibly without proper flushing, could mean formation of less metallic iron. Hence, in literature the gaseous reduction of the ore is usually studied under isothermal conditions as they are heated and cooled under inert gas flow such as argon gas, as shown schematically in figure 6[24, 25].

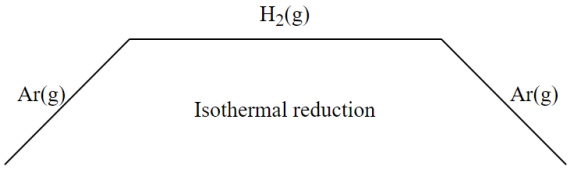

Figure 6. Schematic profile of isothermal reduction.

The reduction rate of iron oxide depends on which parameters are considered. The rate limiting step defines the slowest reaction step and decides the overall rate of the reduction reaction and the production rate. Temperature, diffusion of reducing gas, mass transfer, morphology and composition are all parameters which influence the overall speed of the reaction. An overview of different kinetic parameters that affect the reduction according to the unreacted shrinking core model as it is schematically shown in figure 7[26-28].

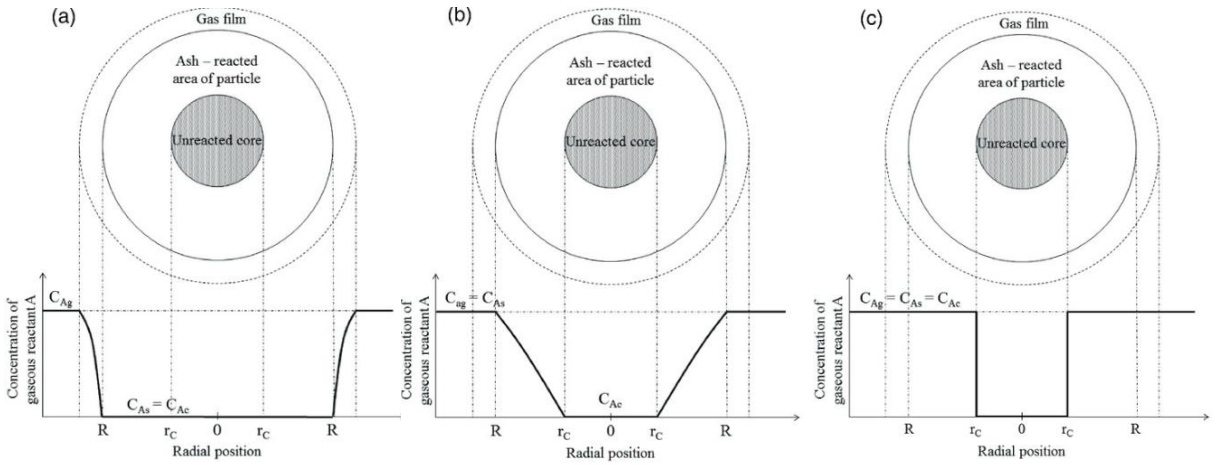

Figure 7. Rate-limiting steps. a) Gas diffusion from gas stream to the particle surface, b) pore diffusion across the product layer and c) chemical reaction at the reaction surface[26].

In figure 7, C_{Ag} represents the reactant gas concentration from the gas mixture, C_{As} the reaction surface concentration of the reactant gas, C_{Ac} is the equilibrium concentration of the reaction, R is the total radius of the particle and r_c the radius of the unreacted core.

As shown in figure 5, the reduction-rate of iron oxides increases with increasing temperature. If the chemical reaction is faster than the transportation of gaseous reactants and products, mass-transfer limits the reaction rate. This includes the diffusion of products such as adsorbed water vapour in the reacted ash layer through the pellets surface to the external gas stream. As opposed to this, since the chemical reaction with hydrogen is endothermic, it demands supplemental energy, thus being strongly temperature dependent. If the temperature is low, the chemical reaction operates slower than the mass transfer at the reaction site and the reduction rate is inhibited by temperature[26].

Higher temperatures in reduction of iron oxides using hydrogen are beneficial. As mentioned, the reaction is most likely rate-controlled by the chemical reaction itself at low temperatures. This is because the kinetics of the reaction such as diffusion of reactants and products slows down at low temperatures. Considering the thermodynamics, the reaction can perform at low temperatures by reduction of H_2 and CO, the latter being more stable at lower temperatures. However, the correlation between the temperatures and kinetics results in low gas utilization which in turn can, economically and environmentally speaking, be problematic from an industrial point of view. As seen in figure 8, the driving force for reduction of iron oxide using hydrogen increases with increasing temperature. The activation energy of the reduction decreases exponentially with increasing temperature, and the reaction is thermodynamically more stable at higher temperatures. Thus, making it mutually beneficial for both kinetics and thermodynamics to use high temperatures in the reduction[26, 28].

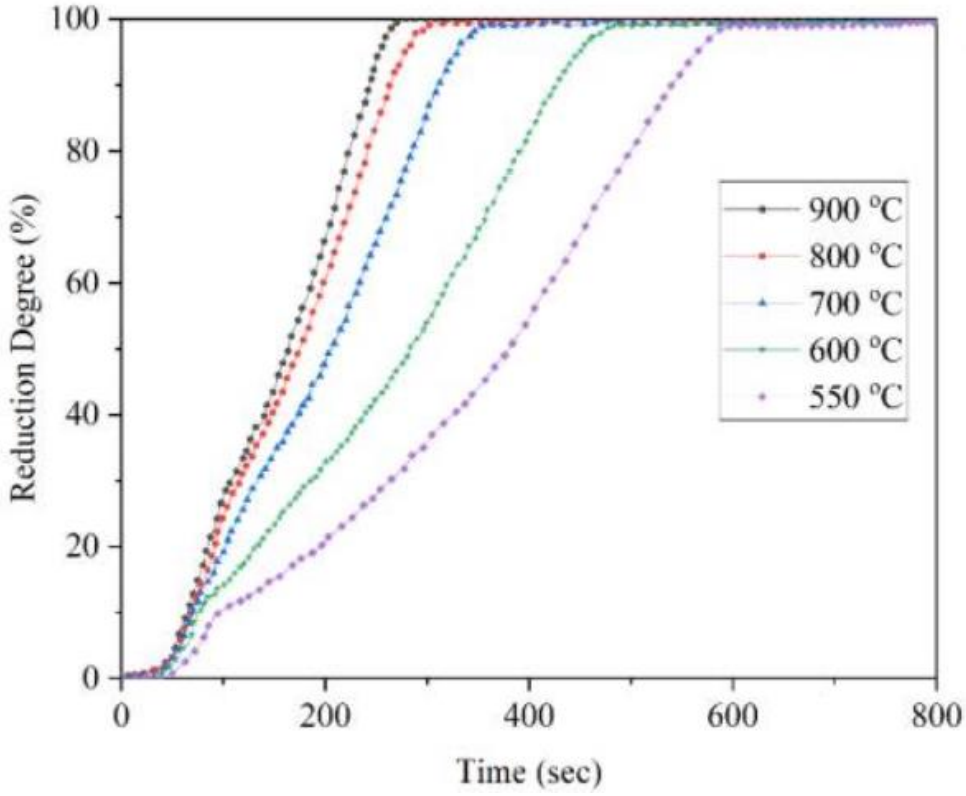

Figure 8. Hydrogen reduction experiments with increasing temperature[28].

Most importantly the reducing agent, in this case hydrogen, must reach the interface of the iron oxide particles. Hence, a porous structure of the pellets is important to ensure sufficient gas transfer. If the structure of the pellet change, and the pores diminishes, the mass transfer of gas becomes the rate-limiting step of the reduction. In this case the reduction can be described by the shrinking core model, as shown in figure 7 b). The reduction starts at the outer surface of the pellet, forming metallic iron whereas the inner oxides remain unreacted. The reductant then must diffuse through the newly formed ash layer to reduce the inner oxides, thus shrinking the core of unreacted oxides. The diffusion through the formed iron then becomes the rate limiting step in the reaction. If the parameters lead to the formation of a dense iron layer around the pellet, the gas is prevented direct access to the oxides, solid-state diffusion is dominant and the reduction rate is greatly inhibited[26, 27].

The particle size and mineral composition of the oxide can affect the rate of the reduction. As shown in figure 9, the reduction rate increases with decreasing pellets size. Smaller pellets can increase surface area of the reaction between hydrogen and iron oxide. However, to a certain point the size becomes rate-limiting. Studies of the reduction of three samples consisting of coarse powder, a sintered piece and nanopowder, show interesting results. Despite the powder samples having a greater surface area for the reduction, during the reduction experiments, they become compact and lose the porosity inhibiting diffusion of reactant thus the reduction. The sintered sample retained its porosity hence being the most reduced sample[28].

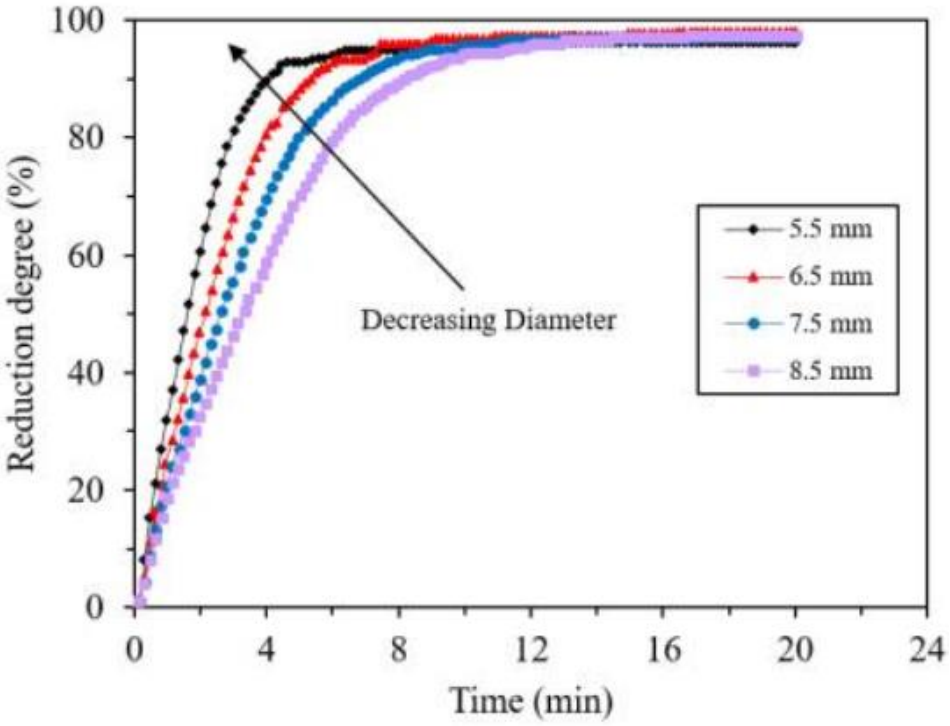

Figure 9. The effect of particle size on reduction degree[28].

The mineralogical composition of the samples is also of importance. Iron oxides usually occurs as hematite but can appear as magnetite. The structure of magnetite forms a denser shell which in turn counteracts the diffusion of hydrogen, making the reduction of this iron phase slower than hematite[28].

2.4 Leaching of calcium-aluminate slags

When extracting alumina from bauxite, the leachability is dependent on the bauxite ore. It is desirable with compositions such as gibbsite and boehmite, in contrary to diaspore[11]. When extracting alumina from bauxite via the Pedersen process, lime is used as flux in the smelting reduction step. This will interact with bauxite and results in the aluminium-containing slag, forming different types of calcium aluminate phases in the slag[20, 29]. Here it is desirable with compositions such as mayenite, and avoid the formation of the non-leachable calcium-aluminate phase gehlenite[10].

The reactions from leaching of various calcium-aluminate phases is yet to be determined, as the compound can be found in multiple stoichiometric relationships, although most of them result in the leaching of aluminum[11]. However, the major and desired phase is mayenite. The leaching of mayenite ($12CaO.7Al_2O_3$) is shown in equation 10[8, 20].

$$12CaO * 7Al_2O_{3(s)} + 12Na_2CO_{3(aq)} + 5H_2O_{(l)} \rightarrow 14NaAlO_{2(aq)} + 12CaCO_{3(s)} + 10NaOH_{(aq)} \quad (10)$$

There has been extended research on leaching of alumina from slags produced from BR[11, 12, 20, 29, 30]. It has been stated that addition of caustic soda is unnecessary, since it decreases aluminium dissolving, while dissolving further silicon[12]. However, recent studies shows that the optimal leaching conditions are 60 g/L Na_2CO_3[8], for one hour, at 60 ℃ for lab scale studies. This can partly be seen in figure 10, from

research done to optimize leaching conditions, in relation to time, temperature and concentration of sodium carbonate. Here the intensity of calcite increases with increasing time of leaching, although most of the alumina is obtained within 90 min. This correlates to the decrease of mayenite, indicating that further amounts of the calcium-aluminium phase have been dissolved[29]. This study found that the rate limiting step during leaching of the intersection, were the diffusion of reactant and product. Further discoveries substantiating the statement was that the activation energy of the leaching reaction was found to be relatively low. If the iron has been extracted beforehand, the residue after this step is grey mud and consists mainly of calcite and associated allotropes[8, 20].

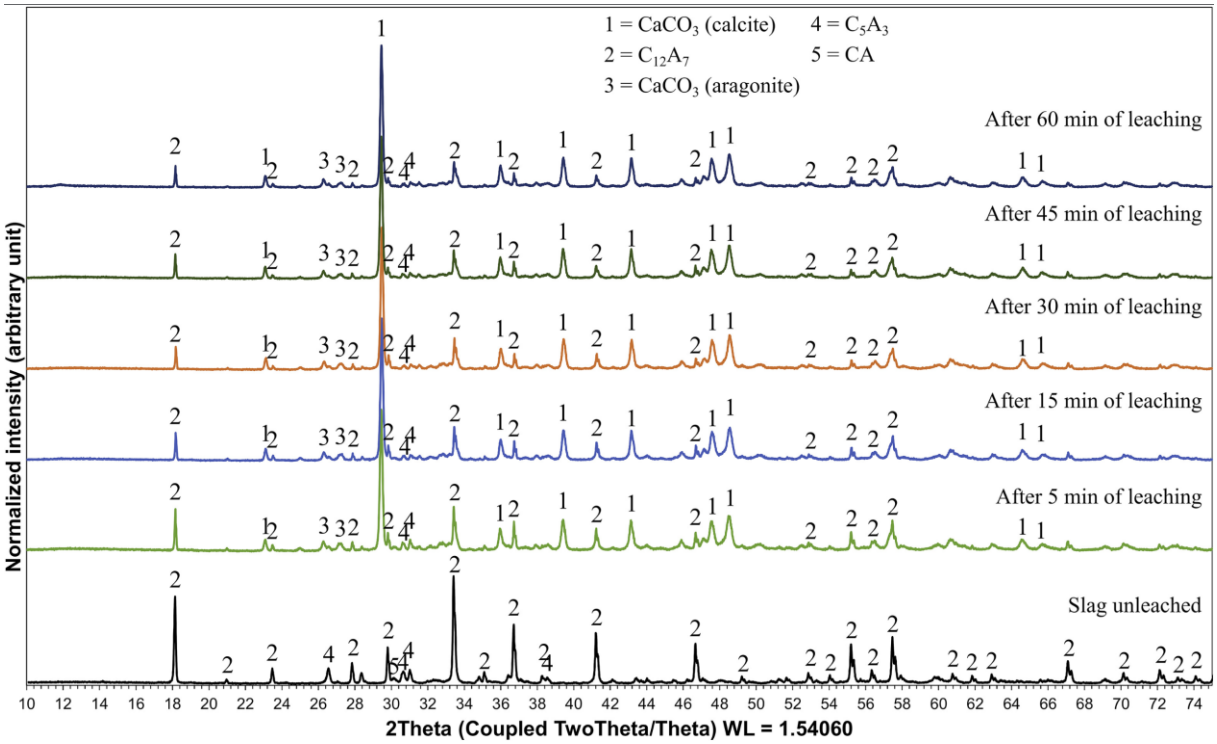

Figure 10. Normalized XRD patterns of the slag and leached slag within 5, 15, 30, 45 and 60 min at 45°C, 300 rpm of stirring rate, and 3 wt% Na_2CO_3 of solvent concentration[29].

After dissolving the calcium-aluminate phase, aluminium is precipitated as aluminium trihydroxides from the leachate. This is done through sparging the solution with carbon dioxide, as shown in formula 11. Lastly, the precipitate is calcined in a furnace and heated, resulting alumina. This is the same calcination process as shown in equation 4 in chapter 2.1[8].

$$2NaAlO_{2(aq)} + CO_{2(g)} + 3H_2O_{(l)} \rightarrow 2Al(OH)_{3(s)} + Na_2CO_{3(aq)} \quad (11)$$

3 Experimental procedures

The experimental procedure for this project includes many experimental steps. The BR used in the samples is from Mytilineos and the limestone ($CaCO_3$, product T802) is from Omya, the BR is produced in Greece while the limestone is produced in Norway. To simplify the experimental procedure, an overview can be viewed in the flowsheet in figure 11. The risk assessment for each experiment can be viewed in attachment I.

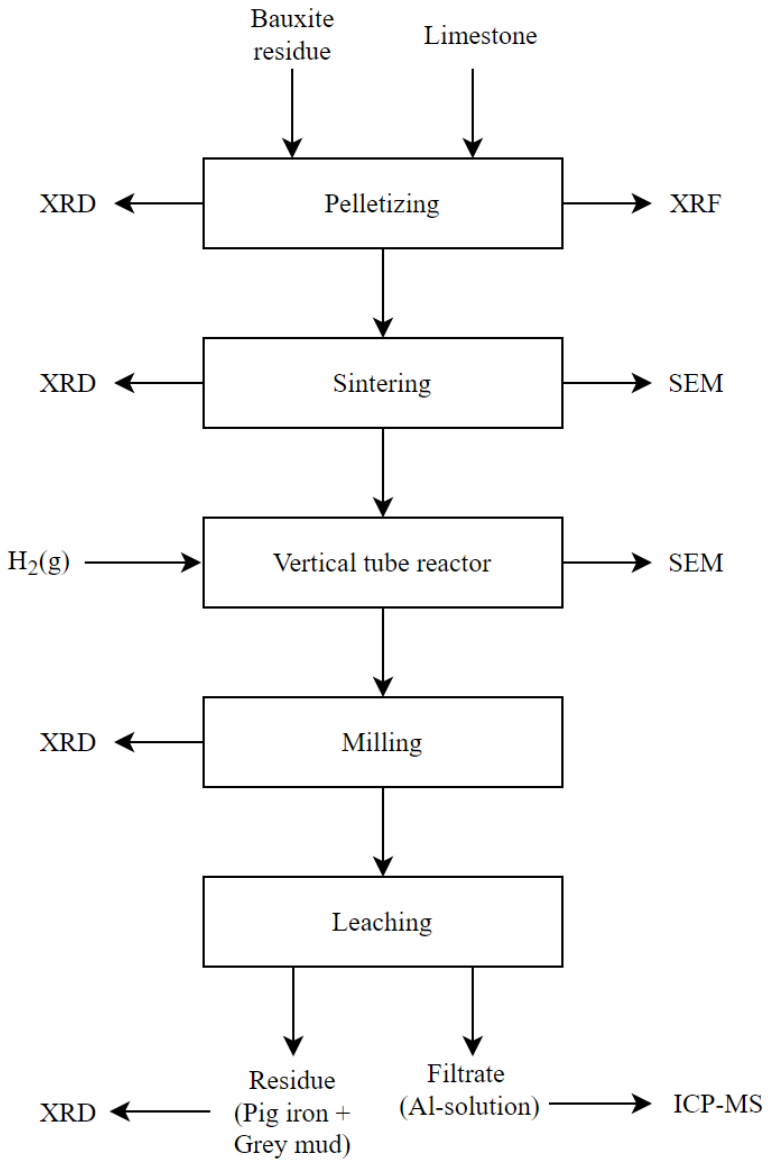

Figure 11. Flow chart of the experimental procedure followed in this project.

The chemical composition of the limestone and BR used to make pellets was characterized with XRF by SINTEF Norlab. The results are presented in Table 1.

Table 1: Chemical composition and sizing of limestone and BR used in the project

Materials	***Limestone [wt%]***	***Bauxite Residue [wt%]***
Al_2O_3	0.90	22.0
CaO	52.70	8.8
Fe	-	28.5
Fe_2O_3	0.15	-
K_2O	0.12	0.09
MgO	0.95	0.23
MnO	-	0.08
Na_2O	-	3.1
P	-	0.05
P_2O_5	0.01	-
S	-	0.38
SO_3	0.06	-
SiO_2	2.07	7.1
TiO_2	0.03	5.0
LOI	42.60	24.67
Mean size [µm]	2.57	-
median size [µm]	1.68	-

3.1 Pelletizing

BR and limestone were crushed in a mortar and milled separately for 1 min in a vibratory ring mill (Retsch RS 200). When all the particles were milled, BR powder (1000 g) and limestone powder (640 g) were mixed for two hours in a turbulent mixer (WAB Turbula Mixer). A home-made disk pelletizer, as shown in figure 12, was used for making pellets. Parts of the mixed powder were applied to the blender and sprayed with water until it formed properly sized pellets. The pellets were then extracted from the pelletizer and sieved. Pellets below the size of 4 mm were returned to the pelletizer to grow.

After pelletizing the pellets were left in a heating oven (VWR DRY-Line® Prime) at 60°C for 24 hours.

Figure 12. Home-made disk pelletizer.

3.2 Sintering

Before sintering, the pellets were sieved to be in the range of 4-8 mm. The pellets (70-90 g) were distributed in two alumina boats and sintered in a Nabertherm N17/HR Muffle Furnace. The heating rate was 20°C/min to the target temperature of 1200°C and sintered for two hours. After sintering, the pellets were left in the furnace to cool down to room temperature for 20 hours. The measured weight prior to sintering is shown in table 2.

Table 2: Weight of dried pellets before sintering

Sintering	1	2	3	4	5	6
Weight [g]	82.6	84.2	85.6	76.0	88.7	78.6

3.3 Hydrogen reduction

The reduction experiments were done in a Entech-18 Furnace. A schematic figure of the furnace is shown in figure 13. The furnace is a vertical tube reactor, built for this type of experiment. It consists of an alumina tube (1), surrounded by heating elements and isolation. A cooling element (2) is twined around the outer layer of the furnace. The sample for reduction is located in a demountable molybdenum crucible (3) inside the alumina tube. There are two gas inlets, where one leads into the alumina tube (4), while the other goes directly into the crucible (5). The outlet is at the top of the alumina tube (6). There are three thermocouples measuring temperature throughout the experiment. One is touching the bottom of the crucible (7), while another touches the pellets from the top (8). The last temperature measurement is from inside the wall of the furnace.

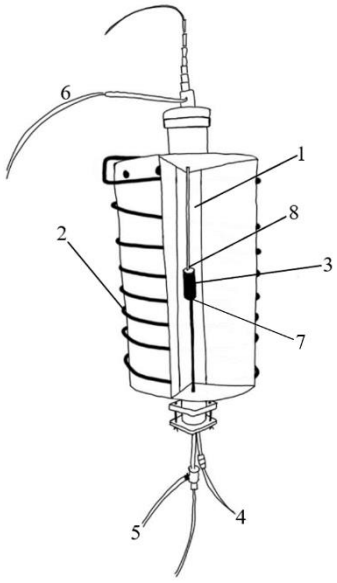

Figure 13. Schematic explanation of the Entech-18 furnace.

First, the furnace was dismantled and cleaned. A molybdenum crucible with a gas inlet in the bottom was used to hold the pellets, while the introduced hydrogen gas moved upwards through the pellet bed. The crucible was removed from the bottom, rubbed with sandpaper, and weighed, before the sample (25 g of sintered pellets) was added to the crucible, as shown in figure 14. The crucible was then mounted back into the furnace.

After the furnace were assembled and all the gas inlets were tightened, He gas flow was introduced through the system. A He-tester were used to check each connection for gas leakages. When the system was cleared of leaks, the flushing with inert gases were started. Prior to hydrogen introduction, flushing was done with Ar (0.05 NL/min) and He (0.05 NL/min) for 24 hours to purge all reactive gases (i.e. oxygen).

The next morning, the furnace was turned on and the temperature programme set. The heating rate was 10°C/min to the target temperature of 1032°C, 1132°C or 1232°C, hydrogen was then introduced, and the reduction lasted for 30, 60, 120 or 150 minutes. The temperature programmes were set to 32°C above target temperature because of difference between wall temperature and the temperature within the sample. Table 3 shows each sample's experimental conditions and weight.

Figure 14. Molybdenum crucible filled with a sintered sample.

Table 3: Experimental conditions during hydrogen reduction and initial weight of each sample

Temperature [℃]	1000				1100				1200			
Hydrogen gas flow	0.2 NL/min											
Time [h]	0.5	1	2	2.5	0.5	1	2	2.5	0.5	1	2	2.5
Reduction sample	1	2	3	4	5	6	7	8	9	10	11	12
Sample weight [g]	25.0	25.2	25.1	25.1	25.0	25.1	–	25.7	24.9	–	–	24.1

3.4 Characterization of samples

Dried pellets, sintered pellets and reduced pellets were characterized both by XRD and SEM. The samples were named in chronological order to simplify the process of identifying them in the report. XRF was done on the dried and the sintered pellets, and the leached samples were analysed by ICP-MS. All the characterization methods were used interchangeably when analysing. XRF results were used for determining elements to detect on EDS with SEM, while the latter were used for determining possible compositions present in XRD analysis.

3.4.1 SEM sample preparation and characterization

3-4 pellets of each reduction sample and 3-4 pellets of sintered pellets were put in separate plastic casting moulds. EpoFix Resin (100 g) were weighed and transferred to a plastic cup. EpoFix Hardener (12 g) were weighed and added to the cup. The mixture was stirred for approximately one minute, until the resin was completely mixed with the hardener. It was then carefully poured into the moulds. Small paper labels were submerged in the epoxy to mark the samples and they were left to dry for twelve hours.

Figure 15. A gold-coated sample of reduced pellets.

The samples were removed from the casting moulds and placed in an automatic grinding and polishing machine (Saphir 550). For one minute the samples were rubbed with sandpaper (grit size: 320, 600, 800, 1200, 2000 and 4000). Between each rubbing the samples were washed in water and rinsed in an ultra-sonic bath (WVR USC 300T), in a solution of isopropanol and water, for three minutes. The final step was polishing with a diamond coated cloth which were done for 30 seconds. All samples were then rinsed in the ultra-sonic bath in methanol, and then dried with compressed air.

Before coating, all samples were dried in vacuum two times each for 15 minutes. The samples were then coated in gold with a sputter coater (Quorom SC7620) for 45 seconds. Reduction 7 were coated in additional 45 seconds. Copper tape was fitted from the top to the bottom of the sample. A sample ready for SEM is shown in figure 15.

Figure 16. Tabletop SEM.

All samples were analysed with different magnifications with SEI and BEI imaging. The SEM (Jeol Tabletop) can be viewed in figure 16. The analysis for each sample consisted of parameters such as porosity, overall structure, phase overview, point analysis and X-ray mapping. Table 4 displays the different magnifications used for each analysis.

Table 4: Systematic analysis of characterization with SEM using SEI and BEI imaging

Imaging	***Magnification***
SEI	20x, 500x
BEI	500x, 1000x
EDS: point analysis	4000x
EDS: x-ray mapping	4000x

3.4.2 XRD sample preparation and characterization

XRD analysis was carried out on all samples; dried pellets, sintered pellets and all of the reduction samples. First, the samples (5 grams each) were milled (30 sec, 800 rpm) to fine powder in a ring mill. In addition to milling, the samples were further crushed with a mortar before analysing.

Small amounts of sample were put on a sample holder and a drop of ethanol was added. After drying they were put into the XRD machine (Rigaku MiniFlex 600), viewed in figure 17, and analysed. The analysis parameters of the XRD are shown in table 5.

Figure 17. The XRD machine used for characterization.

Table 5: Program for XRD analysis

Start [deg]	***Stop [deg]***	***Step [deg]***	***Speed [deg/min]***	***Voltage [kV]***	***Current [mA]***
10.00	120.00	0.02	1.0	40	15
Scan duration		01h, 55 min, 13 sec			

3.4.3 XRF sample preparation

Both the dried (6 g) and sintered pellet (6 g) were milled in a ring mill (30 sec, 800 rpm), before they were sent to SINTEF for XRF characterization.

3.5 Magnetic separation of iron

After the reduction, the produced iron particles in the milled reduced pellets were separated magnetically. The dried samples (5 g) were measured and placed on a watch glass. A stick magnet was placed on a filtrate paper, before being held above the sample. Iron attached to the magnet through the paper were then weighed. The same procedure was done with other magnets, and with different heights between the sample and the filter paper with the magnet.

3.6 Leaching of milled samples

Powder of Na_2CO_3 (60 g) was weighed out and transferred to a volumetric flask (2 L). De-ionized water (100 mL) was added, and the flask were shaken. When the chemicals were dissolved, the flask was filled to the mark with de-ionized water and shaken until the solution were homogenous.

A hot plate with a magnet stirrer and attached thermometer was used to heat a water bath to 60 ℃. A beaker (200 mL) was filled with the Na_2CO_3 solution (100 mL) and placed in the water bath. A magnet was added, and a parafilm put over as a lid to minimize water loss. Figure 18 shows the set-up. When the solution reached 60 ℃, the reduced sample powder (5.0 g) was added, as shown in table 6. The sample was leached for one hour.

Figure 18. Leaching set-up.

Table 6: Initial weight of samples before leaching

Sample nr.	Reduction 2	Reduction 4	Reduction 6	Reduction 8
Weight [g]	5.0107	5.0052	5.0037	5.0039

After leaching, the mixture was filtered with a vacuum set-up until all the liquid had passed. The pore size of the filter used was 11 µm. The filter papers with magnet and filter cake were dried in a heating oven (65 ℃) for 24 hours before weighing. The filtrate for each sample was collected in containers, from which some of the filtrates of each sample (3 mL) were sent to SINTEF for ICP-MS analysis. In addition to the final leachate samples, a blank sample of the Na_2CO_3-solution were taken and sent for ICP-MS as well. The dried filter cakes were collected in containers to preform XRD-analysis.

4 Results

The results of the process are described with tables and figures, whereas additional results can be found in the appendix. Formulas and equations are specified, as opposed to specific examples of calculations.

4.1 Composition analysis (XRF)

The XRF analysis of the dried and sintered pellets are shown in table 7. The original XRF analysis can be found in attachment II. Since iron was registered as Fe, the wt% was normalized and converted to hematite using the chemical relationship between the two, as shown in equation 12. The values were further normalized again, to find the correct wt% in a sintered sample.

$$m_{Fe} * \frac{M_{Fe_2O_3}}{2 * M_{Fe}} = m_{Fe_2O_3} \quad (12)$$

Where m_{Fe} denotes the wt% Fe, and m_{Fe2O3} denotes the wt% of Fe_2O_3, obtained from the XRF in attachment II. M_{Fe} denotes the atomic weight of iron (55.85 g/mol) and M_{Fe2O3} denotes the molecular weight of hematite (159.7 g/mol)[21].

Table 7: Normalized XRF analysis of dried and sintered pellets

Materials	***Dried pellets [wt%]***	***Sintered pellets [wt%]***
Al_2O_3	14.60	18.15
CaO	27.70	34.34
Cr_2O_3	0.11	-
Fe_2O_3	27.07	33.12
K_2O	0.09	0.05
MgO	0.48	0.62
MnO	0.09	0.10
Na_2O	2.09	2.05
P	0.03	0.04
S	0.23	0.31
SiO_2	5.42	6.77
SrO	0.09	0.10
TiO_2	3.25	4.10
V_2O_5	0.09	0.10
ZrO_2	0.11	0.10
LOI 950	18.56	0.07

4.2 Sintering

In the first sintering experiment, seven alumina boats were placed inside the muffle furnace. These batches were smelted when the sintering was done, as shown in figure 19. Figure 14 in chapter 3.3 displays correctly sintered pellets. These smelted pellets were not used further, nor were any mass data collected from them. Before and after the next sintering experiments, the weight of each batch was measured to calculate the mass loss in grams and weight percentage. Only two alumina boats with pellets were sintered at the same time in the later experiments.

Figure 19. The smelted sintered pellets.

Considering the obtained XRF results of the pellets, sent from SINTEF Norlab, theoretical mass loss was calculated and compared to the actual mass loss. The calculations and measurements are displayed in table 8 and the XRF results can be viewed in chapter 4.1.

Table 8: Weight before and after sintering, mass loss and averages

Weight before [g]	***Weight after [g]***	***Mass loss [g]***	***Mass loss [%]***	***Theoretical mass loss [g]***	***Actual:theoretical mass loss [%]***
82.6	63.8	18.8	22.7	17.9	104.8
84.2	65.2	19.0	22.5	18.3	103.9
85.6	66.6	19.1	22.3	18.6	102.7
76.0	58.9	17.0	22.5	16.5	103.0
88.7	68.7	20.0	22.5	19.3	103.8
78.5	60.7	17.8	22.7	17.1	104.4
	Average:	18.6	22.5	17.9	103.8

When calculating the theoretical mass loss, the chemical relation from formula 5 is used, as well as the XRF. The molecular weight used is 56.1 g/mol for CaO and 44.0 g/mol for CO_2[21]. The calculation of theoretical mass loss is shown in formula 13.

$$\frac{\frac{wt\%CaO}{100} * m_{sample}}{M_{CaO}} * M_{CO_2} = m_{CO_2} \quad (13)$$

Where the wt% CaO is wt% from XRF of the dried sample and m_{sample} denotes the initial sample weight prior to sintering. M_{CaO} denotes the molecular weight of lime and M_{CO2} denotes the molecular weight of carbon dioxide.

4.3 Reduction experiments

The program for reducing the pellets was followed, although the heating and cooling rate varied slightly each time. The heating and cooling graph of reduction 1, 5 and 9 is shown in figure 20.

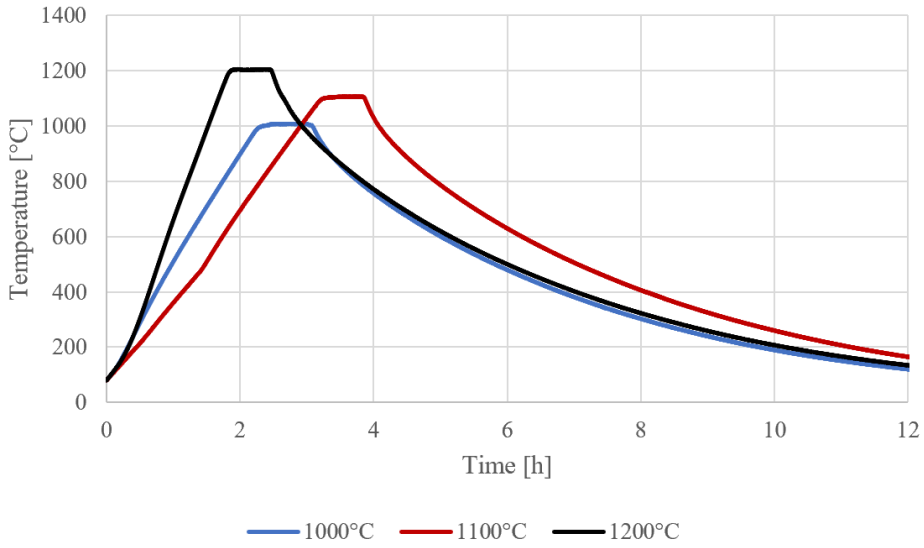

Figure 20. Heating and cooling graphs of reduction 1, 5 and 8 (0.5h).

Only nine of the twelve planned reduction experiments were preformed, because the vertical tube reactor malfunctioned, and it took several weeks to fix it. Thus, reduction experiment 7, 10 and 11 were not preformed. Once the reactor was repaired, reduction 9 and 12 were done. Both reductions at 1200°C were completely melted. The crucibles had to be cut in half to recover the sample within. Cross section of the melted samples and of the crucibles is shown in figure 21.

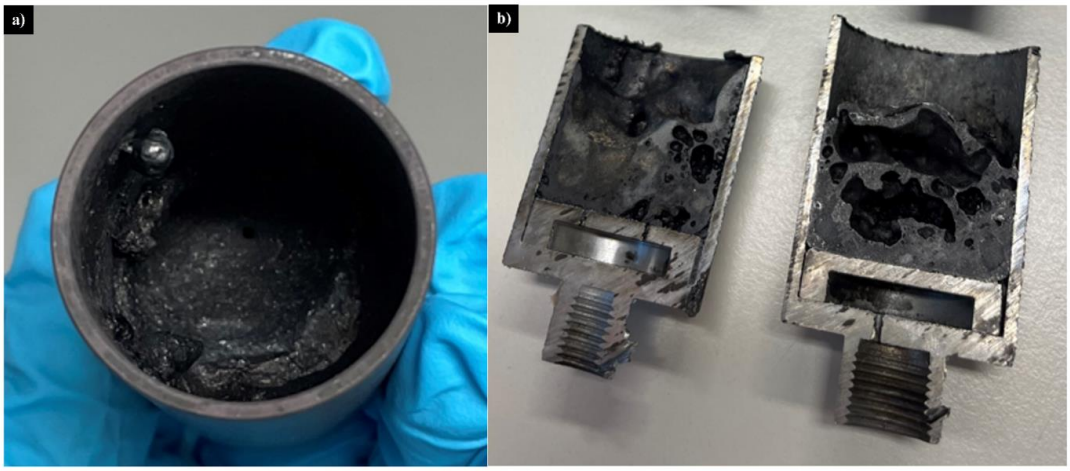

Figure 21. Images of the two reductions which melted. a) shows reduction experiment 9 and b) shows reduction experiment 9 (left) and reduction experiment 12 (right).

Similarly, to the sintering experiments, the masses of the pellets was measured before and after each experiment. The data was compared to theoretic values of mass loss, calculated from the XRF of the sintered pellets. The comparison of the theoretic and initial mass values was then calculated as the actual yield of metallic iron in the reduced samples. The data is displayed in table 9. To enable comparison of different reductions, and examine their kinetics, a fraction conversion from hematite to metallic iron is calculated from formula 14[25].

$$x = \frac{\Delta m}{\left(\frac{wt\%Fe_2O_3}{100}\right)*\left(\frac{3*M_O}{M_{Fe_2O_3}}\right)*m_i} \quad (14)$$

Where Δm denotes the mass difference after reduction, m_i denotes the initial sample mass and $wt\%Fe_2O_3$ denotes the wt% of hematite in the initial sample from table 9. M_O denotes the atomic weight of oxygen (16.0 g/mol), and M_{Fe2O3} denotes the molecule weight of hematite (159.7 g/mol)[21].

Table 9: Reduction sample mass, mass loss, theoretical mass loss and yield Fe

Reduction No.	***Sample mass after reduction [g]***	***Mass loss [g]***	***Mass loss [%]***	***Theoretical mass loss [g]***	***Fe yield [%]***
1	23.59	1.44	5.75	2.49	57.8
2	23.37	1.78	7.07	2.50	71.1
3	23.18	1.92	7.65	2.50	76.8
4	23.00	2.07	8.27	2.50	82.9
5	23.91	1.09	4.34	2.49	43.8
6	23.60	1.46	5.84	2.50	58.5
8	23.56	1.8	7.02	2.55	70.5
9	23.34	0.73	3.04	2.40	30.5

Reduction sample 4 (2.5 h, 1000°C) has the least difference between actual mass loss and theoretical mass loss at 0.42 g and a yield of 82.9%, and reduction sample 9 (0.5 h, 1200°C) has the highest difference, with 1.66 g and a yield of 30.5%.

4.4 Microstructural analysis (SEM)

The sintered pellets and reduced pellets from sample 1-6 and 8 were analysed with SEM. As the samples in reduction 9 and 12 were smelted, SEM was not performed on them. To show the topography and indicate composition and phases of each sample, SEI, BEI and x-ray mapping are presented in images in chapter 4.4.1 and 4.4.2. Point analyses for each sample are shown in chapter 4.4.3.

4.4.1 SEI and BEI

Figure 22-23 shows SEI and BEI in different magnifications (20x, 1000x). Additional magnifications can be viewed in appendix III. The figures are comprised by eight different images marked a) to h); a) reduced sample, b) reduction sample 1, c) reduction sample 2, d) reduction sample 3, e) reduction sample 4, f) reduction sample 5, g) reduction sample 6 and h) reduction sample 8.

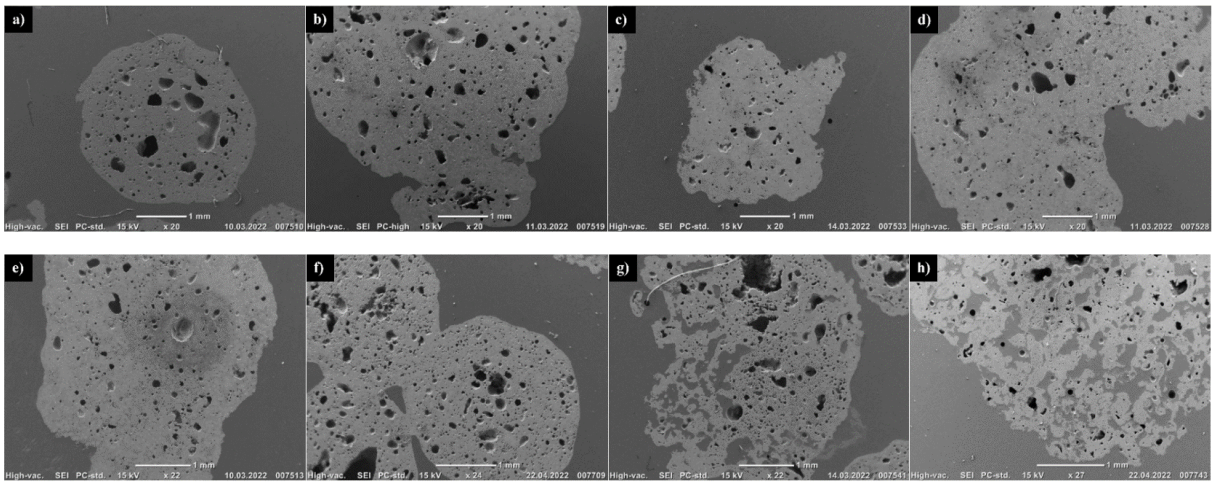

Figure 22. SEM SEI magnified 20x of sintered pellet and reduction sample 1-6 and 8.

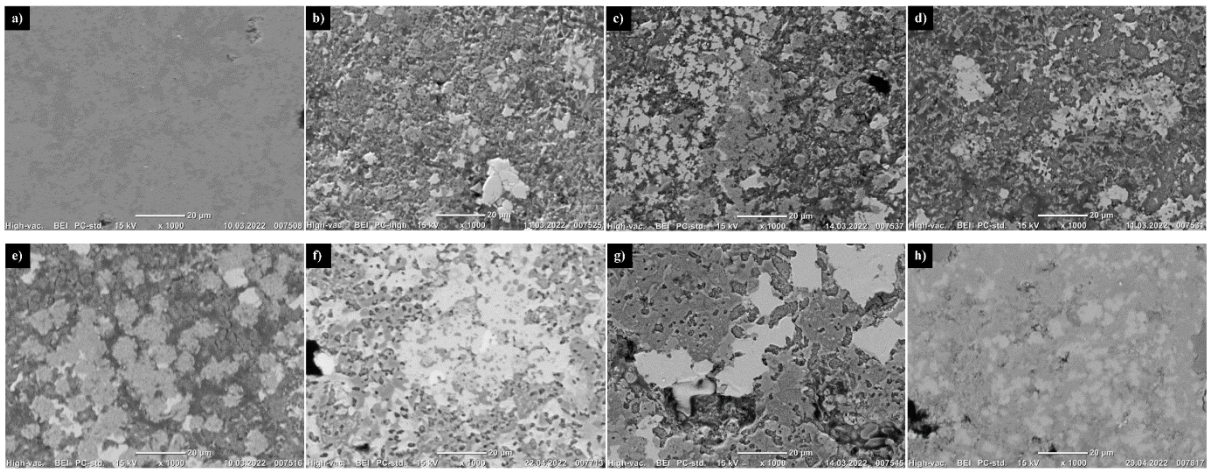

Figure 23. SEM BEI magnified 1000x of sintered pellet and reduction sample 1-6 and 8.

The images show the topography, morphology, and phase-composition of the sample with SEI and BEI. The phases reduced at 1000°C show porous morphology with separated phases. Contrary to this, the phases reduced at 1100°C is more melted together. Heavier elements, such as iron, reside in phases with lighter colours, whereas elements with lower masses is located in darker phases.

4.4.2 X-ray mapping (EDS)

Eight main elements in the pellets are mapped out in the same image of each sample magnified 4000x. The elements are a) Na, b) O, c) Si, d) Mg, e) Ti, f) Ca, g) Al and h) Fe. Each sample is presented with its respective x-ray images and an image of the area on the sample. Starting with sintered pellets and reduction 1 in figure 24-26, the reduction 2 and 3 in figure 27-29, reduction 4 and 5 in figure 30-32 and reduction 6 and 8 in figure 33-35.

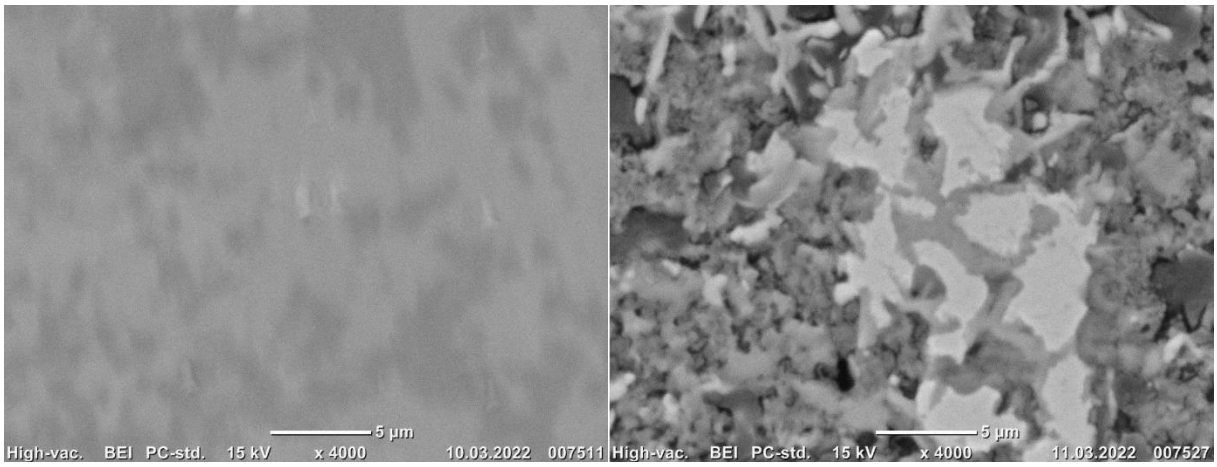

Figure 24. Sintered (left) and reduction 1 (right).

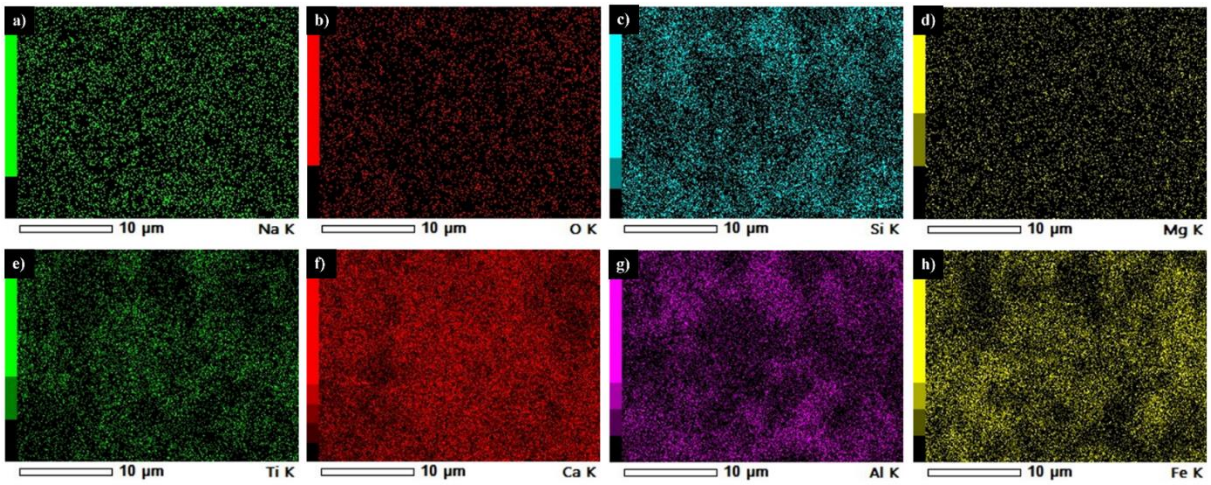

Figure 25. X-ray mapping of the sintered pellets.

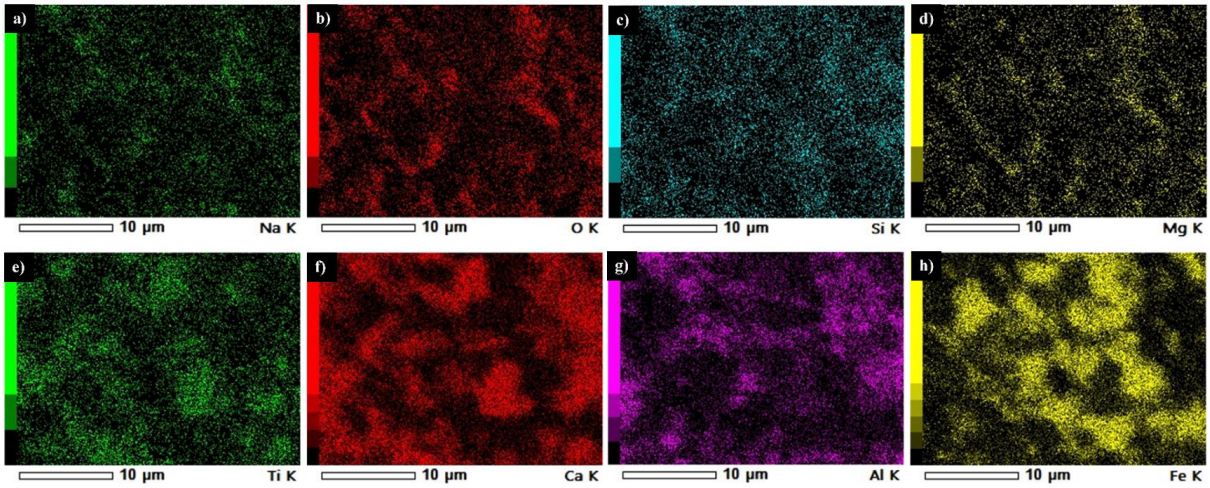

Figure 26. X-ray mapping of reduction sample 1 (1000°C, 0.5 h).

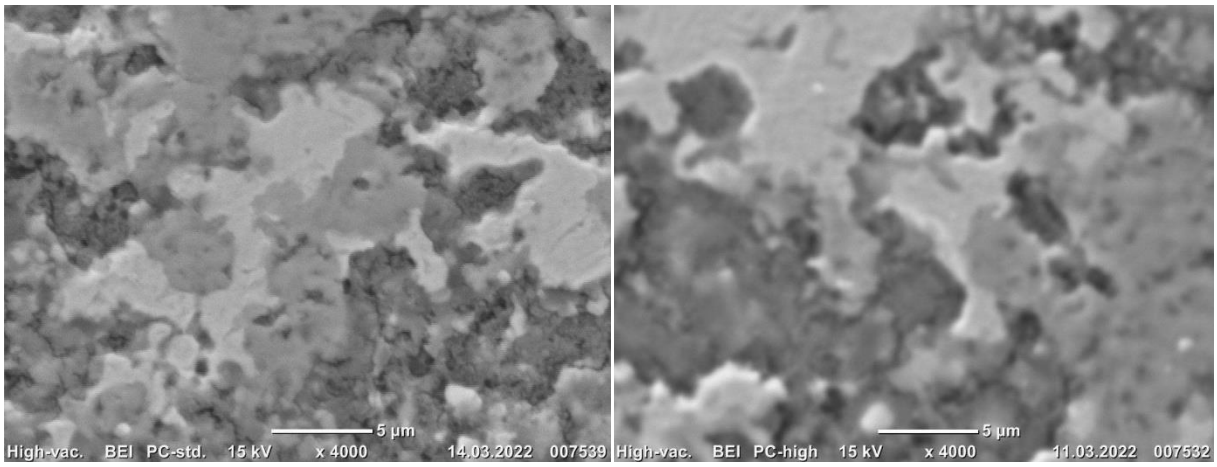

Figure 27. Reduction 2 (left) and reduction 3 (right)

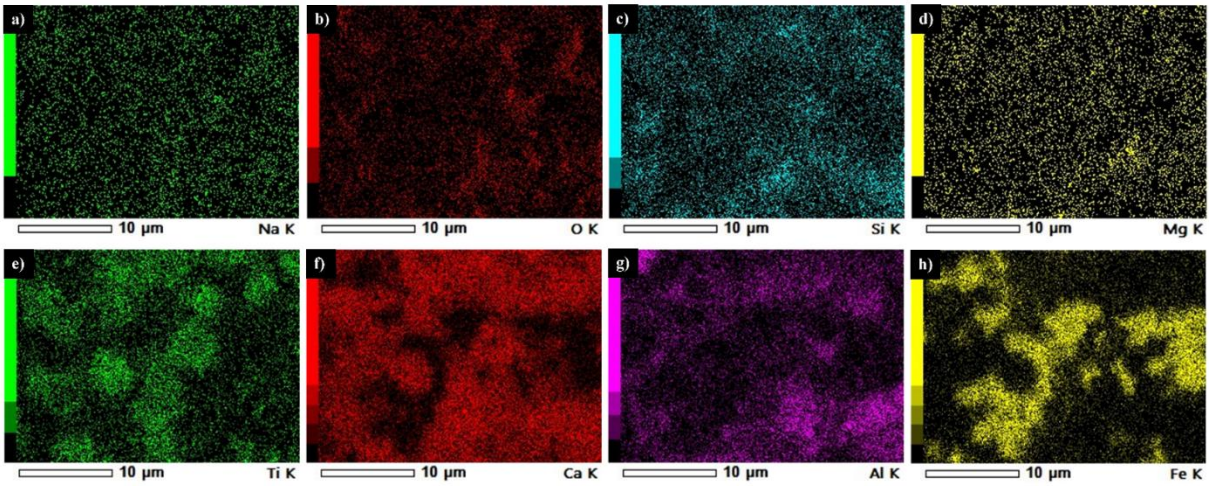

Figure 28. X-ray mapping of reduction sample 2 (1000°C, 1h).

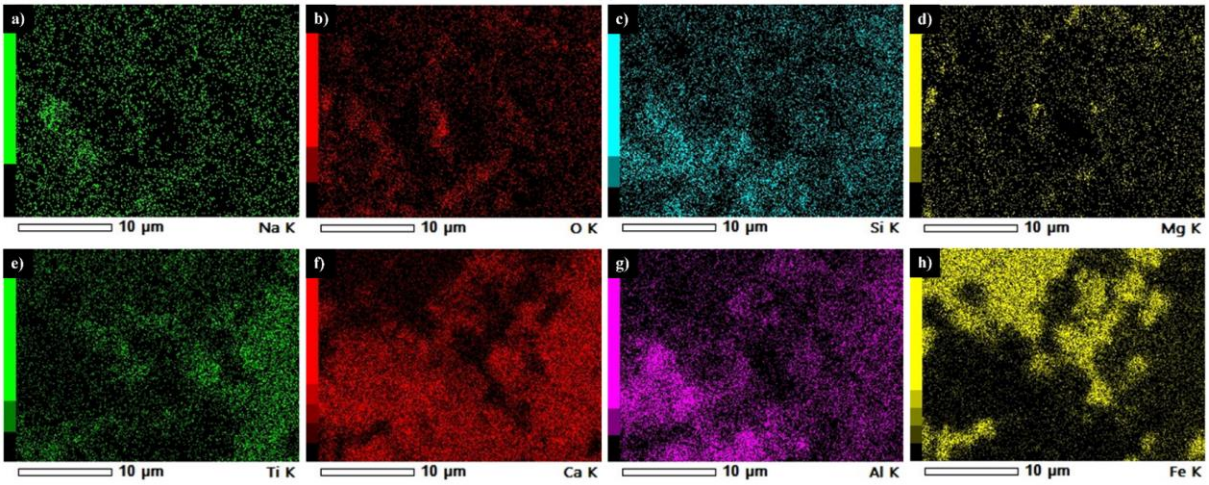

Figure 29. X-ray mapping of reduction sample 3 (1000°C, 2h).

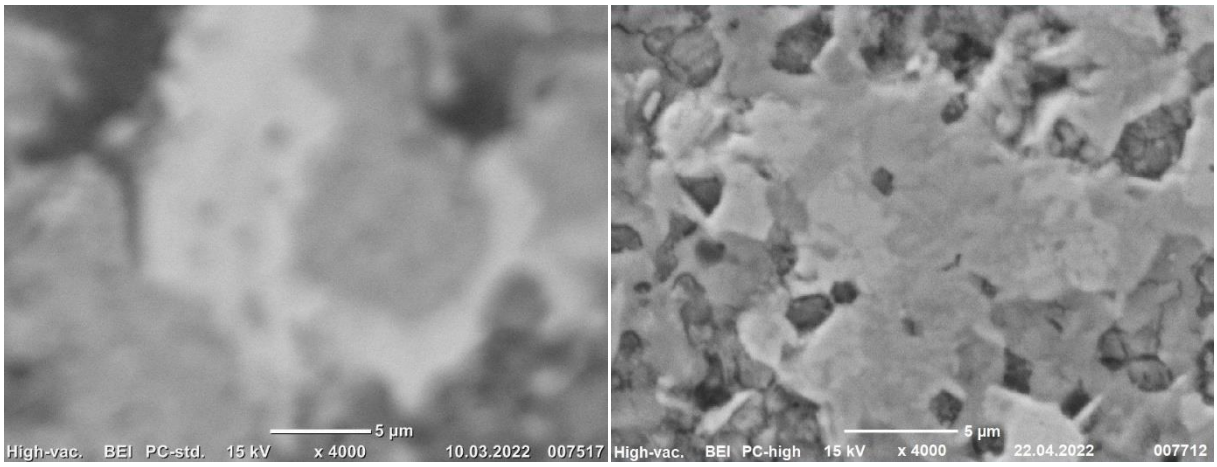

Figure 30. Reduction 4 (left) and reduction 5 (right).

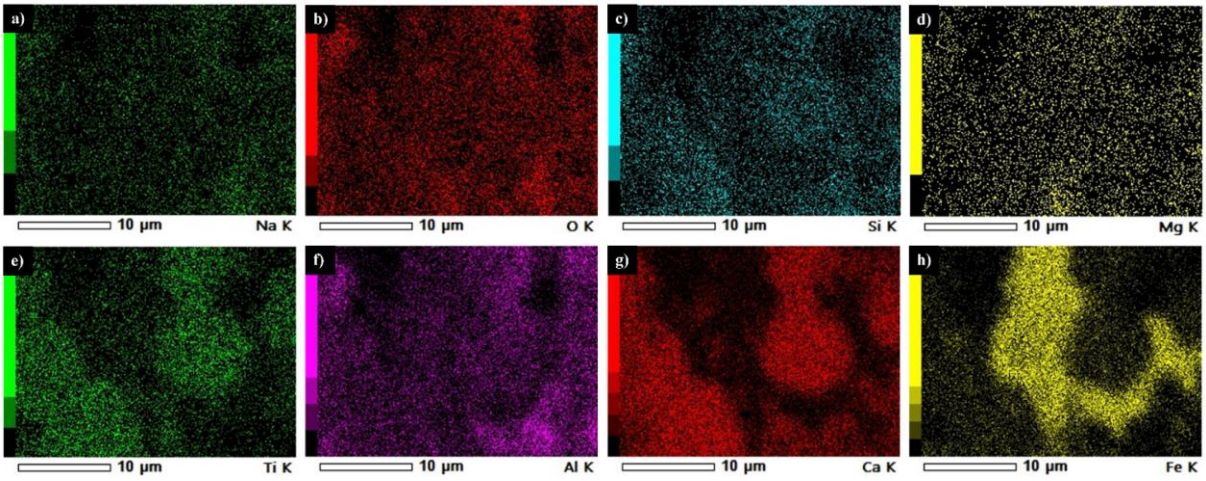

Figure 31. X-ray mapping of reduction sample 4 (1000°C, 2.5h).

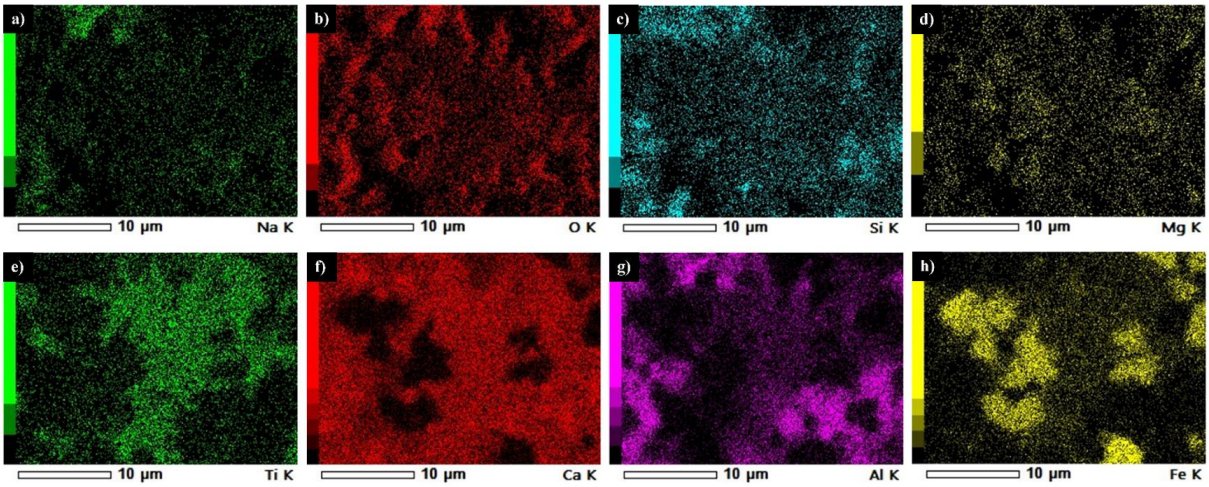

Figure 32. X-ray mapping of reduction sample 5 (1100°C, 0.5 h).

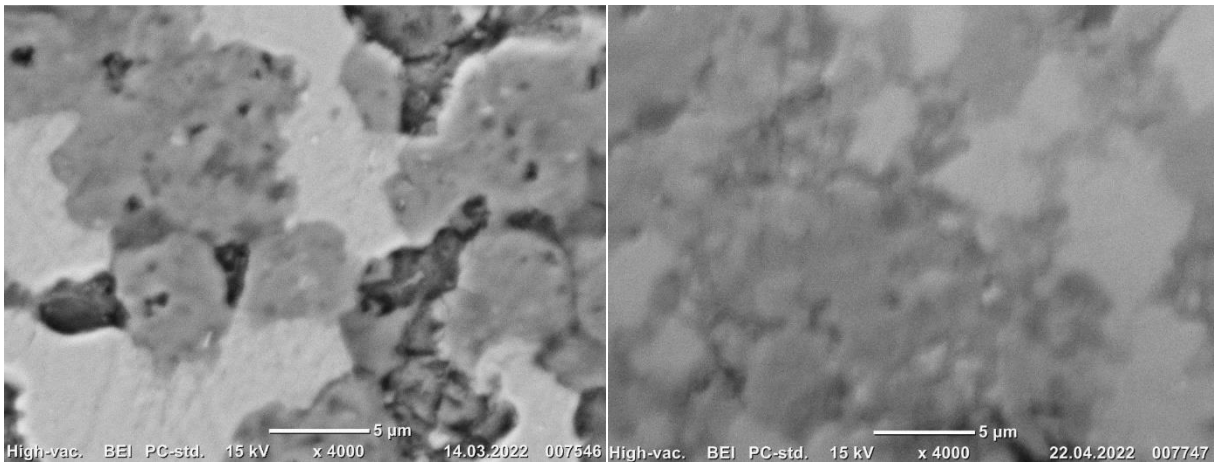

Figure 33. Reduction 6 (left) and reduction 8 (right).

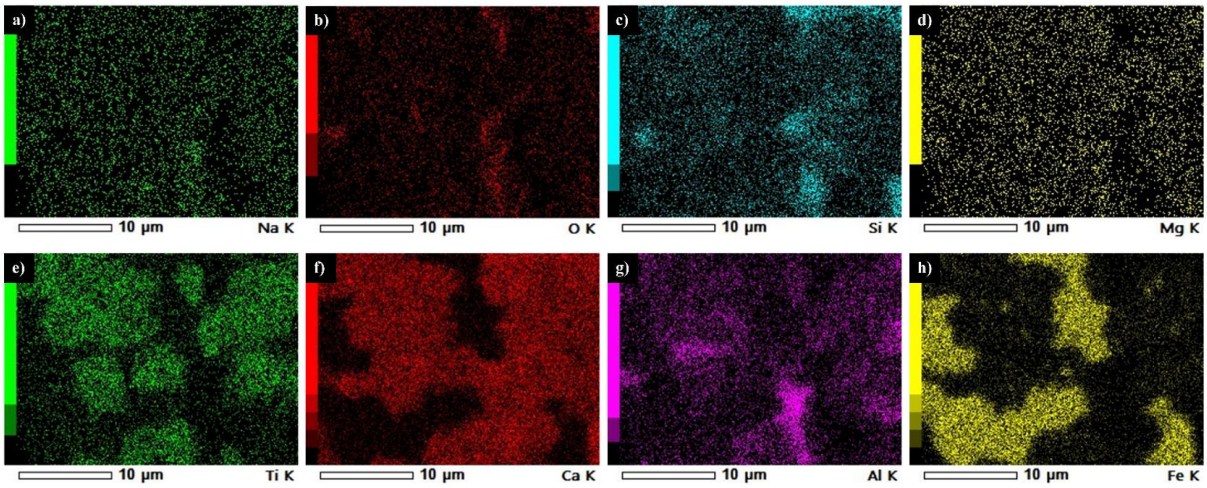

Figure 34. X-ray mapping of reduction sample 6 (1100°C, 1 h).

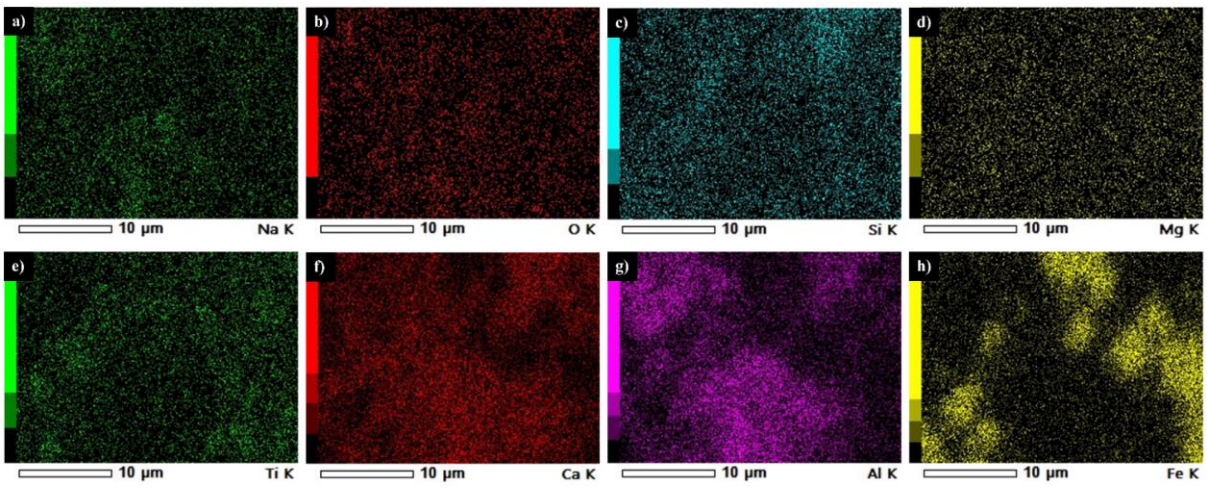

Figure 35. X-ray mapping of reduction sample 8 (1100°C, 2.5 h).

The x-ray mapping of the sintered pellets (fig. 25) shows only slight phase definition as iron and aluminium start to separate, although the phases still are mostly merged. For the reductions at 1000°C (fig. 26, 28, 29 and 31), the x-ray mappings shows that the reduction time affects and changes the phase composition, separating the iron from the others, aluminium in particular. The x-ray mapping for the reductions at 1100°C (fig. 32, 34 and 35) present the intermediate phases of reduced iron where a noticeable layer of oxygen is present on the edges of the iron agglomerates.

4.4.3 Point analysis

The analysis of the phases at 4000x magnification was done with point analysis. For the different samples, each individual point represents a phase with different atomic composition. Every element of interest is displayed with atom% for all spots on the sintered sample, reduction sample 1-6 and 8. The spot mapping for the sintered and the reduced samples are shown in table 10. The coherent location of the points is shown in figure 36.

Table 10: Point analysis [At%] of the sintered sample and reduction samples 1-6 and 8

Sample	***Point***	***Mg***	***Ti***	***Fe***	***Si***	***Na***	***Ca***	***Al***	***O***	***Estimated phase***
Sintered	0.1	0.3	3.7	34.4	0.8	0.5	20.3	13.9	26.2	Brownmillerite*
	0.2	-	0.5	6.8	11.7	1.4	30.2	18.9	30.5	Gehlenite
Red 1	1.1	-	0.0	0.5	1.7	2.2	11.5	18.9	65.2	Mayenite
	1.2	-	0.8	89.4	-	-	1.9	2.7	5.2	Fe
	1.3	-	7.2	10.7	0.2	0.3	20.5	6.1	55.1	Brownmillerite
Red 2	2.1	0.0	8.7	6.0	1.9	0.2	18.9	4.1	60.2	Calcium titanate
	2.2	-	0.5	89.8	-	-	1.9	1.4	6.4	Fe
	2.3	0.3	0.3	0.8	3.9	1.6	14.9	16.7	61.6	Mayenite
Red 3	3.1	0.2	0.2	88.5	-	-	1.6	1.9	7.5	Fe
	3.2	0.1	0.1	1.1	5.2	3.8	13.7	12.3	63.6	Mayenite
	3.3	0.3	6.7	7.1	1.7	0.3	18.0	5.5	60.4	Shulamitite
Red 4	4.1	-	4.4	6.9	2.2	1.7	13.0	4.8	66.9	Shulamitite
	4.2	-	0.6	42.3	-	6.7	2.3	9.5	38.5	Wüstite
	4.3	2.4	0.1	9.8	1.5	5.7	5.0	12.4	63.3	Hercynite**
Red 5	5.1	0.4	5.9	6.1	0.7	0.1	16.2	6.4	64.3	Shulamitite
	5.2	8.5	0.5	43.2	-	2.5	1.5	0.9	43.0	Wüstite
	5.3	0.1	6.2	7.2	0.8	1.0	18.9	6.5	59.3	Shulamitite
Red 6	6.1	0.6	0.4	85.8	0.7	0.4	1.4	2.0	8.8	Fe
	6.2	-	0.1	1.8	0.5	2.9	13.0	22.4	59.3	Mayenite
	6.3	0.1	12.3	4.9	1.1	0.9	20.3	5.2	55.2	Calcium titanate
Red 8	8.1	0.4	1.4	73.7	-	2.4	5.6	8.9	7.5	Fe
	8.2	0.2	0.5	3.6	-	5.2	33.1	19.4	38.0	Mayenite
	8.3	2.7	2.1	11.7	-	2.3	12.8	19.8	48.8	Mayenite***
	8.4	0.2	1.3	75.2	-	1.8	7.2	6.5	7.7	Fe

* the most possible regarding variation in iron and aluminium contents in brownmillerite ($Ca_2(Fe,Al)_2O_3$)
** not found in XRD
*** iron is most likely from the surroundings, because of small particles

Based on the atomic composition of each phase, the corresponding mineral of the phase was estimated.

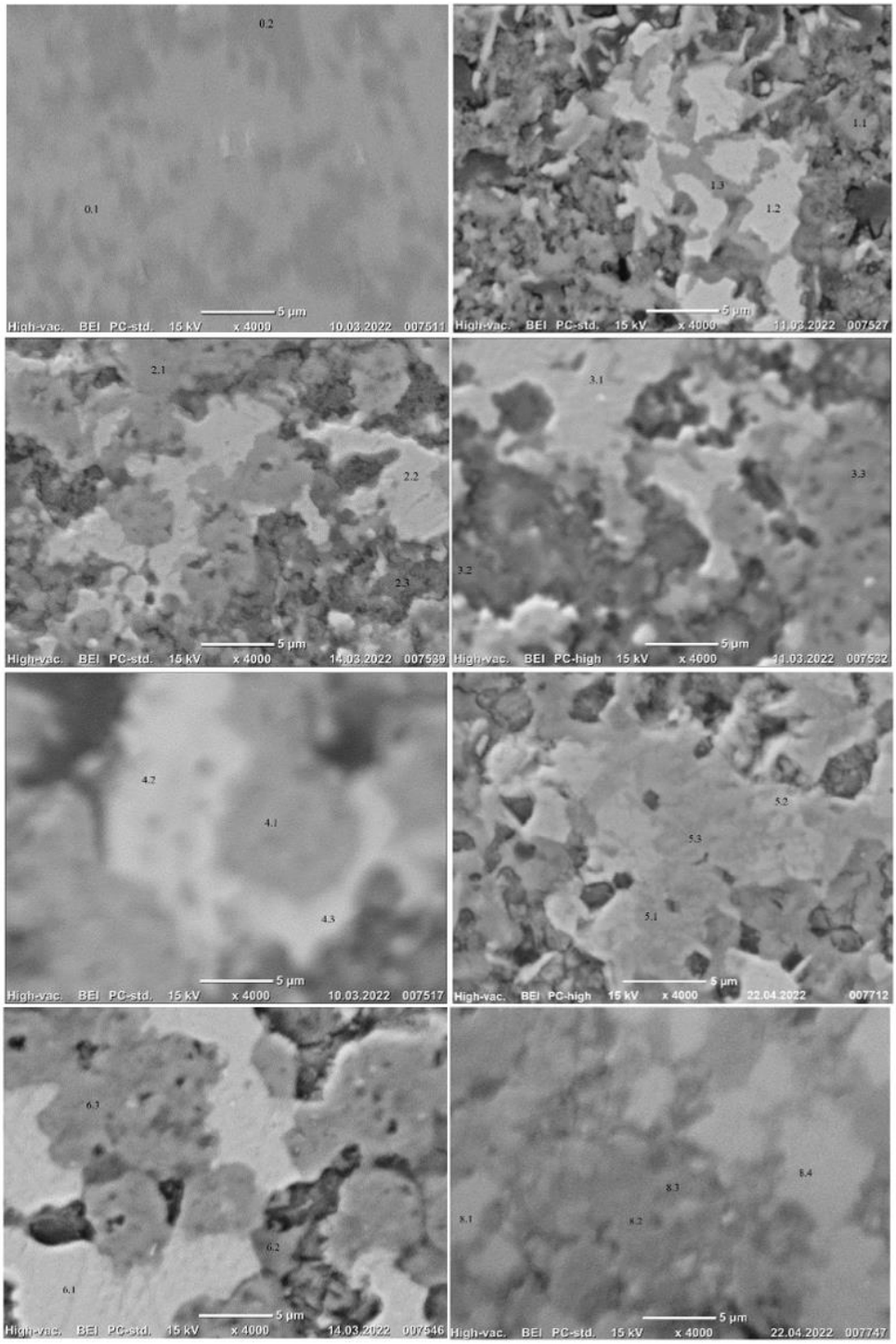

Figure 36. SEM BEI taken at magnification 4000x, with points and coherent numbers.

4.5 Phase analysis (XRD)

The sintered pellets, dried pellets and reduction 1-6, 8, 9 and 12 were analysed with XRD. Figure 37 shows the dried and sintered pellet and figure 38-40 shows the reduced samples sorted by temperature. Figure 41 shows the comparison of each reduction temperature (1000, 1100 and 1200°C) carried out for 0.5 hour and figure 42 shows comparison of the reduction temperatures carried out at 2.5 hour. The raw analyses can be found in attachment IV.

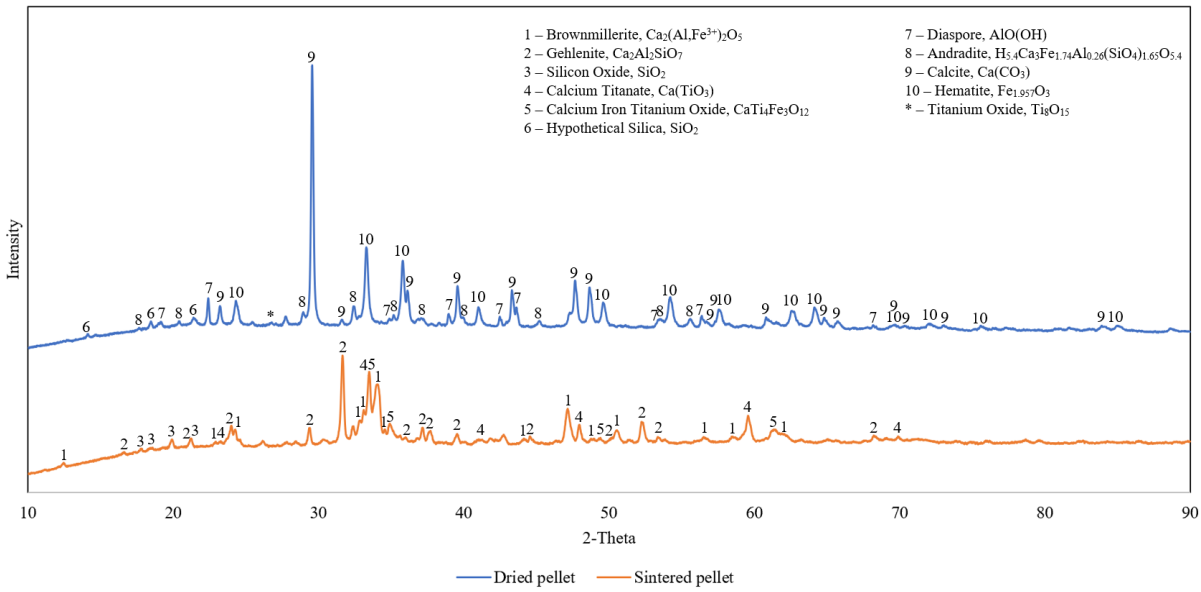

Figure 37. XRD graphs of the dried pellets (blue) and the sintered pellet (orange).

The XRD of the dried and sintered pellets in figure 37 shows that the phase composition change as the volatile components is driven off and more thermodynamically stable phases remain.

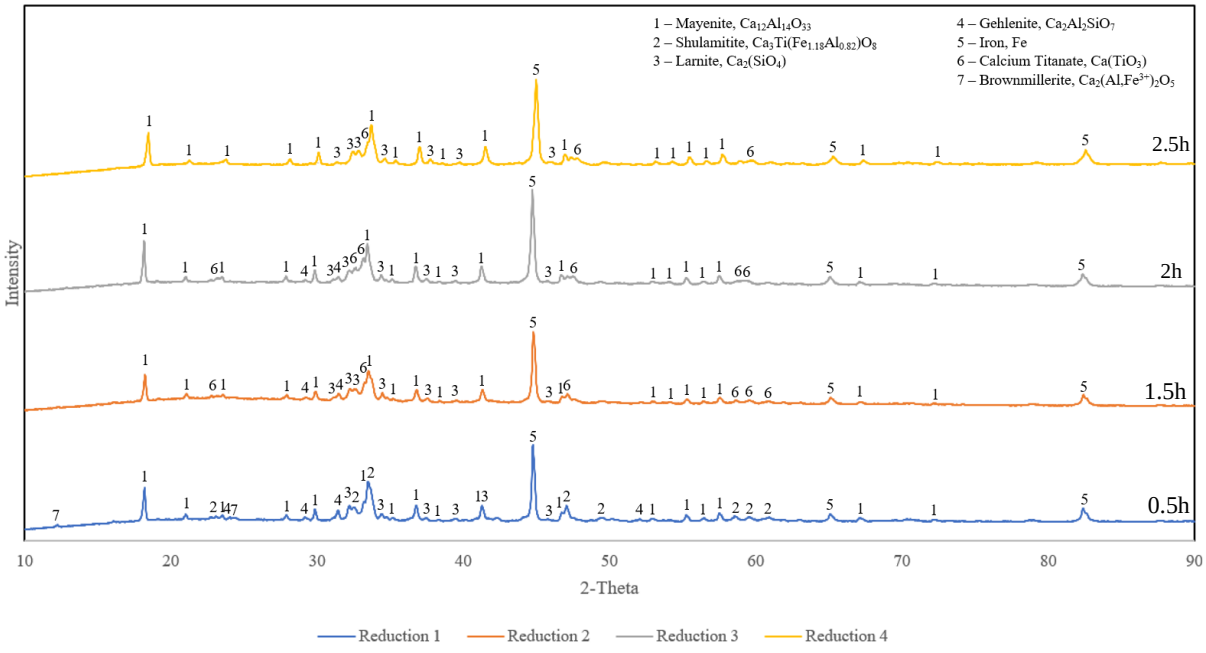

Figure 38. XRD graphs of reduction 1 (blue), reduction 2 (orange), reduction 3 (grey) and reduction 4 (yellow) at 1000°C.

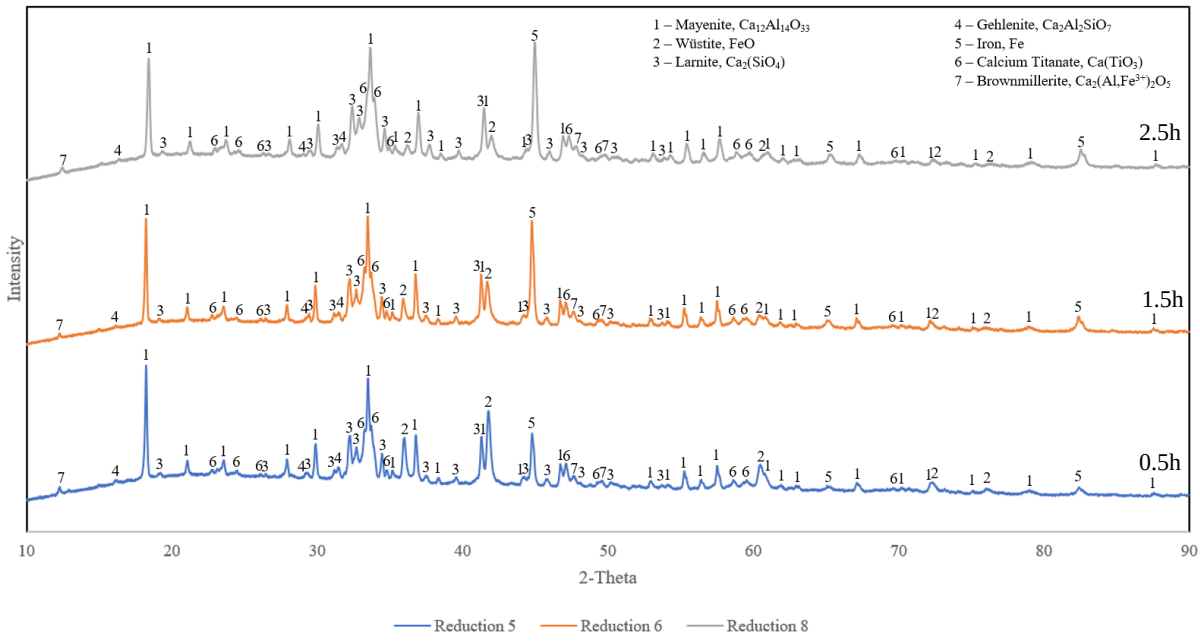

Figure 39. XRD graphs of reduction 5 (blue), reduction 6 (orange) and reduction 8 (grey) at 1100°C.

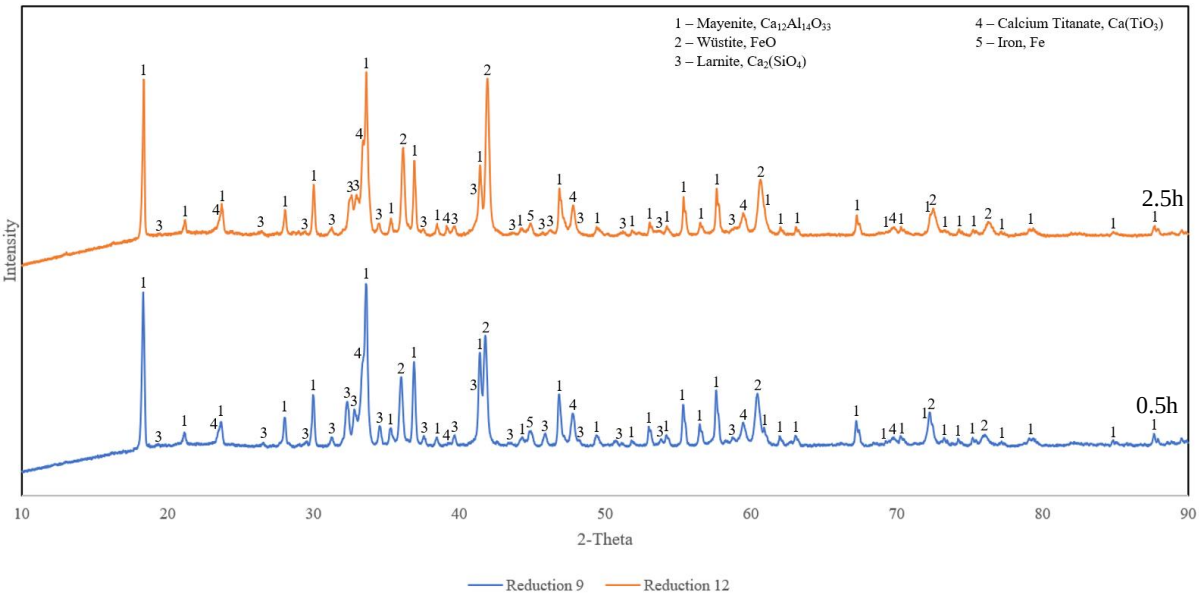

Figure 40. XRD graphs of reduction 9 (blue), and reduction 12 (orange) at 1200°C.

The XRD analysis of the reduction experiments with the same target temperature, with different duration is gathered in figure 38, 39, and 40 with 1000, 1100 and 1200°C respectively. At 1000°C the iron is almost completely reduced except for the reduction at 0.5 hours. The reductions at 1100°C show more intermediate iron phases such as wüstite and brownmillerite, whereas the 1200°C reductions show no significant reduction with iron almost completely residing in wüstite.

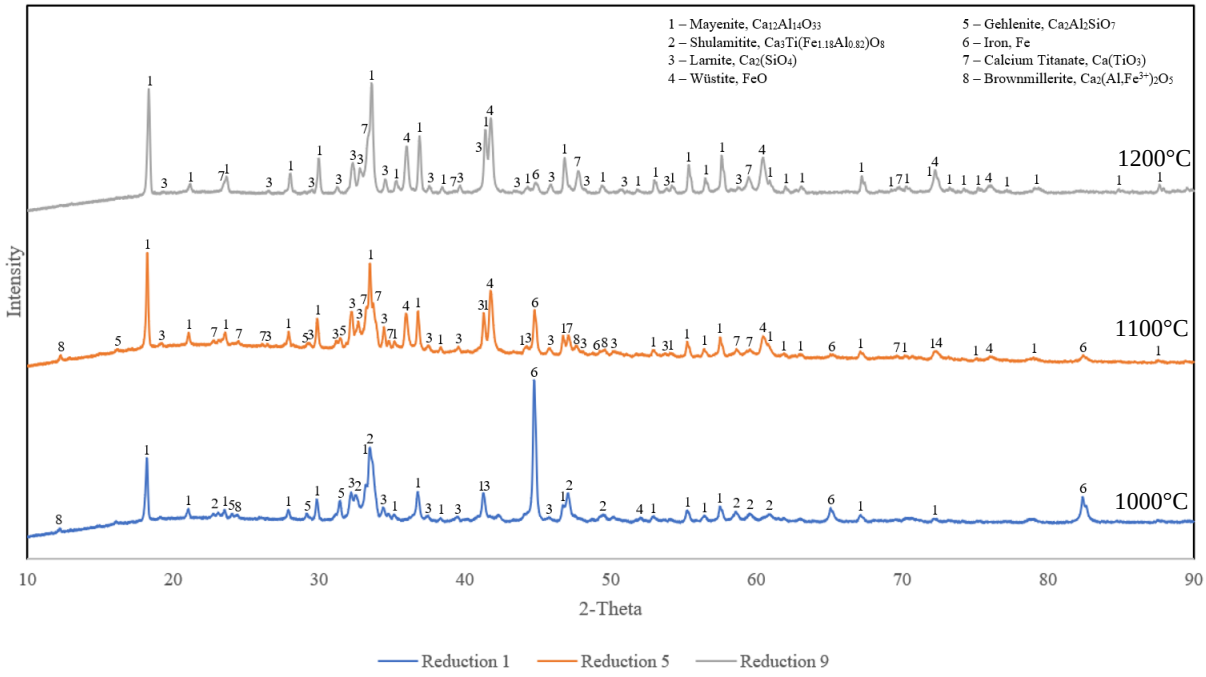

Figure 41. XRD graphs of reduction 1 (blue), reduction 5 (orange) and reduction 9 (grey) after 0.5 h.

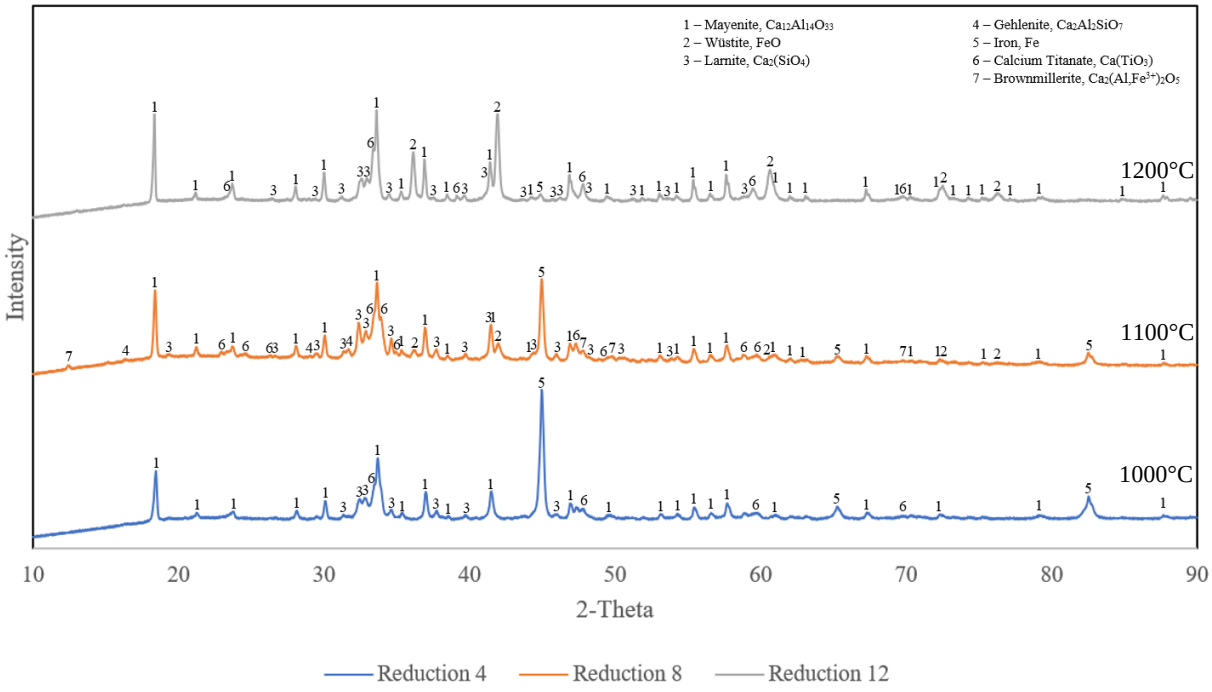

Figure 42. XRD graphs of reduction 4 (blue), reduction 8 (orange) and reduction 12 (grey) after 2.5 h.

As shown in figure 41 and 42, the reduction experiments at the same duration but different times is presented together to compare the effect time has on the reduction. The reductions at 0.5 hours (fig. 41), show considerably more amounts of intermediate phases than the ones at 2.5 hours (fig. 42).

4.6 Magnetic separation

Multiple samples were attempted separated with different magnets and methods, although it did not work as anticipated. The entire sample attached itself to the magnet, so none got separated from the rest. An attempt of magnetic separation is shown in figure 43.

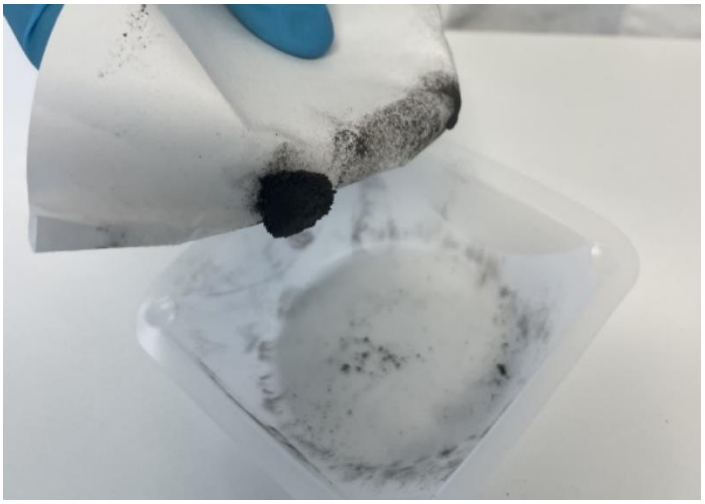

Figure 43. Attempt to separate the magnetic species from the rest of the residue.

4.7 Leaching

The weight of each sample was measured before and after the leaching experiment to record mass loss in grams and percentage. The initial weight of the leaching samples the residue was compared to is presented in table 6. The respective measurements for each sample 2, 4, 6 and 8 are presented in table 11.

Table 11: Weight and mass loss after leaching

Sample nr.	Reduction 2	Reduction 4	Reduction 6	Reduction 8
Weight of residue [g]	4.69	4.70	4.76	4.74
Mass loss [g]	0.32	0.31	0.24	0.26
Mass loss [%]	1.49	1.49	1.08	1.20

4.7.1 XRD results of residue after leaching

The precipitate from the leaching experiments were collected, dried, and analysed with XRD to identify the mineralogical composition of each sample. Results from the XRD analysis of reduction sample 2, 4, 6 and 8 are presented in figures 44-47.

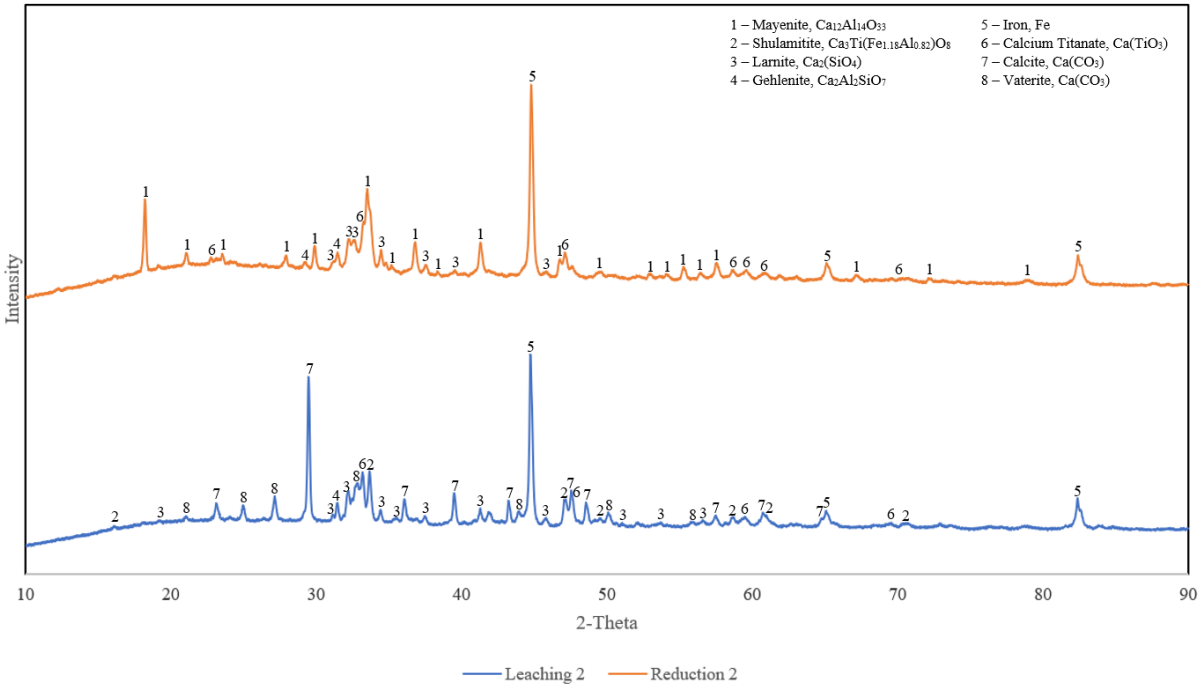

Figure 44. The reduced sample 2 (orange) and the leached sample from reduction 2 (blue). The reduction conditions were 1000°C for 1 h.

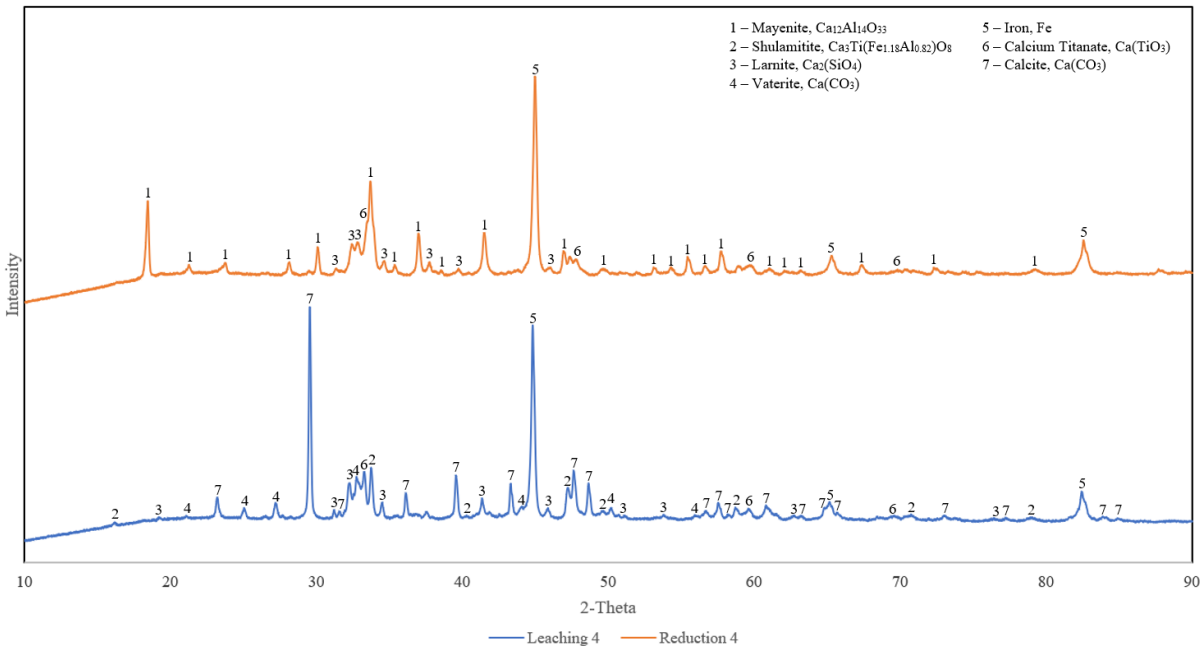

Figure 45. The reduced sample 4 (orange), and the leached sample from reduction 4 (blue). The reduction conditions were 1000°C for 2.5 h.

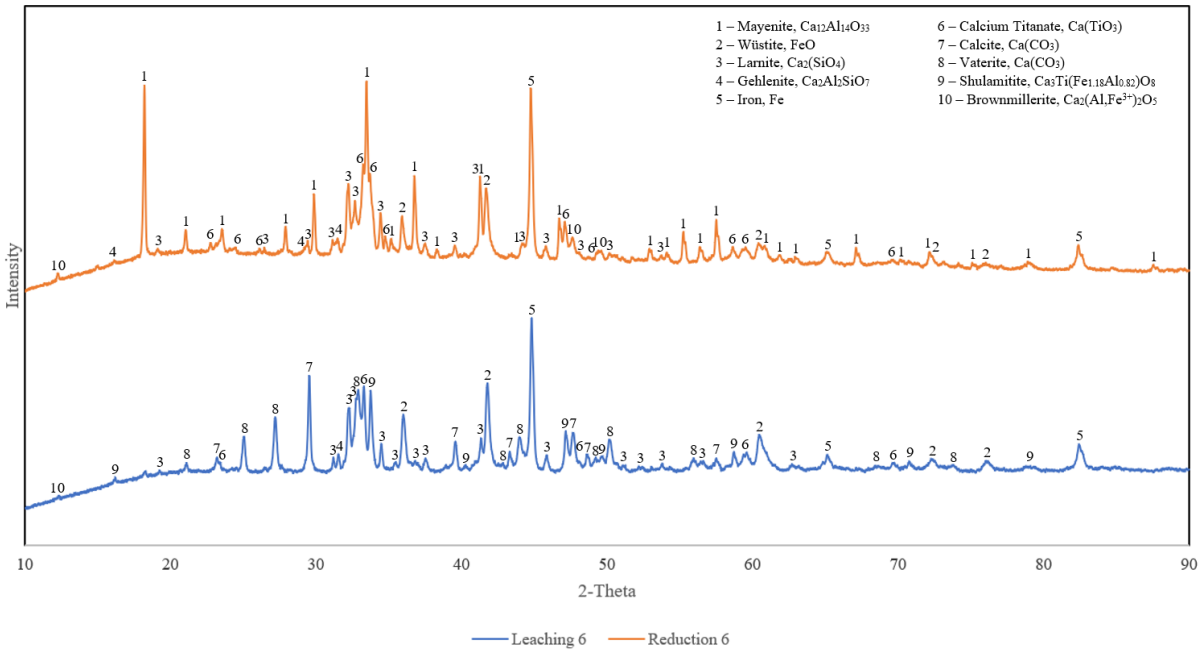

Figure 46. The reduced sample 6 (orange), and the leached sample from reduction 6 (blue). The reduction conditions were 1100°C for 1 h.

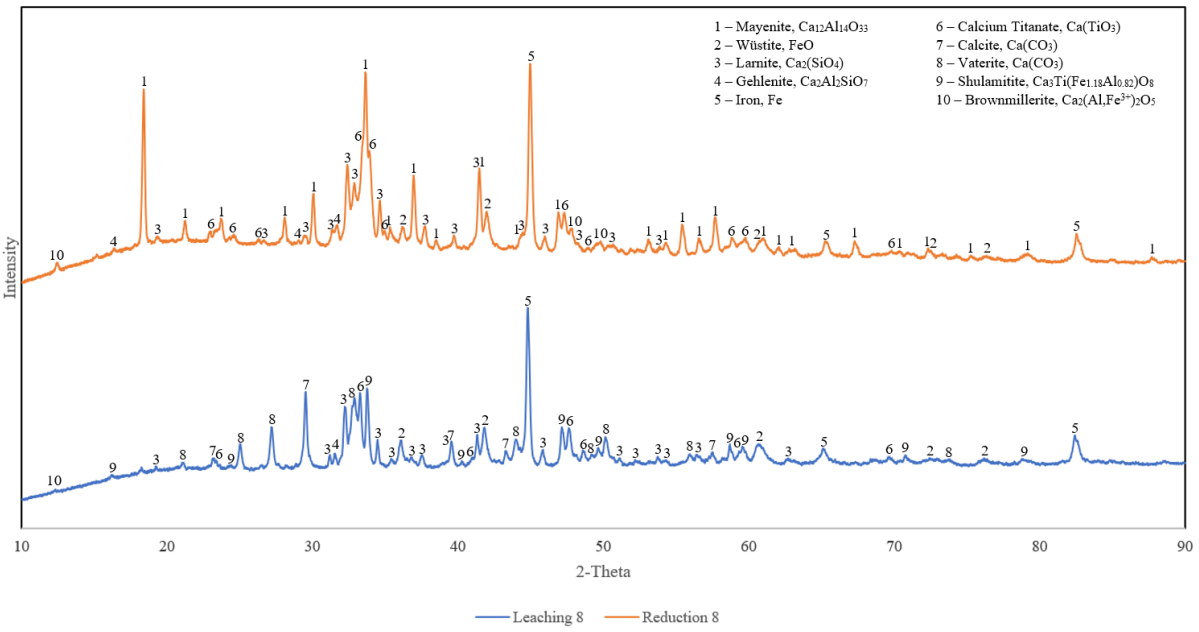

Figure 47. The reduced sample 8 (orange), and the leached sample from reduction 8 (blue). The reduction conditions were 1100°C for 2.5 h.

From the XRD graphs (fig. 44-47), it is visible that the aluminium-rich phase mayenite is leached almost completely, leaving the remaining aluminium in the shulamitite phase. The iron peak is visible with approximately the same intensity in both the reduced and leached sample for all four experiments.

4.7.2 ICP-MS results of filtrate after leaching

The ICP-MS results is presented in table 12. It was provided three blanks of the sodium carbonate solution for analysis and the average value for each element was used for comparison. The full analysis consisted of more elements such as calcium, titanium, and rare earth elements. However, the selected elements such as aluminium, silicon and iron are of most importance. The complete table of elemental composition is presented in attachment V.

Table 12: Concentrations of Al, Si, and Fe in each leached sample, analysed by ICP-MS

Sample	***Concentration [mg/L]***		
	Al	***Si***	***Fe***
Blank	0.12	3.78	0.00
Reduction 2	4163	70	0.78
Reduction 4	3943	66	0.74
Reduction 6	3915	64	0.68
Reduction 8	3647	66	0.55

The leaching yield for aluminium and silicon was calculated with regard to theoretical mass balances, calculated from XRF presented in chapter 4.1, as shown in formula 15.

$$aluminium\ yield = \frac{(C_{Al,sample} - C_{Al,blank}) * V_{sample}}{\left(\frac{2 * M_{Al}}{M_{Al_2O_3}}\right) * \frac{wt\%Al_2O_3}{100} * m_{sample}} * 100\% \quad (15)$$

Where $C_{Al,sample}$ denotes the concentration of aluminium present in the sample from ICP-MS analysis, $C_{Al,blank}$ denotes the aluminium concentration obtained from the blank, and V denotes the volume of the sample when leaching. M_{Al} denotes the atomic weight of aluminium (27.0 g/mol), M_{Al2O3} denotes the molecule weight of alumina, Al_2O_3, (102.0 g/mol) and m_{sample} denotes the initial mass of the leached sample[21]. The wt% of alumina is from the XRF presented in chapter 4.1. The same method applies for the calculation of yield silicon in the sample, except for using the ratio between Si and SiO_2. This is shown in formula 16. The wt% of alumina and silicon oxide is from the XRF presented in chapter 4.1.

$$silicon\ yield = \frac{(C_{Si,sample} - C_{Si,blank}) * V_{sample}}{\left(\frac{M_{Si}}{M_{SiO_2}}\right) * \frac{wt\%SiO_2}{100} * m_i} * 100\% \quad (16)$$

Where $C_{Si,sample}$ denotes the concentration of silicon present in the sample from ICP-MS analysis, $C_{Si,blank}$ denotes the silicon concentration obtained from the blank, and V denotes the volume of the sample when leaching. M_{Si} denotes the atomic weight of silicon (28.09 g/mol), M_{SiO2} denotes the molecule weight of silicon oxide (60.1 g/mol) and m_i denotes the initial mass of the leached sample[21].

Table 13: Yield [%] aluminium and silicon after leaching

Sample	***Yield [%]***	
	Al	***Si***
Reduction 2	86.6	4.40
Reduction 4	82.0	4.14
Reduction 6	81.5	4.07
Reduction 8	75.9	4.14

In table 13 it can be seen that leaching of reduction 2 yields most aluminium and silicon. Reduction 8 yields the least aluminium and reduction 6 yields the least silicon.

5 Discussion

The discussion parts in this report are set up in chronological order according to the experimental plan, to facilitate understanding of the results.

5.1 Characteristics of pellets

The pelletizing and sintering, which were the first two steps in the whole experimental process, is the foundation of the experiments. It is therefore quite important that they were done correctly. The pellets were firm, the right size (4-8 mm) and did not decompose in later experiments and are therefore considered optimal. As mentioned in chapter 4.2, the first pellets were smelted instead of being sintered at the applied temperature, as a consequence of attempting to improve efficiency. Instead of sintering many batches of 70-90 g in two alumina boats, 350 g were distributed into eight alumina boats and put into the furnace at the same time. It proved not to be more efficient as the smelted pellets were not usable. The samples in the back of the furnace were completely melted, whereas the pellets in the boats in the front were closer to being sintered properly. It is therefore suspected that the muffle furnace had a temperature gradient. The later experiments were then revised, and only two alumina boats of pellets, placed in the very front of the furnace, were sintered at the same time. Even though it wasn't recognized at the time, the melting point of the phases in the sintered pellets were around 1200°C.

The observations of experimental and calculation of theoretical mass loss, in chapter 4.2, indicates that the later sintering experiments were very similar to one another. With an average difference between experimental and theoretical mass loss of only +0.6 g, one can also conclude they were successful. The theoretical mass loss is slightly lower than the actual mass loss, most likely due to some loss of hydroxides in addition to CO_2 from the carbonate. From the sintering results (table 8) and the XRF results (table 7) one can see that the actual mass loss is close to the LOI of the dried pellets, which substantiates that it is correct.

5.2 Reduction and sample characteristics

To discuss the reduction experiments, many different parts of the experimental process must be considered. The important parameters in the reduction experiments are time and temperature. The results from direct observations, SEM and XRD are quite important to discuss in order to understand the effect of the parameters.

The direct observations are viewed in figure 20, 21 and table 9. Unfortunately, there are no mass observations from reduction 7 and 10-12 because of the furnace malfunction and melted reductions. These reductions were run at 1200°C and melted completely in the crucible, preventing any significant reduction and produced no usable data. The heating and cooling profiles (fig. 20) for the reductions differ slightly with the various temperatures, although does not indicate anything erroneous. The heating varies more than the cooling does, this is most likely due to the capacity of the system. The cooling profiles are more similar since only natural cooling were performed. The measured results (table 9) suggest that the yield for reductions done at 1000°C increases with reduction time. The pattern can also be viewed in reductions at 1100°C, but because one of them are missing, the pattern cannot be completed. The consensus is that the longer the sample is reduced at a given temperature, the greater the yield of iron. The other pattern is that only from looking at the table, reductions at 1000°C appear to be better than other temperatures considering only iron yield.

The porosity and morphology, important to the mass transfer of products and gaseous reactants in reduction, were analysed with SEM SEI and BEI. If figure 22, 23 and 36 are viewed and considered together, it indicates how porous the different pellets are. The bigger pores (fig. 22) seem to be very similar in all the reduced samples, but the smaller pores and morphology of the samples (fig. 23 and 36) have more differences. Reduction 1-4 have clearer borders between different phases, than reduction 5,6 and 8. The latter three, being reduced at 1100°C, have more connecting phases, seemingly almost molten together, and is perceived semi-molten. This will influence the rate H_2 can penetrate the pellet to reduce iron and can indicate why the reductions preformed at higher temperatures have less metallic iron.

SEM-EDS was used to identify various compositions and phases in the different reduction samples both by x-ray mapping and point analysis. The x-ray mapping and the area of which they were taken are shown in figure 24-35. The elements mapped out in the x-ray map were chosen because of their presence in the samples (see XRF in table 7). The mapping shows the overall distribution of the elements and how they interact with each other. If the x-ray mapping of the sintered sample (fig. 25) is compared to reduction sample 1 (fig. 26), one can see that the reduction clearly changes the elemental phases of the sample. Where the phases are more mixed together in the sintered sample, phases like Fe and Al do not mix in the reduced sample. The x-ray maps were the basis of how XRD were analysed later, as the maps indicate which phases exist in the sample.

EDS was also used for point analysis, at points shown in figure 36. The x-ray maps and BEI of the samples were used to identify interesting points to further study the phases in the samples. Table 10 shows the atom% of the present elements in the exact point and the estimated phases. The points were used in an effort to confirm the phases later found in XRD. The phases in some of the points was not recognized, as the ratio between the elements did not match any of the phases expected. To accommodate for possible cavities beneath each spot, it should have been taken several spots in the same phase to reduce potential errors.

To properly characterize the samples; dried pellets, sintered pellets and each reduction samples, XRD was used to identify mineralogical phases and how they change during the experimental process. Figure 37-42 display all the samples in chronological order. From figure 37, it is possible to state that phases such as hematite and diaspore, changes to brownmillerite and gehlenite respectively, during sintering. When considering the figures 38-40 together, it can be observed that both temperature and time affect the phase composition of the samples during reduction. Generally, during the reduction, the iron containing phases changes from brownmillerite to either metallic iron or to shulamitite and wüstite in the reduced pellets.

All the characterisation methods discussed above should be considered to decide which parameters are more important. Both XRD, SEM x-ray mapping and SEM point analysis should be viewed together to determine phases present in the different samples and thereby ascertain reduction kinetics and what parameters influence them most.

The overall characteristics of the reduction experiments indicate that 1000°C is the most reliable temperature to reduce iron, with little dependence on time. The experiments carried out at 1000°C managed to reduce the iron phases seemingly completely. The only exception being reduction experiment 1 (0.5 h). The XRD analysis of the first four reduction experiments (fig. 38) shows that reduction 1 still has an iron-containing phase, brownmillerite, which indicates that the reduction time was not sufficient to reduce all the iron in the sample. However, point analysis of reduction suggest that both brownmillerite and shulamitite is present in reduction 1 and 4 as shown in table 10. This further shows that the point analysis should have included more points, to determine the phases comprehensively. Especially considering the point analysis for reduction 4, indicating wüstite, is an

unexpected find. This is presumed to be a cavity beneath the surface of the point. The assumption is substantiated by the x-ray mapping (fig. 31), as it does not appear that oxygen is abundant in the same phase as iron. It can also be seen that there are a few cavities in the near area of the point (fig. 30).

The reduction experiments ran at 1100°C shows more complex reduction mechanics. At 1100°C, new phases are introduced as the reduction kinetics start to change. As seen in the XRD (fig. 39) brownmillerite is present in all three reductions as well as wüstite. This can also be confirmed with the point analysis of reduction 5 and 8 in table 10 with consideration to possible error, as these were not found in the points for reduction 6. These phases indicate incomplete reduction of iron and are most present in the shortest experiment, reduction 5 (0.5 h). Reduction 6 (1 h) and 8 (2.5 h) shows that, with increasing time, these intermediate reduction phases decrease, and more iron is reduced. Kinetics and thermodynamics suggest that reduction reaction rate should increase with temperature (fig. 5 and 8)[26, 28]. However, SEM images of reduction 5, 6, 8, image f), g), and h) respectively in figure 23 and 36, shows that the samples have a sub-molten phase throughout the pellet. This sub-molten phase seemingly covers up small pores, inhibiting mass transportation of reactants such as gas and products, limiting the overall rate of the reduction reaction. With a less porous structure, the pore-diffusion decreases, solid-state diffusion increases and become the rate-limiting step of the reaction, thus demanding more time to reduce the sample. This phenomenon can be described in figure 7 (a and b), which explains that pore diffusion decreases the reaction rate with diffusion through the pellets ash compared to a more porous structure which is only inhibited by gas-diffusion through the gas film. Gas diffusion through the gas film a) reaches chemical equilibrium much faster than pore diffusion b) because once the gas has diffused through the gas film, the reduction starts everywhere at once, thus only being inhibited by the chemical reaction and the available reactants.

The experiments carried out at 1200°C shows no remarkable reduction of iron. These samples completely melted in the crucible during the experiments. The XRD of the samples (fig. 40) shows that iron is barely reduced, only leaving a small peak (approximately at 44 degrees) and intermediate iron phases such as wüstite. Since the pellets melted completely, the pores also dissipate, and the mass transfer greatly decreases, possibly due to the dominance of solid-state diffusion. In this case, the melting of the materials causes low porosity (open porosity) in the sample, and hydrogen gas cannot penetrate the material to reduce it - hence the reduction occurs mostly at the external surface of the molten material exposed to hydrogen. This melting effect practically prevents any further reduction of the phases containing iron in the melted pellets. It is conceivable that experiments at this temperature can get sufficiently reduced given enough time. However, compared to the previous experiments, this is an inefficient way to reduce iron.

Considering which parameter is the most important, it seems the parameters is largely dependent on each other. When comparing reduction temperatures at 0.5 hours (fig. 41), it is apparent that reduction 1 (1000°C) is more beneficial. Reduction 5 (1100°C) yields less metallic iron and more intermediate phases like wüstite, while reduction 9 (1200°C) yields significantly less metallic iron. When comparing this to the reductions carried out at 2.5 hours (fig. 42), the XRD graphs suggest that increasing temperature demands more time to achieve sufficient reduction. At 2.5 hours, reductions at 1100°C yields considerably more metallic iron, and less wüstite than the reduction at 0.5 hours at the same temperature. This is also the case for the experiments carried out at 1000°C. The theoretical and experimental mass loss from the reduction experiments, considering iron, is presented in table 9. The respective yields for the experiments at the same temperatures but different times confirms the XRD graphs indication that the metallic iron concentration increases with increasing time. The reduction with the highest iron yield is reduction 4 with 82.9%, while the highest yield at 1100°C is reduction 8 with

70.5%. This further indicates that temperature remains the most important parameter, although time still is important, especially at higher temperatures.

5.3 Magnetic separation

The attempted magnetic separation of iron from the grey mud after leaching was deemed unsuccessful. Despite use of filter paper and different techniques, the precipitate kept latching on to the magnet (fig. 43). The poor separation may be caused by different reasons, but the particle size of the powder was very small, making it difficult to separate the powder magnetically as the iron incapsulated the other phases around the magnet. Even thought it was milled meticulously before leaching, the residue would be small particles of mixed phases. It is plausible that the magnetic separation can be carried out with more advanced equipment than what was used in the lab, although this is speculation.

5.4 Leaching of reduced samples

The leaching procedure of the samples from reduction 2 (1000°C, 1 h), 4 (1000°C, 2.5 h), 6 (1100°C, 1 h) and 8 (1100°C, 2.5 h) were performed under identical conditions. It is expected that the slight variation in results comes from the composition of the samples, due to some inhomogeneities. The mass loss (table 11) is generally alike throughout the samples, with the most mass loss observed in reduction 2 and 4. Theoretically there should not be any mass loss as the calcium carbonate precipitates as the aluminium is dissolved. A possible explanation to this mass loss is that very small amounts of the residue remained in the reaction flasks used in the leaching experiment.

Because of the predominance of iron in the leaching residue samples, the XRD analyses (fig. 44-47) generally shows high intensity of iron. They also show a significant decrease in mayenite after leaching, although there is an increase in the aluminium-containing phase, shulamitite. This indicates that most of the aluminium has been dissolved, whereas the rest remains in the shulamitite phase. Gehlenite is present both prior and post leaching, which substantiate the statement that it is non-leachable[10]. The gehlenite peak at approximately 29 degrees in the reduced samples, is presumed to still be present in the leached samples, although they are overlapping with the calcite peak registered at the same degree. Further, the samples show high intensity of the calcium containing phases calcite and vaterite, as expected[20]. Other calcium containing phases present both before and after leaching are larnite and calcium titanate, indicating that they are not leachable. The less yield of aluminium from sample 6 and 8, correlates with the presence of brownmillerite in the XRD (fig. 46 and 47), indicating that it is not leachable and a stable phase in these leaching conditions. This further substantiate the importance of iron reduction prior to leaching of aluminium.

The ICP-MS results in table 12 and 13 of the leachate generally shows a high yield aluminium in all the samples, although it decreases with increase in reduction time. Leaching of reduction 2 has the most yield aluminium, with 86.6% yield aluminium. All the leached samples displayed small amounts of silicon with mere difference from each sample, which is favourable[8]. However, the sample with the least yield silicon was reduction 6. The ICP-MS also showed an inconsiderable amount of iron in all the leached samples, as desired. Overall, the leaching was deemed successful.

6 Conclusion

In this thesis the valorization of bauxite residue was investigated through experimental work. Hydrogen reduction and leaching of the bauxite residue was studied to recover pig-iron and sodium aluminium hydroxide for further alumina recovery. The following conclusions were drawn from the experimental work:

- Attempts to sinter multiple samples at once resulted in smelting of the samples. Thereafter the sintering was carried out batchwise in the forefront of the furnace to prevent this.
- The hydrogen reductions at 1000°C and 1100°C successfully yielded iron whereas the reductions at 1200°C melted completely. This indicates that the melting point of the mixture is approximately 1200°C.
- The reduction which yielded most metallic iron was performed at 1000°C for 2.5 hours with 82.9%.
- Reduction experiments performed at temperatures 1100°C and 1200°C hosted more intermediate phases such as brownmillerite and wüstite than the ones at 1000°C.
- Generally, the iron yields were higher at lower temperatures and longer durations, revealing that temperature was the most important parameter for iron reduction with time being increasingly important at higher temperatures.
- Leaching of the reduced samples resulted in the dissolving of aluminium where leaching of the reduction sample performed at 1000°C for 1 hour, yielded the most aluminium with 86.6%.
- Overall, the reduction condition yielding most of both iron and aluminium was at 1000°C for 2.5 hours.

7 Recommendations for further work

For further research of hydrogen reduction of bauxite residue, the following suggestions are made. Investigation of isothermal reduction with a temperature range around 1000°C, in example 950-1050°C is interesting. Longer and shorter reduction intervals at 1000°C in order to study appearance of intermediate phases and yield of metallic iron. Additional parallels of each reduction would also be desirable.

8 Reference list

(1) Nations, U. *The Paris Agreement*. United Nations, 2022. https://unfccc.int/process-and-meetings/the-paris-agreement/the-paris-agreement (accessed 2022 May 14th).
(2) CORDIS, e. r. r. *Horizon 2020: Hydrogen as the Reducing Agent in the Recovery of metals and minerals from metallurgical waste*. European Commision, 2022. https://cordis.europa.eu/project/id/958307 (accessed 2022 May 14th).
(3) Change, I. P. o. C. *The evidence is clear: the time for action is now. We can halve emissions by 2030.* 2022. https://www.ipcc.ch/2022/04/04/ipcc-ar6-wgiii-pressrelease/ (accessed 2022 May 15th).
(4) HARARE. *HARARE*. 2021. https://h2020harare.eu/ (accessed 2022 May 13th).
(5) Pilla, G.; Kapelari, S. V.; Hertel, T.; Blanpain, B.; Pontikes, Y. Hydrogen reduction of bauxite residue and selective metal recovery. *Materials Today: Proceedings* **2022**, *57*, 5. DOI: 10.1016/j.matpr.2022.02.152.
(6) production, E. S. a. *Background*. ENSUREAL: Sustainable alumina production, 2021. https://ensureal.com/background/ (accessed 2022 May 14th).
(7) HARARE. *Let's talk about red mud (bauxite residue)*. 2021. https://h2020harare.eu/lets-talk-about-red-mud-bauxite-residue (accessed 2022 13th May).
(8) Mwase, D. J. M.; Safarian, J. Production of Aluminum Tri-hydroxides from Secondary Bauxite Materials. *Proceedings of EMC* **2021**, 547 - 557. DOI: 10.5281/zenodo.5012308.
(9) production, E. S. a. *Results*. ENSUREAL: Sustainable alumina production, 2021. https://ensureal.com/results/#WPs (accessed 2022 May 14th).
(10) Lazou, A.; Eijk, C. v. d.; Tang, K.; Balomenos, E.; Kolbeinsen, L.; Safarian, J. The Utilization of Bauxite Residue with a Calcite-Rich Bauxite Ore in the Pedersen Process for Iron and Alumina Extraction. *Metallurgical and materials transactions B* **2021**, *52* (3), 11. DOI: 10.1007/s11663-021-02086-w.
(11) Azof, F. I.; Kolbeinsen, L.; Safarian, J. The Leachability of Calcium Aluminate Phases in Slags for the Extraction of Alumina. **2017**, *46*, 12.
(12) Azof, F. I.; Vafeias, M.; Panias, D.; Safarian, J. The leachability of a ternary CaO-Al2O3-SiO2 slag produced from smelting reduction of low-grade bauxite for alumina recovery. *Hydrometallurgy* **2020**, *191*, 12. DOI: 10.1016/j.hydromet.2019.105184.
(13) Hind, A. R.; Bhargava, S. K.; Grocott, S. C. The surface chemistry of Bayer process solids: a review. *Colloids and Surfaces A: Physicochemical and Engineering Aspects* **1999**, *146* (1-3), 15. DOI: 10.1016/S0927-7757(98)00798-5.
(14) Safarian, J.; Kolbeinsen, L. Sustainability in Alumina production from Bauxite. *Mineral Processing* **2016**, *5*, 7.
(15) Institute, T. I. A. *Aluminium for Future Generations - Refining process*. The International Aluminum Institute, 2018. https://bauxite.world-aluminium.org/refining/process/ (accessed 2022 April 26th).
(16) Silveira, N. C. G.; Martins, M. L. F.; Bezerra, A. C. S.; Araújo, F. G. S. Red Mud from the Aluminium Industry: Production, Characteristics, and Alternative Applications in Construction Materials—A Review. *Sustainability* **2021**, *13* (22), 21. DOI: 10.3390/su132212741.
(17) Soceities, T. I. F. o. R. C. a. R. C. *Chemical spill: Red sludge*. The International Federation of Red Cross and Red Crescent Soceities, 2020. https://oldmedia.ifrc.org/ifrc/techbiohazards/red-sludge/ (accessed 2022 April 26th).
(18) Balomenos, E.; Beaulieu, S.; Ken Evans, C. L.; Rosani, D.; Tentes, G.; Tormo, E. *Bauxite Residue (BR) produced by Alumina refineries in Europe*; RemovAL, 2019. https://www.removal-project.com/wp-content/uploads/2021/09/removal-policy-report-20210923.pdf.
(19) Safarian, J.; Kolbeinsen, L. Smelting-reduction of bauxite for sustainable alumina production. *Mineral Processing* **2016**, *5*, 158.
(20) Azof, F. I.; Yongxiang; Panias, D.; Kolbeinsen, L.; Safarian, J. Leaching characteristics and mechanism of the synthetic calcium-aluminate slags for alumina recovery. *Hydrometallurgy* **2019**, *185*, 17. DOI: 10.1016/j.hydromet.2019.03.006.
(21) Allan Blackman, L. G. *SI Chemical Data*; John Wiley & Sons Australia, Ltd, 2014.

(22) Kolbeinsen, L. *Sintring*. Store Norske Leksikon, 2019. https://snl.no/sintring (accessed 2022 April 7th).
(23) Spreitzer, D.; Schenk, J. Iron Ore Reduction by Hydrogen Using a Laboratory Scale Fluidized Bed Reactor: Kinetic Investigation - Experimental Setup and Method for Determination. *Metallurgical and materials transactions B* **2019**, *50* (5), 13. DOI: 10.1007/s11663-019-01650-9.
(24) Lazou, A.; Eijk, C. v. d.; Balomenos, E.; Kolbeinsen, L.; Safarian, J. On the Direct Reduction Phenomena of Bauxite Ore Using H2 Gas in a Fixed Bed Reactor. *Journal of Sustainable Metallurgy* **2020**, *6* (2), 11. DOI: 10.1007/s40831-020-00268-5.
(25) Safarian, J. Extraction of Iron and Ferrosilicon Alloys from Low-Grade Bauxite Ores. *Extraction 2018* **2018**, 12. DOI: 10.1007/978-3-319-95022-8_66.
(26) Spreitzer, D.; Schenk, J. Reduction of Iron Oxides with Hydrogen—A Review. *steel research international* **2019**, *90* (10). DOI: 10.1002/srin.201900108.
(27) Patisson, F.; Mirgaux, O. Hydrogen Ironmaking: How It Works. *Metals* **2020**, *10* (7), 16. DOI: 10.3390/met10070922.
(28) Heidari, A.; Niknahad, N.; Iljana, M.; Fabritius, T. A Review on the Kinetics of Iron Ore Reduction by Hydrogen. *Materials* **2021**, *14* (24), 19. DOI: 10.3390/ma14247540.
(29) Safarian, J.; Azof, F. I. Leaching kinetics and mechanism of slag produced from smelting-reduction of bauxite for alumina recovery. *Hydrometallurgy* **2020**, *195*, 13. DOI: 10.1016/j.hydromet.2020.105388.
(30) Azof, F. I.; Kolbeinsen, L.; Safarian, J. Kinetics of the Leaching of Alumina-containing Slag for Alumina Recovery. *EMC 2019* **2019**, 15.

8 Appendix

I – Risk assessment

II – Original XRF results from SINTEF Norlab

III – Additional SEM imaging

IV – Raw analysed data for XRD

V – Complete ICP-MS results from SINTEF

I – Risk assessment

RISK ASSESSMENT (RiskManager alternative)			
Unit/Institute:	Department of Materials Science and Engineering	**Date:**	25.01.2021
Responsible line manager (name):	Einar Magne Hjorthol	**Revised:**	09.05.2022
Responsible for activities being risk assessed (name):	Frida Hemstad Danmo		
Participants in the risk assement (names):	Sander Ose Velle, Olivia Bogen Skibelid, frida Vollan, Arman Hoseinpur Kermani, Jafar Safarian		

Description of the activity, process, area, etc.:

The activities was done in several labs in Berg at Gløshaugen and at Kalvskinnet. Each activity is described and risk assessed beneath.

Activity / process	**Unwanted incident**	**Existing risk reducing measures**	**Probability (P)**	**Consequence (C)** Evaluate the categories individually. *Health should always be evaluated.*				**Risk value (P x C)**	**Risk reducing measures: suggestions** Measures reducing the probability of the unwanted incident happening should be prioritized.	**Residual risk after measures being implemented (S x K)**
			(1-5)	Health (1-5)	Material values (1-5)	Environment (1-5)	Reputation (1-5)			
Measuring out and mixing metal oxide powders in addition to transferring the mixture to a pelletizer.	Spill which means inhaling or contact with the substance on the skin or in the eye which can cause serious internal injury.	Protective gear: gloves, lab coat, glasses and respiratory protection. Fume hood as a barrier and ventilation.	*2*	*3*	*1*	*3*	*2*	*6*	Always use lids that can fully keep the substance sealed in when transporting the material from one station to another.	3
Pelletizing the mixture of oxides.	Heavy machinery can cause physical injury.	Protective gear: Lab shoes, gloves, glasses.	2	2	3	1	1	4	Know the machine well and how to use it.	2
Sintering the dried pellets	High temperatures which can cause burn damage and is some cases even explosions.	Protective gear: Heat resistant gloves, lab coat and glasses for protection. Crucible tongs to avoid direct contact with the heat from the pellet container. Brushes or ventilators for cleaning the furnace making sure that nothing unwanted is in the furnace. Lab rules clearly state that you need to know the material you are working with.	2	3	3	2	2	6	Let it cool down in the furnace for extra safety.	3

Cross sectioning and milling for analyses (SEM, XRF, XRD).	Cuts and fragments of the material being shot outwards from the cross sectioning and milling machines.	Protective gear: Face shield, gloves.	2	2	1	1	1	4	Do not touch the machines while they are preforming their task.	2
Reduction experiment using hydrogen gas flow.	Burn damage from high temperatures and in some cases even explosions. Gas suffocation from odourless and colourless gas or gas poisoning from leakage. High pressure gas in which can cause explosions in high temperatures or in direct sunlight when in gas tank/bottle.	Protective gear: Heat resistant gloves, as the resina furnace is relatively safe, a lab coat and glasses are fine. Built in alarm system in the lab for when concentration of gas exceeds a certain unsafe limit. Personal mobile gas detector. Leak detector and pressure test to know if something is leaking. Ask the people who are certified to move the bottles to do it. Warning signs on the door. Flushing the chamber after the experiment with vacuuming and then filling the chamber with Ar and then opening the chamber. checking the gas atmosphere around the gas burner of the RESINA furnace from time to time to measure the poisonous gases (this can be done by gas detectors or Dräger tubes)	1	4	3	3	3	4	Be familiar with the gas and regulators. Listen for leakage sounds.	2
Cutting crucible	Severe injuries from sawblade.	Protective gear: lab coat, glasses, and gloves. Saw is incapsulated in plastic screen.	1	5	1	1	2	5	Close protective screen and wear protective gear before use	1
Leaching of (Na_2CO_3)	Severe eye irritation and skin irritation. From anhydrous powder and solution	Protective gear: Lab coat, gloves and glasses.	2	2	1	1	1	4	Keep workspace tidy and spacious. Wear protective gear	1
Casting of SEM samples with epoxy	Spill of given chemicals EpoFix Resin: serious eye irritation, skin irritation, release to environment EpoFix Hardener: Severe skin and eye damage	Protective gear: Lab coat, gloves and glasses.	1	4	1	4	1	4	Keep workspace tidy and spacious. Wear protective gear	1

II – Original XRF results from SINTEF Norlab

SINTEF NORLAB

SINTEF AS
Arman Hoseinpur-Kermani

SINTEF Norlab AS
Org. nr.: NO 953 018 144 MVA
Postboks 611
NO-8607 Mo i Rana
www.sintefnorlab.no

Tlf: (+47) 404 84 100

Ordrenr: 113176
Sted: Mo i Rana
Antall prøver: 2
Bestillingsnr:

ANALYSERAPPORT

Mineralske materialer

Resultater er rapportert på glødet prøve

Prøvenr.:	Prøvetype:	Dato:	Prøvemerking:			Prøvetaker:	Mottaksdato:
113176-001			Dried Pellets			Oppdragsgiver	15.02.22
Analyse/Parameter		Resultat	Enhet	Usikkerhet	Analysedato	Metodbeskrivelse	
*) Al2O3		17.5	%	-	23.02.22	Intern metode, XRF	
*) CaO		33.2	%	-	23.02.22	Intern metode, XRF	
*) Cr2O3		0.13	%	-	23.02.22	Intern metode, XRF	
*) Fe		22.7	%	-	23.02.22	Intern metode, XRF	
*) K2O		0.11	%	-	23.02.22	Intern metode, XRF	
*) MgO		0.57	%	-	23.02.22	Intern metode, XRF	
*) MnO		0.11	%	-	23.02.22	Intern metode, XRF	
*) Na2O		2.5	%	-	23.02.22	Intern metode, XRF	
*) P		0.04	%	-	23.02.22	Intern metode, XRF	
*) S		0.28	%	-	23.02.22	Intern metode, XRF	
*) SiO2		6.5	%		23.02.22	Intern metode, XRF	
*) SrO		0.11	%	-	23.02.22	Intern metode, XRF	
*) TiO2		3.9	%	-	23.02.22	Intern metode, XRF	
*) V2O5		0.11	%	-	23.02.22	Intern metode, XRF	
*) ZrO2		0.13	%	-	23.02.22	Intern metode, XRF	
*) LOI 950		22.24	%		23.02.22	Intern metode	

Prøvenr.:	Prøvetype:	Dato:	Prøvemerking:			Prøvetaker:	Mottaksdato:
113176-002			Sintered			Oppdragsgiver	15.02.22
Analyse/Parameter		Resultat	Enhet	Usikkerhet	Analysedato	Metodbeskrivelse	
*) Al2O3		17.7	%	-	23.02.22	Intern metode, XRF	
*) CaO		33.5	%	-	23.02.22	Intern metode, XRF	
*) Fe		22.6	%	-	23.02.22	Intern metode, XRF	
*) K2O		0.05	%	-	23.02.22	Intern metode, XRF	
*) MgO		0.6	%	-	23.02.22	Intern metode, XRF	
*) MnO		0.1	%	-	23.02.22	Intern metode, XRF	
*) Na2O		2.0	%	-	23.02.22	Intern metode, XRF	
*) P		0.04	%	-	23.02.22	Intern metode, XRF	
*) S		0.3	%	-	23.02.22	Intern metode, XRF	
*) SiO2		6.6	%	-	23.02.22	Intern metode, XRF	
*) SrO		0.1	%	-	23.02.22	Intern metode, XRF	

Rapportert av:
Avdelingsingeniør
Ingunn Hilton

23.02.22 kl 13.29

Prøvenr.:	Prøvetype:	Dato:	Prøvemerking:			Prøvetaker:	Mottaksdato:
113176-002			Sintered			Oppdragsgiver	15.02.22
Analyse/Parameter		Resultat	Enhet	Usikkerhet	Analysedato	Metodbeskrivelse	
*) TiO2		4.0	%	-	23.02.22	Intern metode, XRF	
*) V2O5		0.1	%	-	23.02.22	Intern metode, XRF	
*) ZrO2		0.1	%	-	23.02.22	Intern metode, XRF	
*) LOI 950		0.07	%		23.02.22	Intern metode	

Angitt måleusikkerhet er beregnet med dekningsfaktor k=2. Ved intervallangivelse viser det høyeste tallet usikkerheten nært rapporteringsgrensen. For nærmere informasjon gjeldende usikkerhet, vennligst ta kontakt. SINTEF Norlab er akkreditert med test nr. 032. Hvilke analyser som inngår i akkrediteringen fremkommer i rapporten, *) = Ikke akkreditert, mod = modifisert standard, n.d. = Ikke påvist

Rapportert av:
Avdelingsingeniør
Ingunn Hilton

23.02.22 kl 13.29

III – Additional SEM imaging

Figure 48 and 49 shows the SEM SEI and BEI magnified 500x, respectively. The figures are comprised by eight different images marked a) to h); a) reduced sample, b) reduction sample 1, c) reduction sample 2, d) reduction sample 3, e) reduction sample 4, f) reduction sample 5, g) reduction sample 6 and h) reduction sample 8.

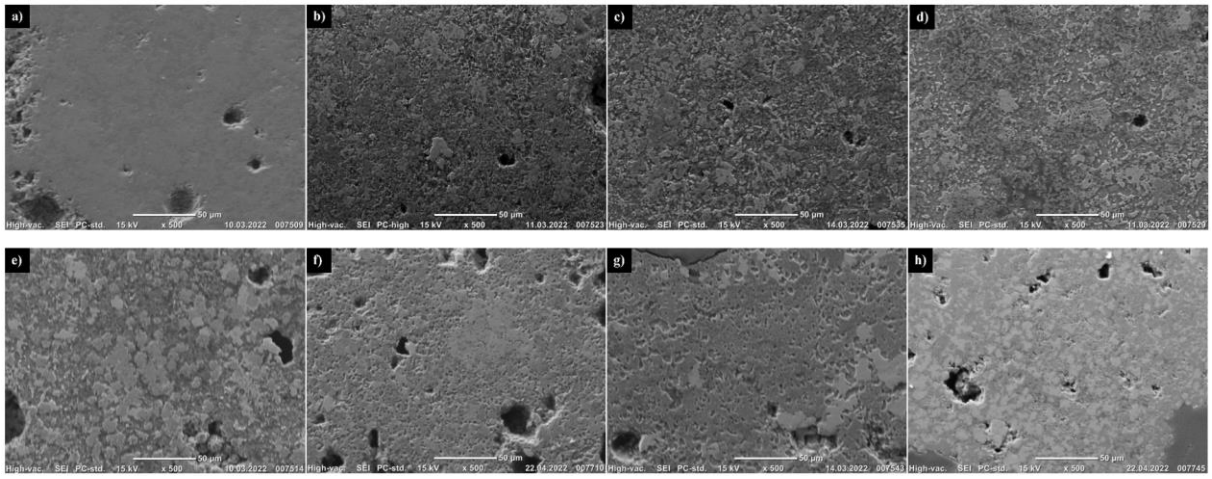

Figure 48. SEM SEI magnified 500x.

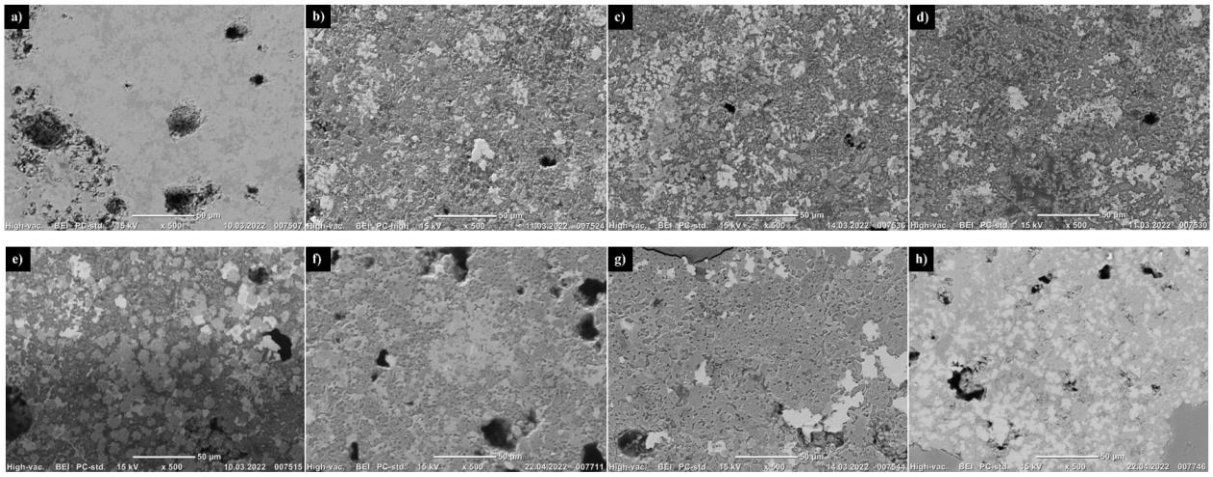

Figure 49. SEM BEI magnified 500x.

IV – Raw analysed data from XRD

The analysed XRD results are shown in figure 50-64. They are analysed in Rigaku PDXL 2.

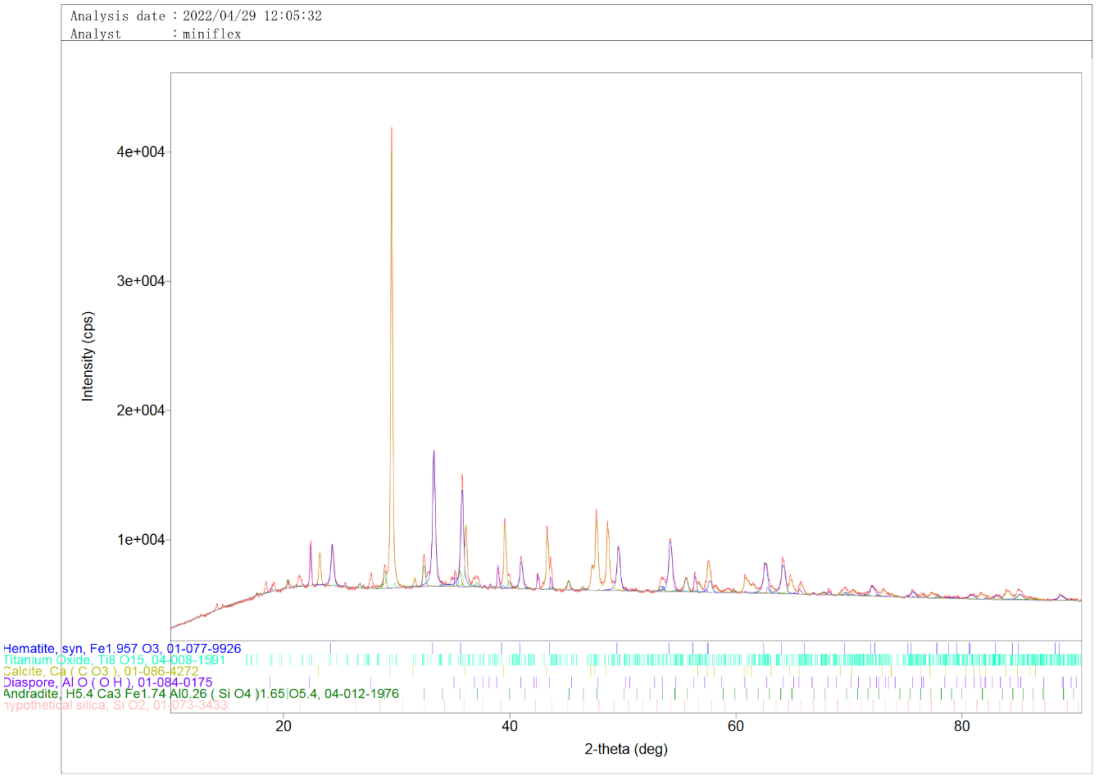

Figure 50.The analysed XRD results of dried pellets (red).

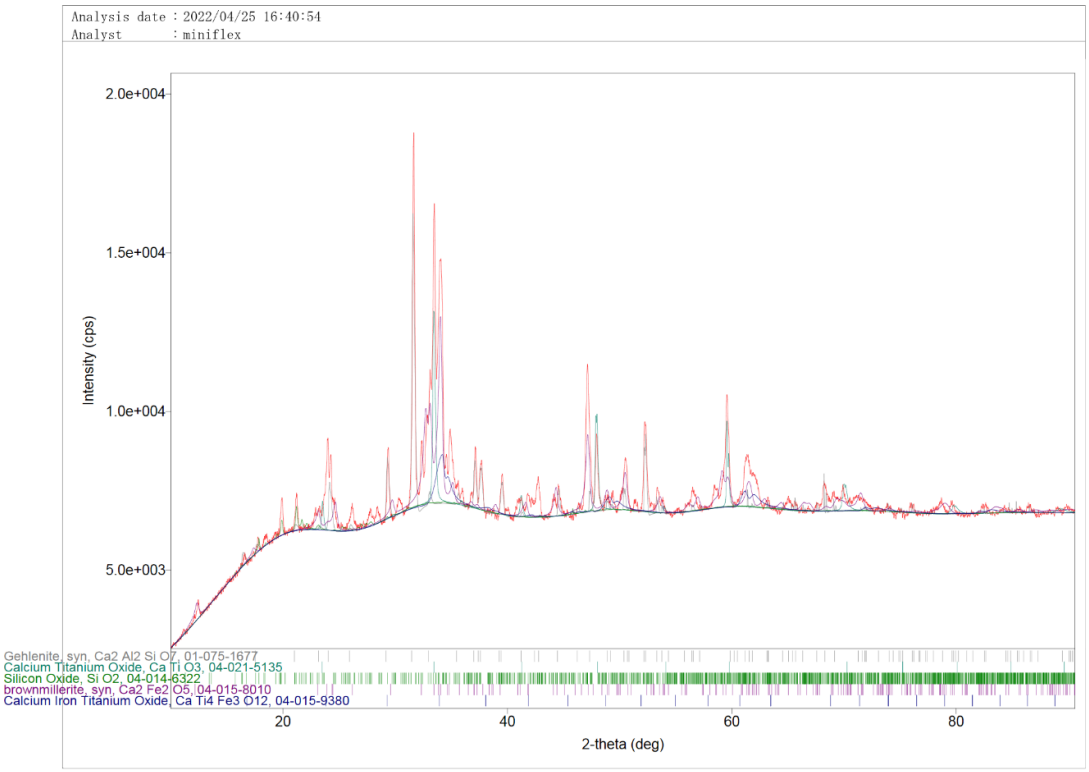

Figure 51. The analysed XRD results of sintered pellets (red).

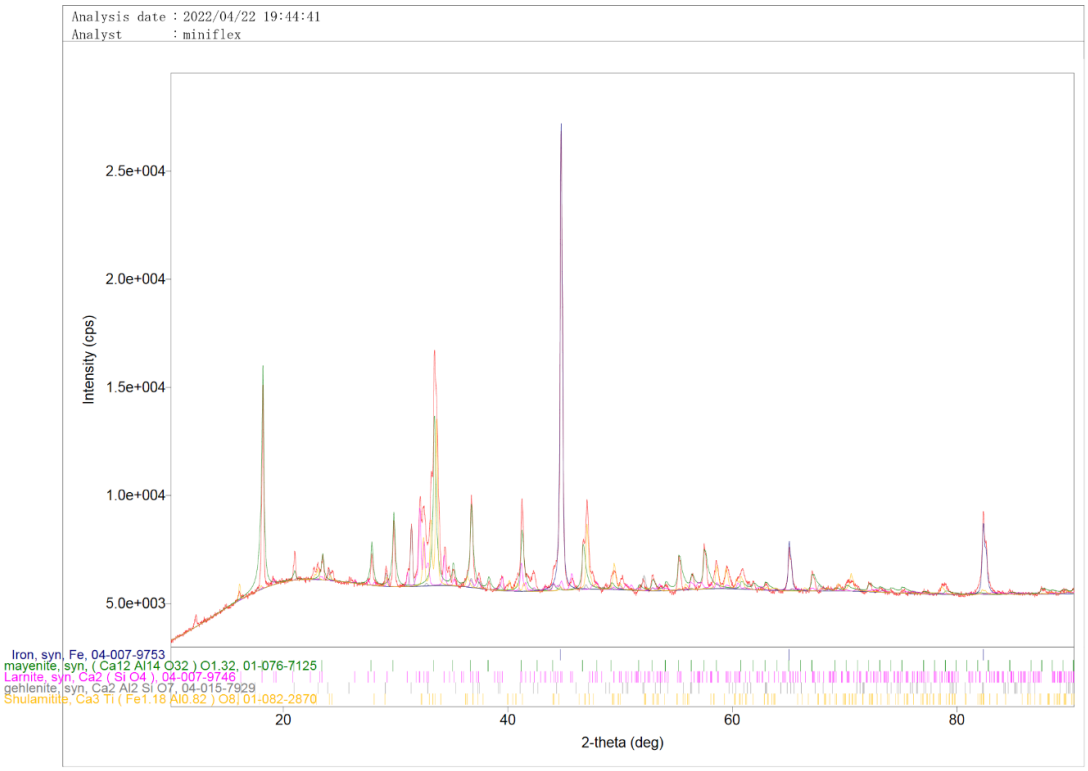

Figure 52. The analysed XRD results of reduction 1 (red).

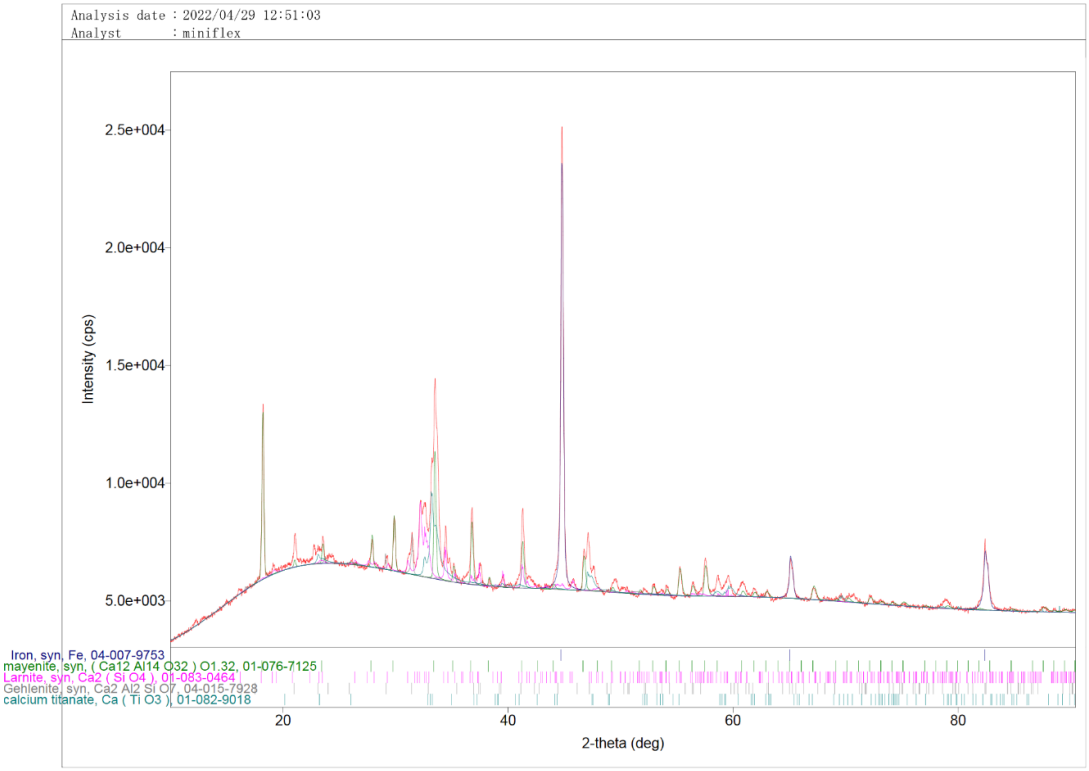

Figure 53. The analysed XRD results of reduction 2 (red).

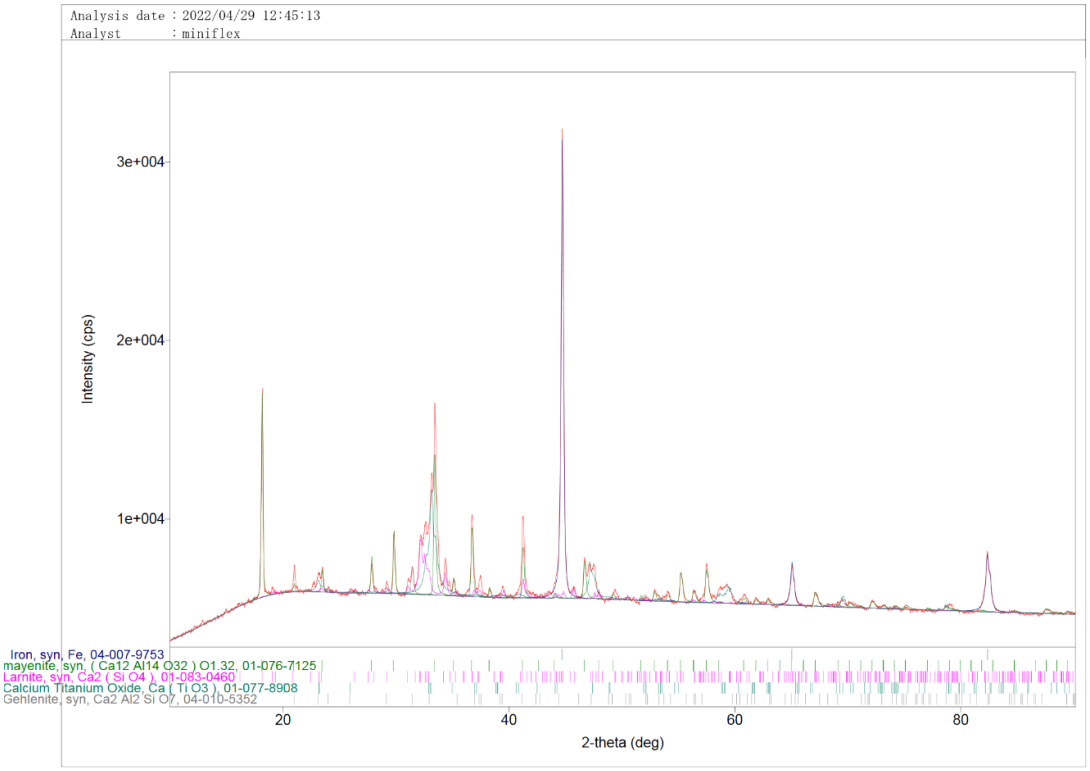

Figure 54. The analysed XRD results of reduction 3 (red).

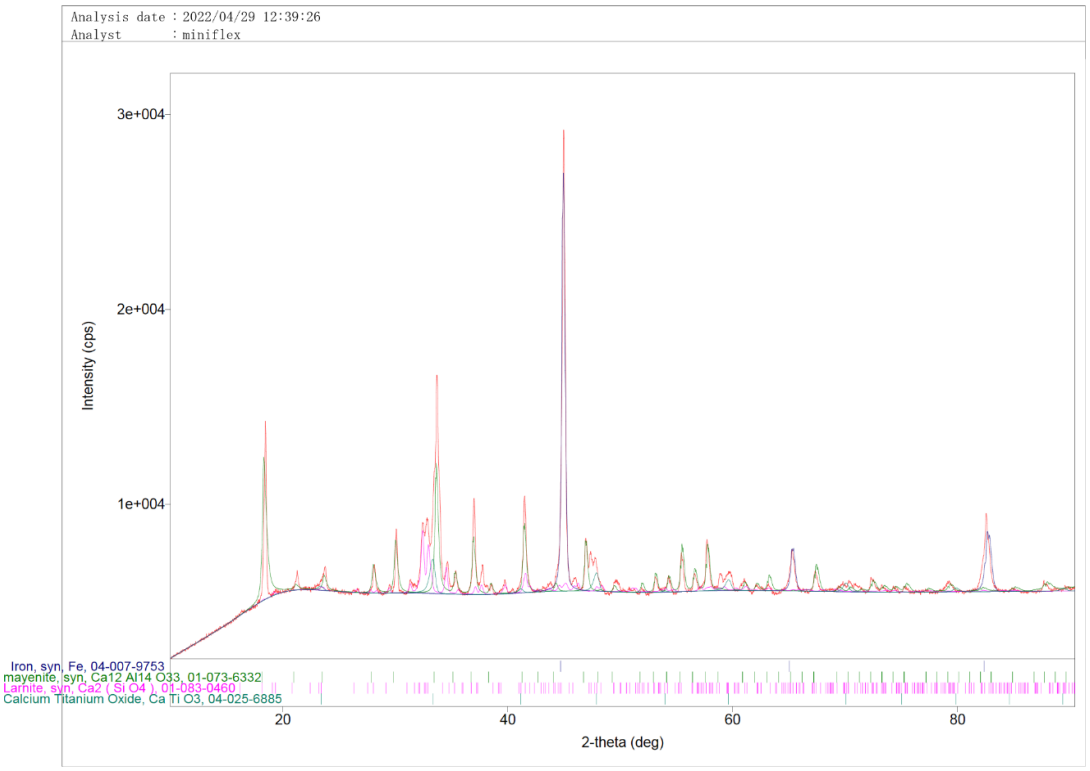

Figure 55. The analysed XRD results of reduction 4 (red).

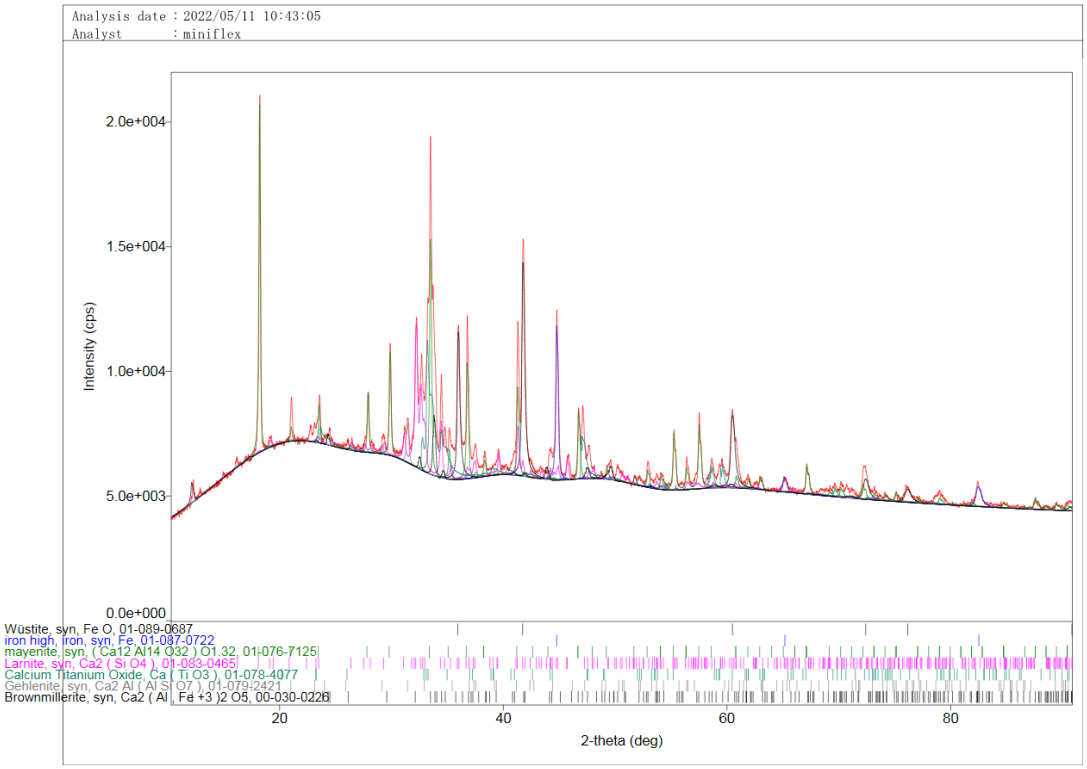

Figure 56. The analysed XRD results of reduction 5 (red).

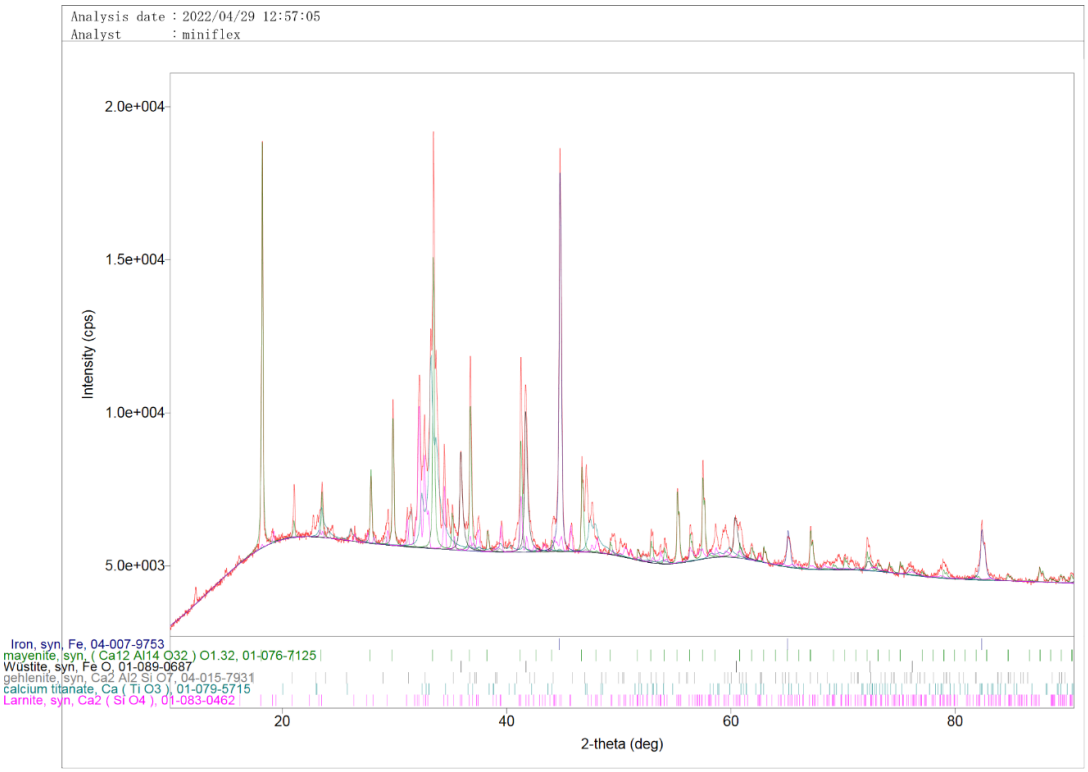

Figure 57. The analysed XRD results of reduction 6 (red).

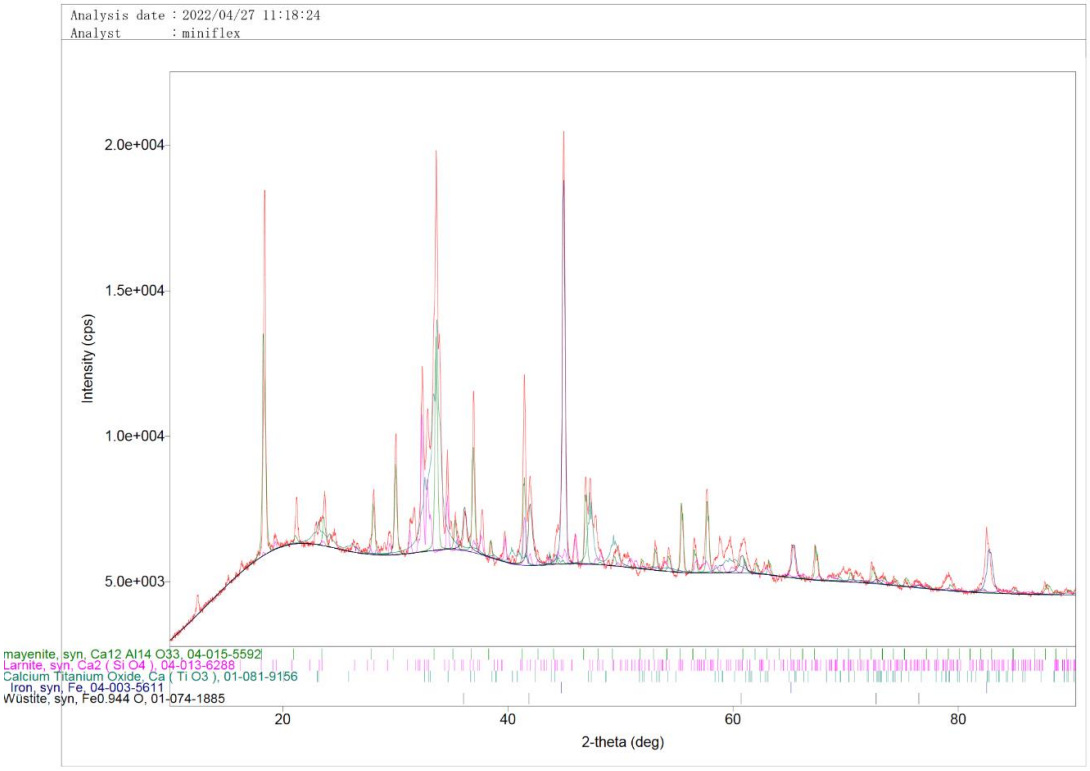

Figure 58. The analysed XRD results of reduction 8 (red).

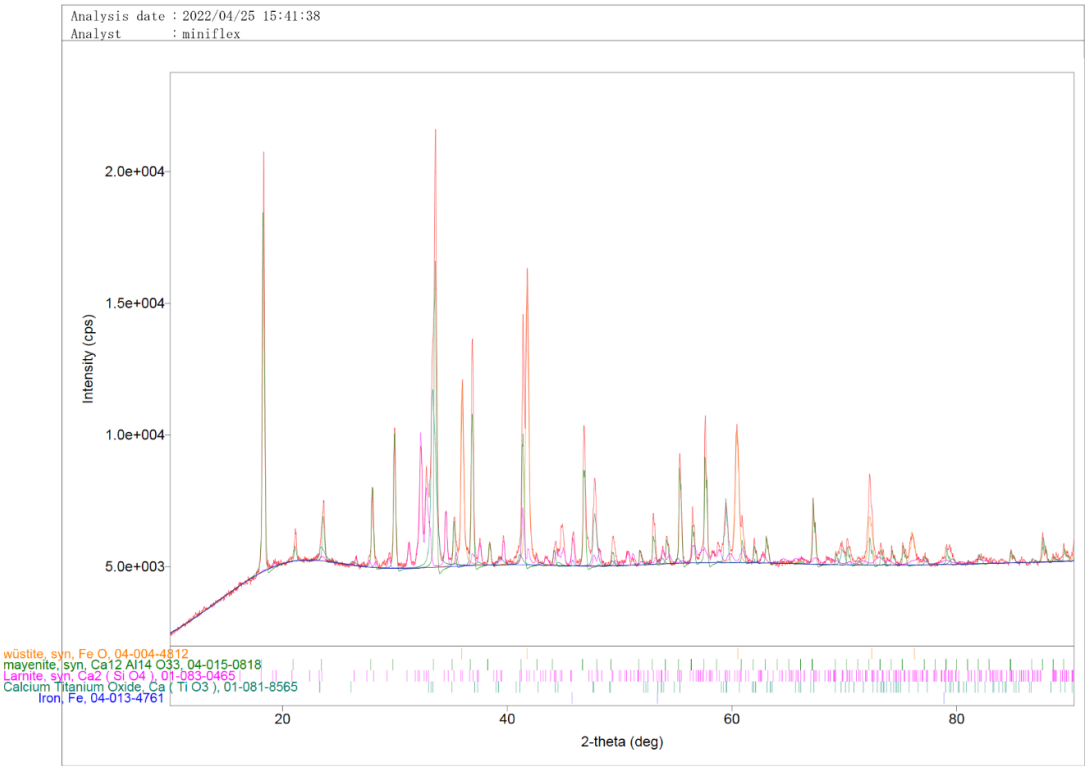

Figure 59. The analysed XRD results of reduction 9 (red).

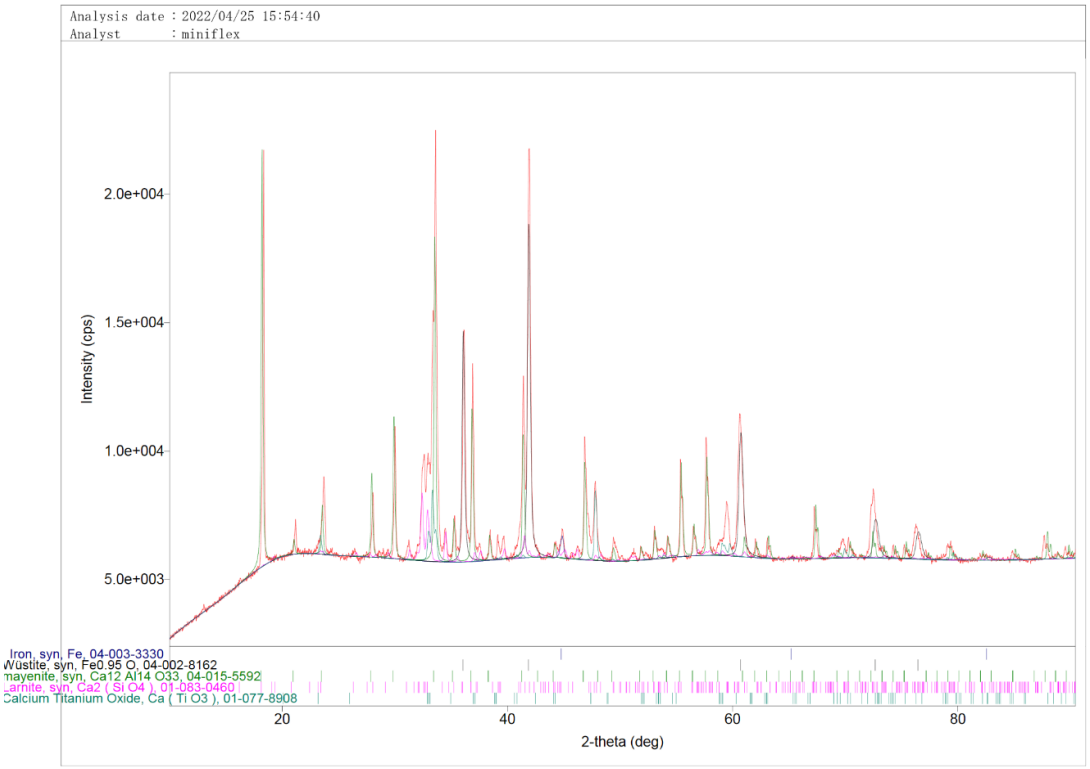

Figure 60. The analysed XRD results of reduction 12 (red).

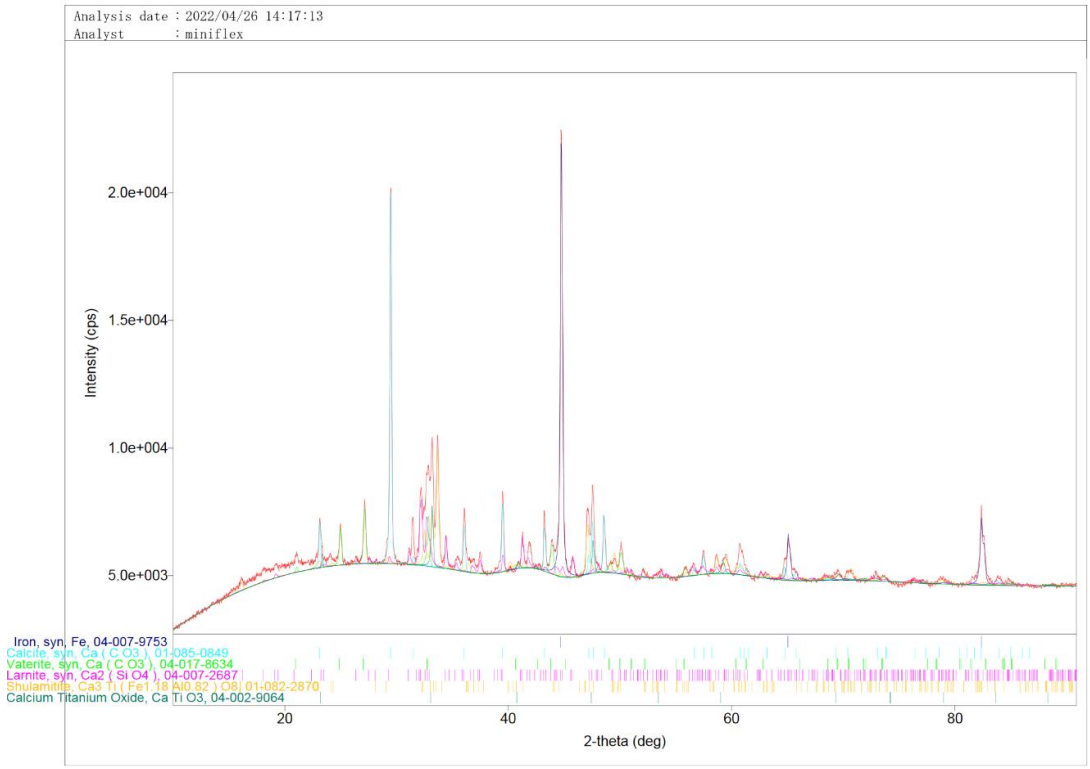

Figure 61. The analysed XRD results of leaching 2 (red).

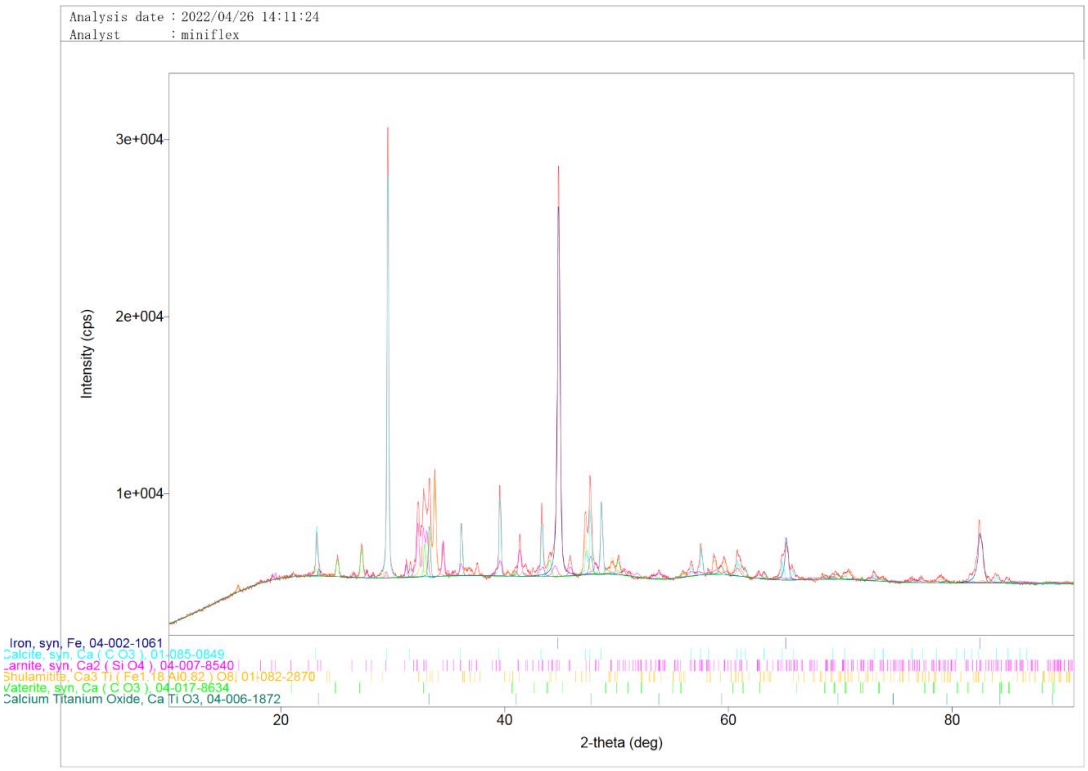

Figure 62. The analysed XRD results of leaching 4 (red).

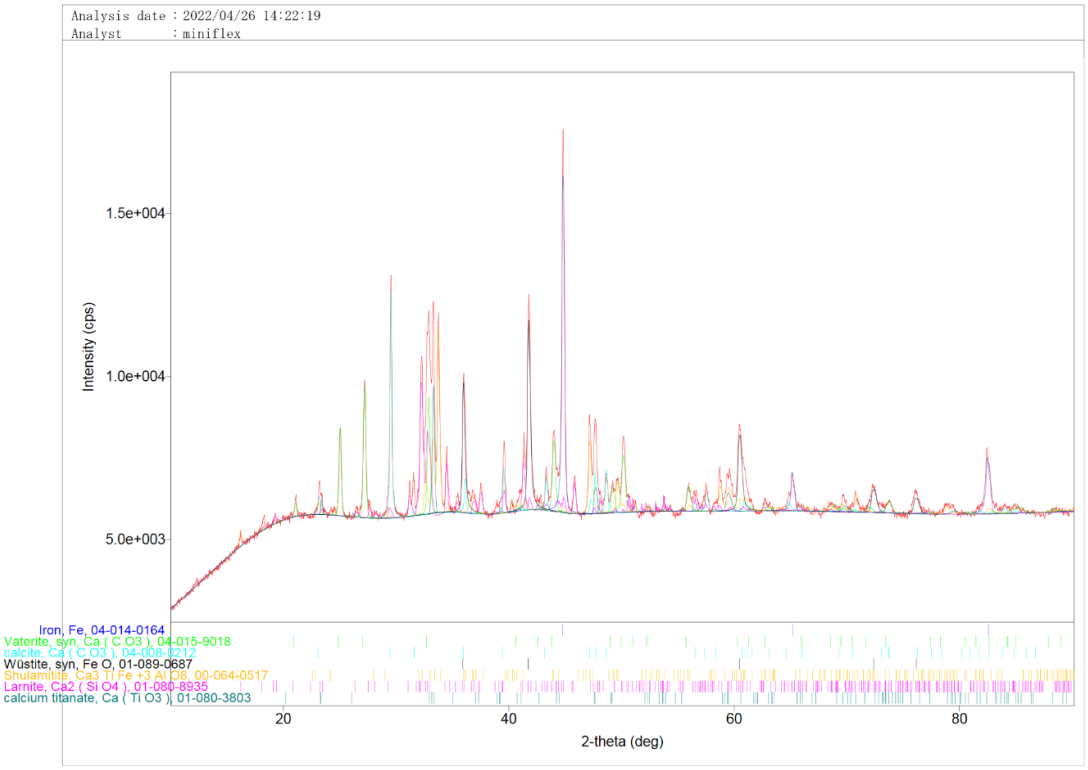

Figure 63. The analysed XRD results of leaching 6 (red).

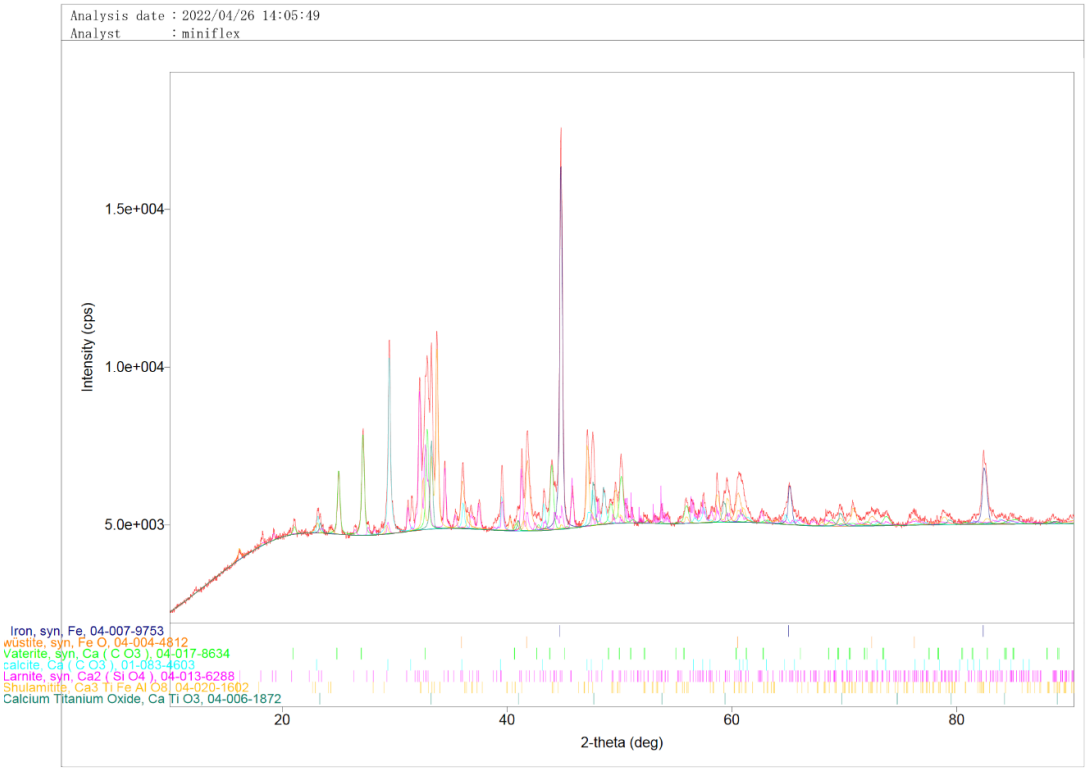

Figure 64. The analysed XRD results of leaching 8 (red).

V – Complete ICP-MS results from SINTEF

Table 14 shows the complete results from the ICP-MS analysis done by Sr. Engineer Marianne Kjos at SINTEF. The samples were diluted in 5% HNO3 and analysed with an Agilent 8800 Triple Quadropole ICP-MS (ICP-QQQ) with SPS 4 Autosampler. They are quantified against standards from Inorganic Ventures with 115In as internal standard.

Table 14: Complete table for ICP-MS analysis

Element	***Concentration [mg/L]***				
	Blank	***Reduction 2***	***Reduction 4***	***Reduction 6***	***Reduction 8***
Na	26742	27203	27323	26765	25201
Mg	2.09	0.23	< 0.2	< 0.2	< 0.2
Al	0.12	4163	3943	3915	3647
Si	3.78	70	66	64	66
P	< 0.2	5.8	6.7	2.9	2.6
S	0.51	77	64	63	52
K	0.29	25	44	55	43
Ca	3.49	2.7	2.4	2.4	3.9
Sc	< 0.001	< 0.001	< 0.001	< 0.001	< 0.001
Ti	0.002	0.030	0.015	0.011	0.012
V	< 0.002	8.2	9.6	5.3	5.4
Cr	0.003	< 0.002	< 0.002	< 0.002	< 0.002
Mn	< 0.002	< 0.002	< 0.002	< 0.002	< 0.002
Fe	0.003	0.78	0.74	0.68	0.55
Sr	0.004	0.024	0.021	0.026	0.028
Y	< 0.001	< 0.001	< 0.001	< 0.001	< 0.001
Zr	0.001	0.004	0.004	0.003	0.002
Nb	< 0.001	< 0.001	< 0.001	< 0.001	< 0.001
La	< 0.001	< 0.001	< 0.001	< 0.001	< 0.001
Ce	< 0.001	< 0.001	< 0.001	< 0.001	< 0.001
Pr	< 0.001	< 0.001	< 0.001	< 0.001	< 0.001
Nd	< 0.001	< 0.001	< 0.001	< 0.001	< 0.001
Sm	< 0.001	< 0.001	< 0.001	< 0.001	< 0.001
Eu	< 0.001	< 0.001	< 0.001	< 0.001	< 0.001
Gd	< 0.001	< 0.001	< 0.001	< 0.001	< 0.001
Tb	< 0.001	< 0.001	< 0.001	< 0.001	< 0.001
Dy	< 0.001	< 0.001	< 0.001	< 0.001	< 0.001
Ho	< 0.001	< 0.001	< 0.001	< 0.001	< 0.001
Er	< 0.001	< 0.001	< 0.001	< 0.001	< 0.001
Tm	< 0.001	< 0.001	< 0.001	< 0.001	< 0.001
Yb	< 0.001	< 0.001	< 0.001	< 0.001	< 0.001
Lu	< 0.001	< 0.001	< 0.001	< 0.001	< 0.001
Th	< 0.001	< 0.001	< 0.001	< 0.001	< 0.001
U	< 0.001	0.069	0.050	0.073	0.083